FACULDADE DE ENGENHARIA DA UNIVERSIDADE DO PORTO

Development of a multi-station creep testing machine for adhesive joints

Luis Pedro Laja Pina

Mestrado Integrado em Engenharia Mecânica

Supervisor: Prof. António Mendes Lopes

Co-Supervisors: Inv. Carlos Moreira da Silva
Prof. Lucas F.M. da Silva

December 2016

Development of a multi-station creep testing machine for adhesive joints

Luis Pedro Laja Pina

Mestrado Integrado em Engenharia Mecânica

December 2016

Resumo

As juntas adesivas oferecem diversas vantagens em relação aos métodos de fixação convencionais, sendo o seu estudo e caracterização impulsionado pelo Grupo de Adesivos da Faculdade de Engenharia da Universidade do Porto (ADFEUP). Devido ao limitado conhecimento sobre o comportamento das juntas em condições de fluência, é do interesse do ADFEUP ter à sua disposição um dispositivo capaz de realizar ensaios de fluência para juntas adesivas.

Este projeto surge no intuito de desenvolver e implementar uma máquina de ensaios de fluência para juntas adesivas sendo a continuação do trabalho desenvolvido na tese de mestrado de Freire, onde foi definido o sistema de atuação e o projeto mecânico.

A máquina desenvolvida deverá ter estações independentes, ter uma câmara térmica para impor as condições de temperatura, e ser capaz de manter constante a força aplicada no provete. Deverá também medir e registar a força e o deslocamento aplicados em cada provete ao longo do ensaio.

Foi feito um ante projeto da câmara climática para saber os seus requisitos e limitações de montagem. De seguida foi feita a revisão e aprimoramento do projeto mecânico, de modo a facilitar a sua fabricação e implementação. Em paralelo, os componentes de instrumentação e de actuação foram definidos e adquiridos, e a lógica de controlo e comando foi projetada para garantir o correto funcionamento da máquina, e permitir ao utilizador, via interface gráfica, a definição dos parâmetros e vizualização dos resultados dos ensaios.

Abstract

Adhesive joints have many advantages when compared to the traditional joining methods and their study and characterisation is driven at FEUP by the Adhesives Group (ADFEUP). Due to the lack of knowledge of the adhesive joints' behaviour under creep conditions, it's in the best interest of ADFEUP to have a device capable of performing creep tests in adhesives.

This work's purpose is to develop and implement a machine capable of performing creep tests and stress relaxation tests on adhesive joints. This thesis follows Freire's master's thesis, in which the actuation was defined and the mechanical design was performed. The machine should have a climatic chamber to apply the temperature conditions and independent stations able to maintain a constant load applied on the specimen. It should also be able to measure and record the load and displacement applied on each specimen along the test.

A brief design of the climatic chamber was done, to acknowledge the possible assembly requirements and limitations. The mechanical design was revised and improved to allow for easier manufacture and assembly. The actuation and instrumentation components were defined and ordered and the control and command logic were carried out to ensure the correct functioning of the machine and allow, via graphical user interface, the setup and visualization of the tests.

Acknowledgements

Firstly, I wish to express my gratitude to Prof. António Mendes Lopes, Inv. Carlos Moreira da Silva and Prof. Lucas da Silva, supervisors of this thesis, for all the support, patience and availability during the development of this machine and for providing me with the opportunity to work in such an interesting project.

To all the members of ADFEUP, particularly Ricardo Carbas and Eduardo Marques, for the support and contributions made to this project.

To Mr. Joaquim for the insight and help with the command logic circuit. To António Ramos Silva, for the help with the *LabView* graphical interface.

To Mr. José and Mr. Albino, for all the input and hard work in the workshop.

To João Dias, David Calado, Ricardo Maia, Tiago Costa, David Costa for their friendship and company in this steps of my academic life.

To Clara Viegas, for all support and insight.

To my family, for being always supportive.

To my girlfriend, Francisca Viegas, who encouraged me in all my decisions, right or wrong, and motivated me to accomplish the best possible.

Luis Pina

"Simplicity is the ultimate sophistication."

Leonardo da Vinci

Contents

List of Figures

List of Tables

Acronyms

FEUP	Faculdade de Engenharia da Universidade do Porto
ADFEUP	Adhesives Group from Faculdade de Engenharia da Universidade do Porto
SLJ	Single Lap Joint
GUI	Graphical User Interface
AI	Analogue Input
AO	Analogue Output
DI	Digital Input
DO	Digital Output
GND	Ground
DC	Direct Current
VPPX	VVPX proportional pressure regulator valve
DADE	DADE measured value transducer
UTM	Universal Test Machine
DAQ	Data Acquisition

Symbols

σ_r	Ultimate Tensile Strength
σ_y	Tensile Yield Strength
σ_w	Admissible Tensile Stress
τ_w	Admissible Shear Stress
σ	Tensile Stress
τ	Shear Stress
E	Young's modulus
λ	thermal conductivity
A_s	Surface area
A_c	Cross-sectional area
ϕ	Diameter
T_{amb}	Ambient Temperature

Chapter 1

Introduction

This chapter aims to introduce the reader to this thesis, and contains a brief background, the motivation, the objectives, the methodology and the thesis outline of the project developed.

1.1 Background

Adhesive bonding is a surface-to-surface joining technique of independent bodies using an adhesive, which adheres to the surface of the two adherents to be joined, transferring the forces from one to the other. This bonding technique offers uniform stress distribution, the possibility of joining large surfaces and of joining dissimilar materials. It has reduced weight, sealing capabilities, good damping properties as well as improved fatigue and corrosion resistance, altogether providing the designer with great flexibility. On the other hand, the adhesive joints have limited stability to heat and need surface preparation [1].

This bonding technique has become an interesting and valid replacement for welding, mechanical fasteners and rivets and is used in many different industries: from automotive to aerospace, electronics, medical, sports, and construction. Adhesive bonding is very distinct from the other joining techniques used in the industries, as it is not applicable to every situation, but it is particularly well-suited for lightweight construction in the automotive and aeronautic industry where reliability and durability are the most important characteristics, and adhesive joints meet these criteria better than most others [2].

1.2 Motivation

In automotive and aerospace industry applications, where adhesives are increasingly being used in safety-critical areas, it's necessary to carefully evaluate any possible decrease in performance that may occur when the adhesive bonded joints are subjected to creep loading. Creep is a time dependent slow deformation of materials under constant stress. This phenomenon usually occurs at lower stress than the yield strength and higher temperatures values. The rate of deformation of the material is dependent on the stress value, material properties, temperature and time.

Although the behaviour of adhesive joints under static conditions is well known, the creep behaviour of adhesives needs to be further studied. Creep may have catastrophic consequences, and therefore it's imperative that, by using testing methods, we are capable of studying and determining its behaviour [1].

The importance of the study and characterization of adhesive bonds is constantly growing. FEUP's Adhesives Group (ADFEUP) is responsible for various research projects in this area and has an electromechanical test system with a climatic chamber available, which is capable of running creep tests. However, creep tests are very time-consuming, so it's in the ADFEUP best interests to have access to a multi-station creep test machine enhancing throughput with the possibility of performing simultaneous, independent tests, leaving the electromechanical test system available for other necessary more dynamically demanding tests.

1.3 Objectives

The main goal of this thesis is to develop a multi-station creep test machine able to execute creep tests of adhesive joints. The specifications of the creep test machine were partially defined in Freire's thesis [3] with the help and expertise of ADFEUP:

- Load capacity : 2500 N
- Maximum displacement : 300 mm
- Temperature range: from -100 ^{o}C up to +200 ^{o}C

A load capacity of 2500 N and a 300 mm of maximum displacement, which was updated from the original value of 200 mm, were considered enough to test most specimens. The creep test machine should have three stations, making it possible to load each specimen separately, and the climatic chamber should enforce temperature conditions between -100 ^{o}C and +200 ^{o}C. The data acquisition system (DAQ) of the machine should acquire and plot, in a graphical user interface (GUI), the displacement and load applied to the specimen. A GUI was developed to enable user friendly communication with the DAQ system allowing for a parameter setup of the test and the control of the machine.

During the development of this thesis it was suggested that the creep test machine should also run stress relaxation tests, which occur under constant strain instead of under constant load.

1.4 Methodology

The first step in this project was to specify what would be necessary to make a fully functional creep test machine. As Freire [3] had already modelled a draft project for the mechanical structure, the project of the climatic chamber was advanced enough to acknowledge possible assembly requirements. After a brief project of the climatic chamber, where the design, insulation and temperature control components were defined, the focus was changed to the review, improvement and

manufacturing of the mechanical structure, leaving the climatic chamber for future progress of the machine.

The gripping system was designed, and the connections between cylinders, grips, load cells and the mechanical structure were revised. The mechanical structure itself, suffered several improvements in relation to Freire's original work [3], and after a final design was approved, the workshop started manufacturing and assembling the components.

At the same time, the instrumentation and actuation components were revised, redefined and ordered, and the command and control logic components and graphical interface of the machine were defined and designed.

1.5 Thesis Outline

The thesis' chapters follow each system of the creep test machine. The second chapter contains a brief Literature Review on creep tests and the machines available to perform it. The third chapter explores the Mechanical Design of the creep test machine. The Climatic Chamber is described in the fourth chapter. The fifth chapter addresses the Actuation and Instrumentation components. The sixth chapter encompasses the Command and Control of the machine. And finally, the seventh chapter outlines the main conclusions.

Chapter 2

Literature Review

This chapter contains a brief literature review about creep testing and commercial models of machines as well as machines available at FEUP which are able to perform creep tests.

2.1 Creep Tests of Adhesive Joints

Two different kinds of tests can be performed to study the behaviour of adhesive joints. The first one, is the characterization of the bulk adhesive, where the properties are intrinsic to the adhesive and not influenced by the adherents. The other one, is the determination of adhesive properties in joints, where the adhesive layer is in a complex state of stress. The Single Lap Joint (SLJ), due to its ease of manufacturing, represents the most common joint configuration. The creep test machine will be able to perform tests with both bulk specimens (Figure 2.1) and SLJ specimens (Figure 2.2).

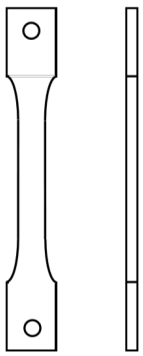

Figure 2.1: Bulk specimen

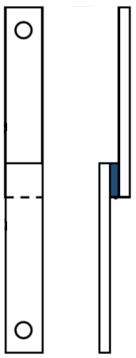

Figure 2.2: SLJ specimen

Creep is the deformation that occurs over a period of time when a material is subjected to constant stress at constant temperature. Data obtained in a creep test is usually presented as a plot of creep *versus* time with constant load and temperature. Creep tests can be performed at constant stress or at constant load resulting in slight differences. In practical terms the constant

load condition is more usual, therefore its study becomes more interesting than the constant stress condition [4].

In metals, creep usually occurs only at high temperatures. However, polymeric materials such as adhesives can undergo creep deformation at room temperature. The creep of a material can be divided into three stages after the initial elastic deformatio, shown in Figure 2.3. The first stage, or primary creep, exhibits a decreasing creep rate. Then, the second stage or secondary creep begins, in which the creep rate is relatively constant. The third stage, or tertiary creep, has an accelerating creep rate and terminates when material failure occurs [4].

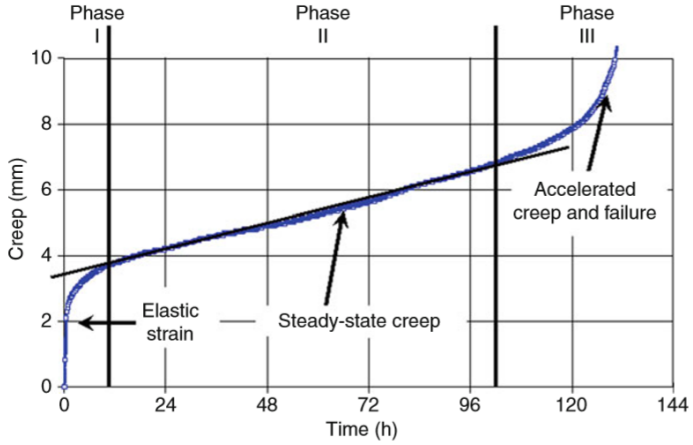

Figure 2.3: Creep Curve [2]

The time-dependent deformation of adhesive joints under constant load is known as creep or retardation. If, somehow, the joint was subjected to a defined strain condition, the adhesive's creep-related behaviour would lead to a time-dependent reduction of stress, which is known as relaxation [2]. A creep test's purpose is to determine the creep or relaxation behaviour of the adhesive joints. To determine the creep properties, the joint is subjected to prolonged constant load at constant temperature and its deformation is recorded. If specimen failure occurs within the test's designated duration, the test ends, and the time it took to rupture is recorded. If the specimen does not fracture, the creep recovery may be measured. To determine the relaxation behaviour of the joint, the specimen is deformed a given amount and exposed at constant temperature while the load applied is recorded. Although the mechanisms responsible for creep are different from those responsible for stress relaxation, both kinds of tests are conducted slowly, typically over long periods of time.

2.2 Creep Testing Solutions in FEUP

The ADFEUP group has an INSTRON 3367 electromechanical dual column tabletop model [5] with an INSTRON 3119 environmental chamber [6] available in the laboratory (Figure 2.4), which is capable of performing creep tests. However, the ADFEUP members use this machine in a daily basis, and a creep test would occupy it for extended periods of time. The cost of acquisition of

this universal test machine (UTM) is around 45000 € not including the climatic chamber which would add about 15000 € to the total cost.

In the *Laboratório de Ensaios Tecnológicos* (LET) there are currently two screw driven creep test machines for steel specimens, which have a lesser maximum deformation, higher load capacity and a high temperature furnace (Figure 2.5).

Figure 2.4: ADFEUP's UTM

Figure 2.5: LET's creep test machines

2.3 Creep Testing Solutions in the Market

To be capable of performing a creep test, a machine needs to expose the specimen to a constant load and a constant temperature. There are many manufacturers of universal test machines like ZWICK, MTS, SHIMADZU and INSTRON with the option of including a climatic chamber, making it able to perform creep tests. Although the test system suppliers offer many options of single station universal test machines with a load capacity matching our needs, most of the universal test machines that allow the implementation of a climatic chamber have a minimum load capacity of 30 kN, way above the necessary to test adhesive joints. There is not much offer for multi-station test machines, with or without climatic chambers, and by the law of demand, the ones existent would be very expensive.

INSTRON offers a multi-station system with a climatic chamber and a load capacity of 30 kN (Figure 2.6). It has a single load frame with five load axis allowing for simultaneous and independent testing. The load capacity of each station is the system load capacity divided by the number of stations being used. However, only the central load station can accommodate full capacity while the others are rated to a maximum of 10 kN. It's not clear how the machine guarantees a correct load distribution as the test stations are assembled to the same crosshead. The climatic chamber is may be removed from the work area and operates between -40 ºC and +200 ºC [7].

Figure 2.6: INSTRON Multi Station System [7]

ZWICK also offers a multi station creep test machine (Figure 2.7), but with five stations, each with a single screw drive with a load capacity of 10 kN. The climatic chamber is assembled to the test frame and can operate between -70 ºC and +250 ºC [8].

Figure 2.7: ZWICK Multi Station Creep Test Machine [8]

2.4 Conclusions

After analysing the commercial solutions, the design principle of the creep test machine was defined with the help and expertise of ADFEUP. An independent loading of each specimen and a partially removable climatic chamber was also defined.

Chapter 3

Mechanical Design

This chapter addresses the mechanical design of the creep testing machine. The machine and its components must be able to withstand the maximum load applied while presenting a low deflection and its stations should be aligned to provide reliable data of the creep behaviour of the adhesive joints. The mechanical project outlined up to the date this thesis started [3] was revised, and although every component of the old machine suffered alterations or was replaced, the current mechanical project is inspired in it and the optimization or replacement of each component is studied in further detail along the chapter.

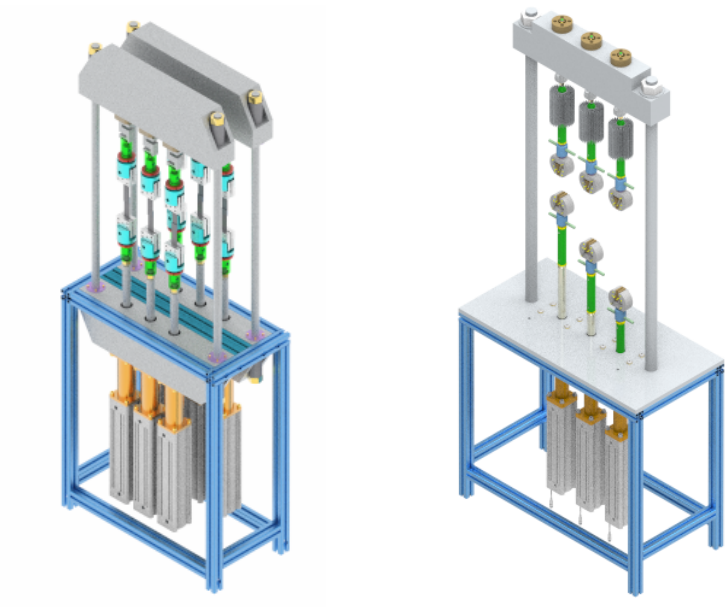

(a) Original machine (b) Improved machine

Figure 3.1: Creep testing machine comparison

The creep testing machine conceived by Freire [3] consists in a test frame based on an upper beam and a lower beam with two columns connecting one another; a support frame where the load frame would be supported; and the necessary connections for the cylinder, load cell and

grips (Figure 3.1(a)). Freire's [3] concept contains two modules of three stations supported by one support frame, but due to the Climatic Chamber specifications [Chapter 4], a three station per support frame design, as shown in Figure 3.1(b), was a more viable solution.

The mechanical design (Figure3.2) can be divided in four different sub-assemblies that will be studied in four different sections:

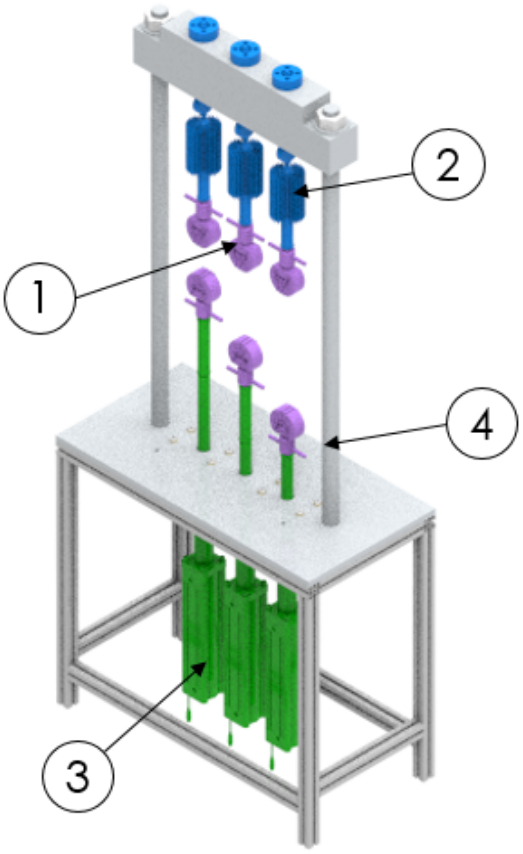

Figure 3.2: Creep Test Machine sub-assemblies

1. Mechanical Wedge Action Grips [Section 3.1]

2. Upper Assembly [Section 3.2]

3. Lower Assembly [Section 3.3]

4. Mechanical Structure [Section 3.4]

As the sub-assemblies of the machine have repercussions in one another, the project of each sub-assembly and of the Climatic Chamber was undertaken simultaneously and the components were designed and assembled with *Solid Edge* to check for assembly interference.

3.1 Mechanical Wedge Action Grips

The grips are a crucial sub-assembly of the creep testing machine as they are responsible for tightening the specimen while it's subjected to the load conditions of the creep test. To obtain a fully functional creep testing machine, the grip system needed to be defined. The ADFEUP laboratory has a clamping tool available for one station, but the machine needs one pair of grips for each of the three stations. A choice had to be made between either manufacturing two clamping tools equal to the existing one, acquiring three pairs of grips on the market or designing a new set of grips.

3.1.1 Clamping system available in ADFEUP laboratory

The ADFEUP laboratory has a clamping system for one station available to use with the *INSTRON* machine. Figure 3.3 shows on the left a representation of the complete clamping system, including the specimen, and on the right is shown the SLJ tool needed to clamp each side of the specimen. The specimens need to have an alignment hole on each side, which is responsible for aligning it to the clamping system through the use of a pin in each SLJ tool. After the alignment of the specimens, both SLJ tools are tightened and the clamping system is ready to use. This is a slow process, that occurs outside the work area of the machine.

(a) Clamp with SLJ specimen

(b) Tool for SLJ specimen

Figure 3.3: Clamping system available at ADFEUP laboratory

Manufacturing two sets of grips equal to the available one would solve the problem for SLJ specimens but not for the bulk specimens, so the clamping system available for that option wouldn't completely satisfy the requirements of the ADFEUP group.

3.1.2 Commercial models of grips

The testing systems suppliers like *INSTRON*, *MTS*, *SHIMADZU* and *ZWICK* have available grips that would suit the creep testing machine. They offer pneumatic grips, hydraulic grips and mechanical grips, mainly with side action or wedge action principle. The side action design consists in compressing two jaw faces together via pneumatic, hydraulic or screw action. The wedge design takes advantage of the inclined faces of both the body and the jaws, forcing the simultaneous movement of the jaws against each other.

(a) *MTS* Hydraulic Wedge Action Grip [9]

(b) *INSTRON* Pneumatic Side Action Grip [10]

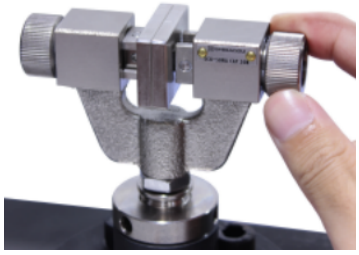

(c) *SHIMADZU* Mechanical Side Action Grip [11]

(d) *MTS* Mechanical Wedge Action Grip [12]

Figure 3.4: Commercial models of grips

The hydraulic grips (Figure 3.4(a)) are used for gripping specimens at much higher loads than the 2500 N at which the creep test machine will work and would require a hydraulic circuit. The pneumatic grips(Figure 3.4(b)) , despite being more appropriate to the loads used and being able to use the pneumatic circuit necessary for the cylinders [Chapter 5], would have been, like the hydraulic grips, an unnecessary investment. The mechanical side action grips (Figure 3.4(c)) would be similar to the clamping system available. The mechanical wedge action grips (Figure 3.4(d)) would be a good option for the creep testing machine, but despite having the simpler operating principle, a fast tightening method and a good performance, they also had an excessive cost, around 700 € per pair, which would go against making a low budget creep testing machine. It was decided that designing a new set of grips with the features of the commercial ones was the route to take.

3.1.3 Mechanical Wedge Action Grip

To design a new set of grips we had to analyse the design of the existing grips on the market. Although we found a few schematics of mechanical grips, most of those available on the market don't have the technical drawing and the *modus operandi* available for the common client, so a lot of guessing work was involved. As designing a new set of grips was the option chosen, we wanted to make sure that it was an improvement of the current solution. Therefore, we needed to make it easier and faster to setup the specimens, and make sure it had a better performance during tests. The type of grip adopted was the mechanical wedge action grip. There are two main types of mechanical action wedge grips: a moving body type and a moving wedge type (Figure 3.5). They are both based on the relative vertical movement between the body of the grip and the wedges, which occurs due to both the grip's Body and Jaw Face inclined faces, tightening the specimen in the process. The moving wedge type grips have the body in a fixed position and need the use of a lever mechanism or a screw action to push the jaw faces. The moving body type grip has the jaw faces in a fixed position via another component and needs some mechanism (usually a threaded connection) to control the vertical movement of the body.

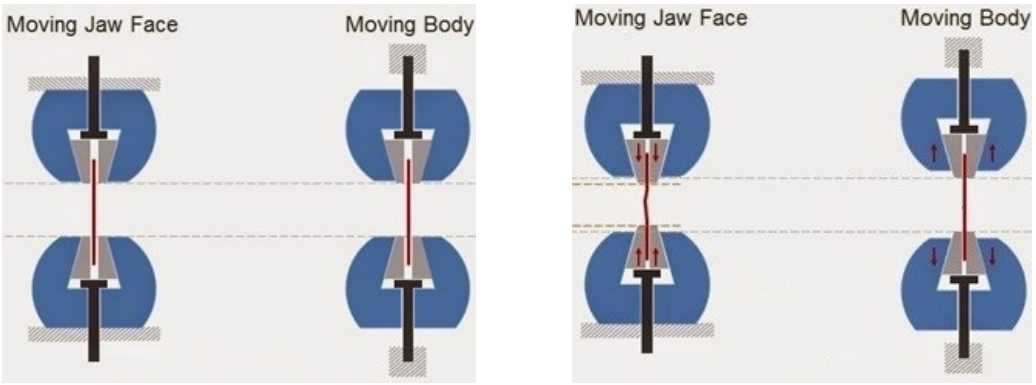

(a) Before clamping (b) After clamping

Figure 3.5: Comparison between moving body and moving jaw face design

The Mechanical Wedge Action Grip [Drawing GP-00 in Apendix A.1] is designed for easy specimen loading and alignment. The grip moving body design allows it to be tightened to a specimen without altering the vertical position of the Jaw Faces in relation to it (Figure 3.5). This design feature makes it possible to pre-select the exact point at which the specimen will be held and no compressive force is applied which could cause specimen buckling. The open design of the grip Body allows the Jaw Faces to be easily interchanged as well as easy specimen loading. The Jaw Faces are spring loaded against a Shoe which is in a fixed position. When the Body is drawn up, the inclined sides push against the matching side of the Jaw Faces forcing its simultaneous movement relative to the grip centerline, ensuring correct specimen alignment (Figure 3.6). A strong clamping force can be applied through a high mechanical advantage achieved by the tightening mechanism. However, only a light initial gripping force needs to be applied to the specimen

as the wedge-shaped design of the Jaw Faces causes the gripping force to increase, as tension is applied during the test. Because the Jaw Faces are held in fixed position, there is no recoil, or loosening, when the specimen ruptures.

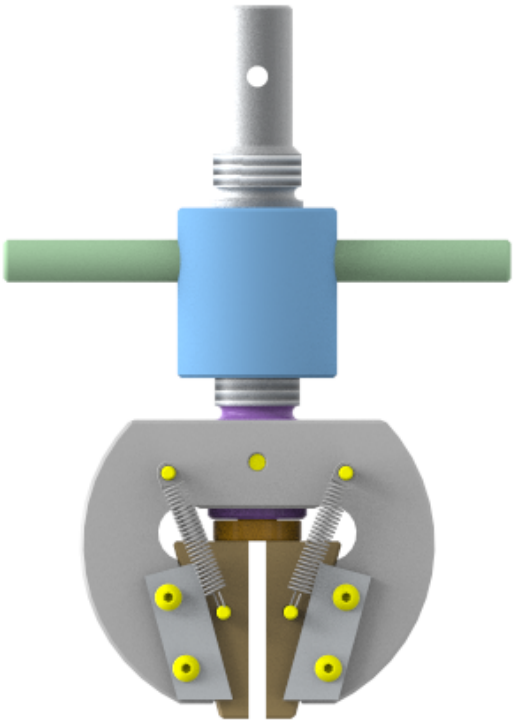

Figure 3.6: Mechanical Action Wedge Grip

3.1.4 Effects of temperature on mechanical properties

The selection of the material to be used is an essential step of designing. The main goal is to minimize the cost of the material while meeting the performance goals. The material adopted for the construction of the grips and other components inside, or at least partially inside, the chamber was the AISI 304 austenitic stainless steel because of its good balance between mechanical resistance and thermal conductivity and also due to its corrosion resistance (Table 3.1). The thermal conductivity of the AISI 304 stainless steel is $k = 16$ W/(m.K).

Table 3.1: Mechanical Properties of AISI 304 steel at room temperature

Ultimate Tensile Strength, σ_r	510 MPa
Tensile Yield Strength, σ_y	205 MPa
Young's modulus, E	190 GPa

The mechanical properties of AISI 304 slightly decrease along the range of temperatures the components will work. When a material is subjected to constant load at high temperatures for long periods of time, it creeps. Altough, a temperature of 200 ^{o}C is not high enough for us to consider

that the stainless steel is at creep conditions [13], it still has a slight degradation in properties like the Tensile Strength, Yield Strength and Young's Modulus, as shown in the following Figures 3.7, 3.8 and 3.9.

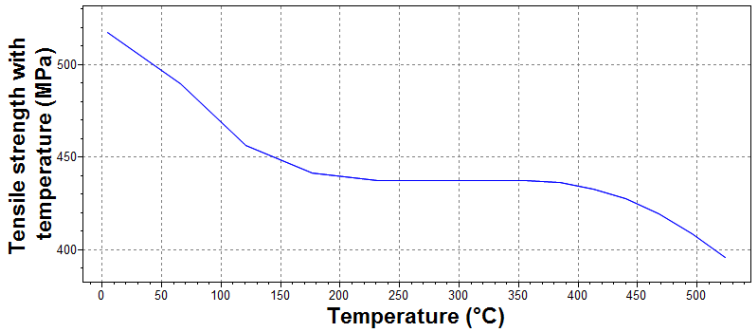

Figure 3.7: Effect of temperature in AISI 304 Tensile Strength [14]

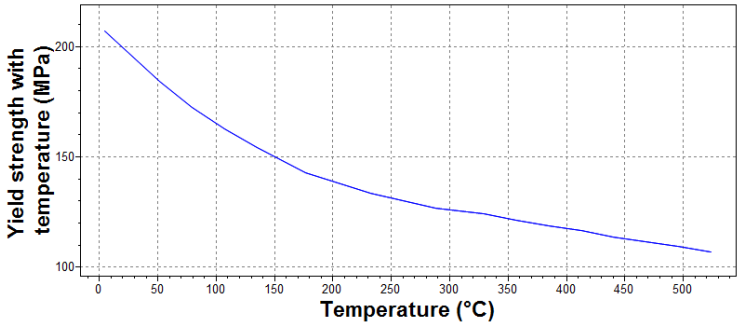

Figure 3.8: Effect of temperature in AISI 304 Yield Strength [14]

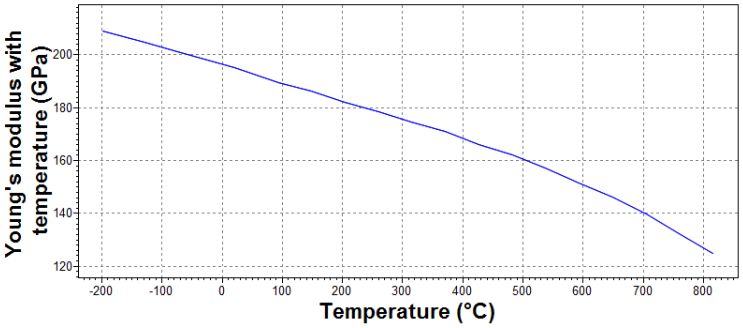

Figure 3.9: Effect of temperature in AISI 304 Young's Modulus [14]

As the climatic chamber's operating temperature goes up to 200 ^{o}C, we took this degradation of the mechanical properties into account and used the lowest values of those properties within the operating temperature range (Table 3.2).

Table 3.2: Mechanical Properties of AISI 304 steel at 200 °C

Ultimate Tensile Strength, σ_r	440 MPa
Tensile Yield Strength, σ_y	139 MPa
Young's modulus, E	182 GPa

For the design calculations of the components using AISI 304 stainless steel, we will assume an admissible tensile stress σ_w = 70 MPa and therefore an admissible shear stress τ_w = 40 MPa.

3.1.5 Jaw Faces

The Jaw Faces [Drawing GP-01 in Apendix A.1](Figure 3.10) are responsible for the tightening of the specimens through the wedge action principle. To accomplish the griping of the specimens, the faces' surfaces were serrated with a diamond cut teeth with an angle of 60° and a tooth pitch of 1 mm, as shown in Figure 3.11. These parameters were chosen with the help and expertise of the ADFEUP group within those available in *INSTRON* Jaw Faces.

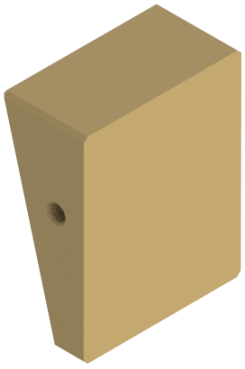

Figure 3.10: Jaw Face

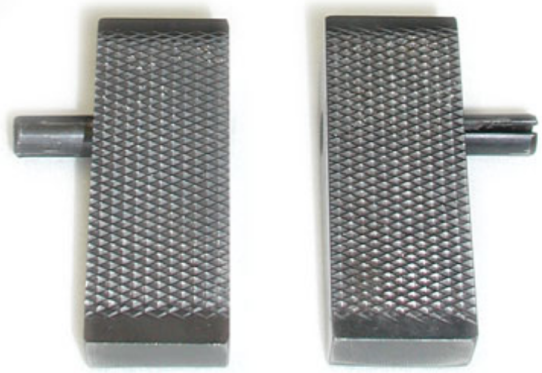

Figure 3.11: *INSTRON* Jaw Face with desired serration [15]

This Jaw Face has a gripping range between 0 mm and 5 mm. To obtain different gripping ranges to grip thicker specimens, the Jaw Face must be slimmer (Table 3.3).

Table 3.3: Jaw Faces' gripping ranges

Jaw Face maximum width	**Gripping Range**
21.5 mm	0...5 mm
20 mm	3...8 mm
19 mm	5...10 mm

Both the angle of the Jaw Faces and the angle of the internal faces of the Body determine the relation of vertical movement of the Body and the horizontal movement of the Jaw Faces towards or away from one another. The angle chosen was 15°, thus for each 1 mm the Body moves

vertically, the Jaw Faces will move $2\tan(15^o)$ mm. With a gripping range of 5 mm, the equivalent vertical range of the grip is approximately 9 mm.

The Jaw Faces were manufactured using a DIN 20 MnCr 5 case-hardening steel, so after manufacturing in the workshop they returned to the supplier for the surface hardening process and then to the workshop again for grinding.

3.1.6 Body

The Body [Drawing GP-02 in Apendix A.1](Figure 3.12) commands the movement of the Jaw Faces which in turn tightens the specimen to be tested. When the Body moves vertically, the Shoe prevents the Jaw Faces from following the vertical movement and the inclined faces of the Body, which have the same angle of the Jaw Faces, forcing their horizontal movement.

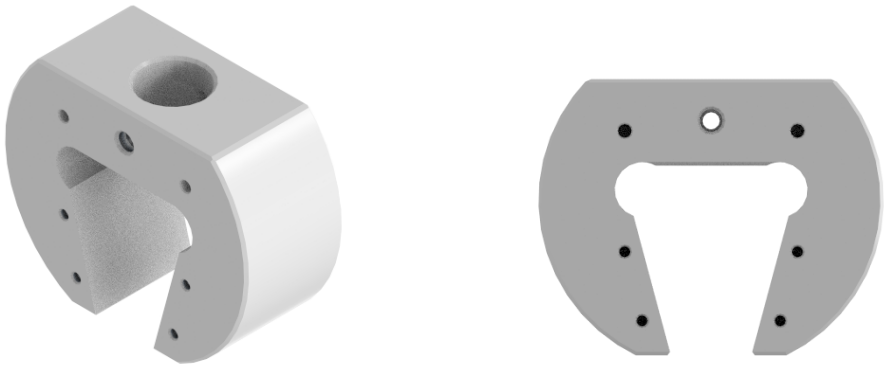

(a) Isometric view (b) Front view

Figure 3.12: Body

The forces acting on the Body during the test are the reactions to the Jaw Faces when gripping a specimen (Figure 3.13).

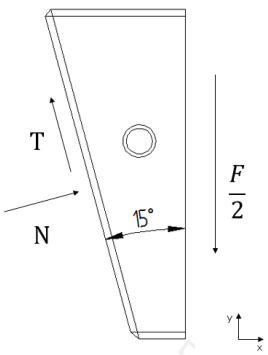

Figure 3.13: Forces acting on the Jaw Faces during the test

Neglecting the weight of the Jaw Faces and their spring load, and considering only the maximum work load of 2500 N, the forces acting on the Body are given by

$$\begin{cases} N \cdot cos(15) - T \cdot sin(15) = 0 \\ N \cdot sin(15) + T \cdot cos(15) - \frac{F}{2} = 0 \end{cases} \quad \begin{cases} N = 324 \text{ N} \\ T = 1207 \text{ N} \end{cases} \tag{3.1}$$

As confirmed via *Solid Edge Simulation*, fixing the Body in a circular surface that is supported by the Bushing and loading each face with the loads previously calculated, assures that the Body withstands the maximum load applied. Figure 3.14 shows that the maximum stress occurs due to the horizontal component of the reaction between the Body and the Jaw Faces, on the cylindrical parts of the hollow of the Body.

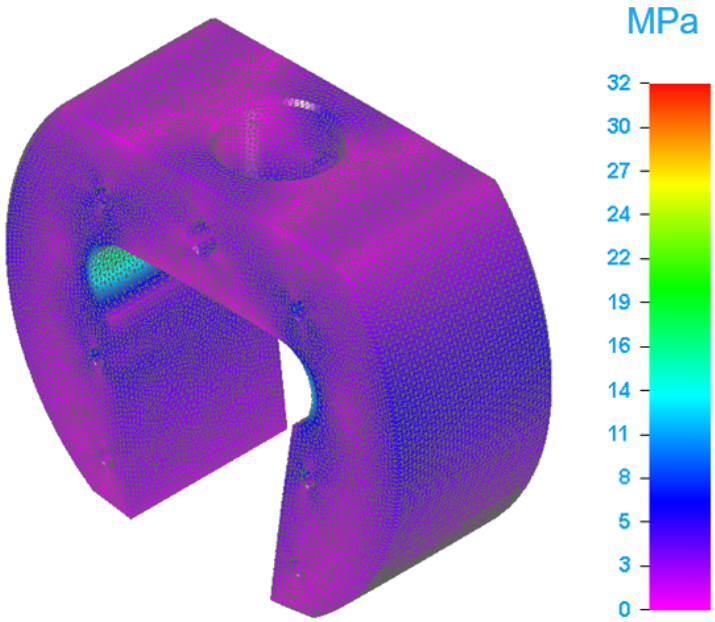

Figure 3.14: Von Mises Stress on the Body of the Grip

3.1.6.1 Retaining Plate

The Retaining Plates' [Drawing GP-03 in Appendix A.1] function is to limit the horizontal movement of the Jaw Faces, perpendicular to the gripping movement, driving them along the desired path and allowing for a good tightening. The Retaining Plates are fixed to the Body with two ISO 7382 screws each, having a button head, as shown in Figure 3.15, which is the most appropriate design for a component with great user interaction.

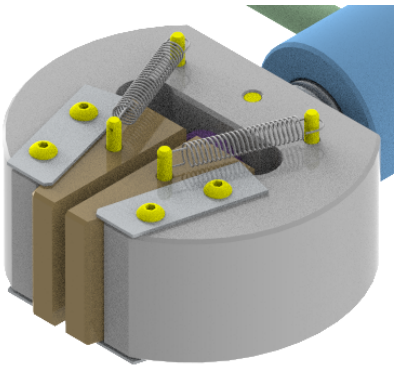

Figure 3.15: Retaining Plates assembly

3.1.6.2 Extension Springs

The extension springs are used to pull the Jaw Faces against the Shoe. This ensures that the Jaw Faces are being pushed down symmetrically, therefore ensuring the correct tightening of the specimen. During setup, the forces acting in the Jaw Face are its weight, the spring load and the reaction forces from the Shoe and the Body. A spring must be defined to ensure that at the maximum grip opening, when the springs are less deformed, they endure the gravity force of the Jaw Faces pulling them against the Shoe. These springs are connected to the Body and to the Jaw Faces through the use of DIN 1469 C half-length grooved pins with a rounded neck in the end to accommodate the spring hook (Figure 3.16).

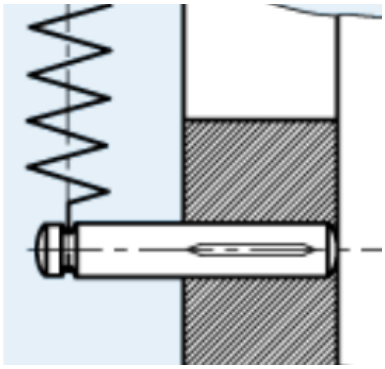

Figure 3.16: Extension Spring assembly

3.1.6.3 Bushing

The Bushing [Drawing GP-04 in Appendix A.1] is responsible for the vertical movement of the Body, which is fundamental to the grip tightening process. Ideally the Bushing (Figure 3.17) and the Body would be a sole component, but due to the FEUP workshop limitations, it had to be adapted to an assembly of two components of easier manufacturing.

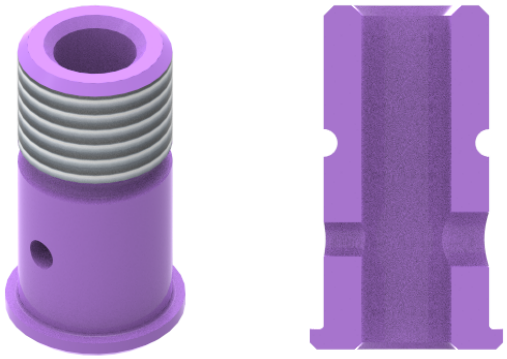

(a) Isometric view (b) Front section view

Figure 3.17: Bushing

The Bushing ledge has to support the Body, so it needs to be checked for shear stress and for compression stress. An admissible tensile stress of σ_w = 70 MPa, and therefore an admissible shear stress τ_w = 40 MPa were considered. For the shear stress on the ledge we have

$$\tau \leq \tau_w \Leftrightarrow \tau = \frac{F}{A_\tau} \leq \tau_w \tag{3.2}$$

where F is the maximum load applied, which is 2500 N and the shear area A_τ of the ledge is given by

$$A_\tau = \pi D h = \pi \cdot 24 \cdot h \tag{3.3}$$

Replacing Equation 3.3 into Equation 3.2 we obtain

$$\frac{2500}{\pi \cdot 24 \cdot h} \leq 40 \tag{3.4}$$

thus the minimum height h of the ledge of the bushing is

$$h \geq 0.829 \text{ mm} \tag{3.5}$$

For the compression stress on the ledge

$$\sigma \leq \sigma_{adm} \Leftrightarrow \sigma = \frac{F}{A_c} \leq \sigma_{adm} \tag{3.6}$$

where the area of compression A_c is given by

$$A_c = \frac{\pi}{4} \cdot (D_m^2 - D^2) = \frac{\pi}{4} \cdot (D_m^2 - 24^2) \tag{3.7}$$

obtaining

$$\frac{2500}{\frac{\pi}{4} \cdot (D_m^2 - 24^2)} \leq 70 \tag{3.8}$$

thus the minimum diameter of the ledge is

$$D_m \geq 24.929 \text{ mm} \tag{3.9}$$

The ledge ended up with $\phi 28$ mm and a height of 3 mm. The assembly between the Body and the Bushing was assured through a transition fit (a compromise between clearance and interference) [16] and through a parallel pin DIN 6325 5×12 m6 (Figure 3.18) which prevent the relative rotation between the components and align the Bushing to the Body, allowing the assembly of the Rotation Set Screw [Section 3.1.8.1].

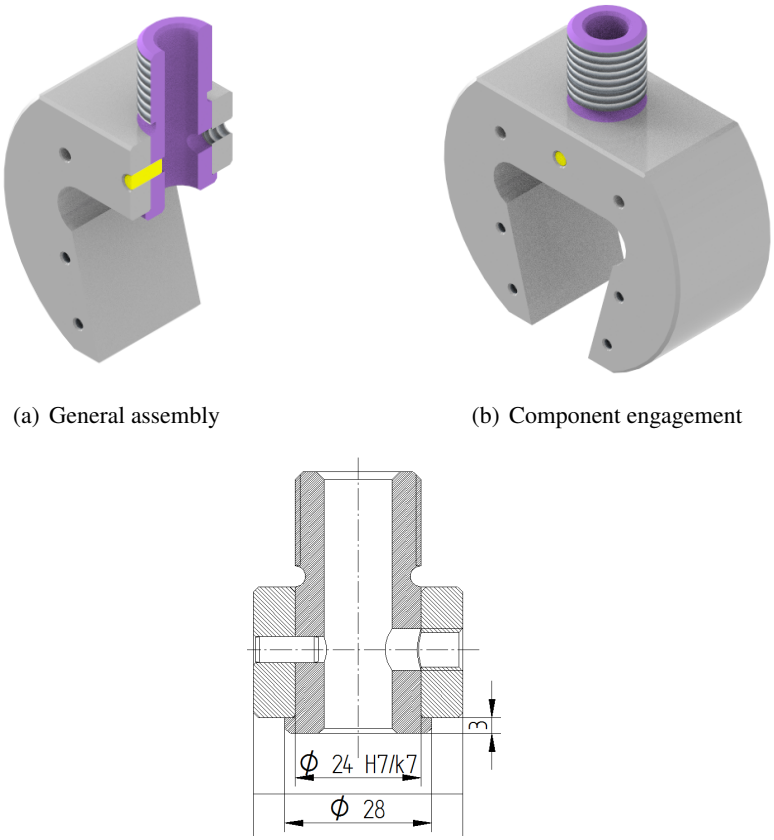

(a) General assembly (b) Component engagement

(c) Dimensioning scheme

Figure 3.18: Body - Bushing assembly

3.1.7 Control Nut

The Control Nut [Drawing GP-05 in Appendix A.1], due to its internal thread, is the component responsible for transforming the rotation of the Handles which are assembled to it, into a vertical movement of the Bushing and through assembly, of the Body (Figure 3.19). The axial movement of the Control Nut is limited by the Spindle shoulder feature and by the Sleeve. This puts the Control Nut in a fixed position and pulls the Body against itself when tightening the grip.

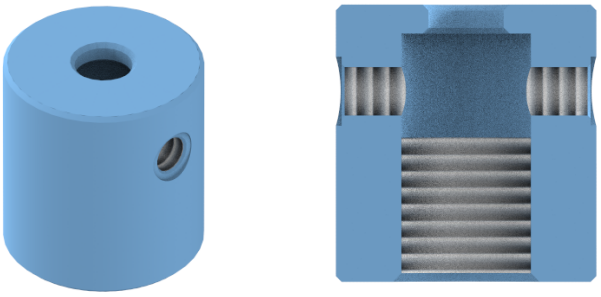

(a) Isometric view (b) Front section view

Figure 3.19: Control Nut

The connection between the Control Nut and the Bushing was made through a M24×1.5 fine pitch metric thread. The Bushing has a greater engagement in the Control Nut when the grip is at the maximum value of the gripping range and a lower engagement when the grip is at the minimum value. When it's at the maximum value of the gripping range, the thread engagement of the Bushing in the Control Nut is slightly greater than 10 mm (Figure 3.20).

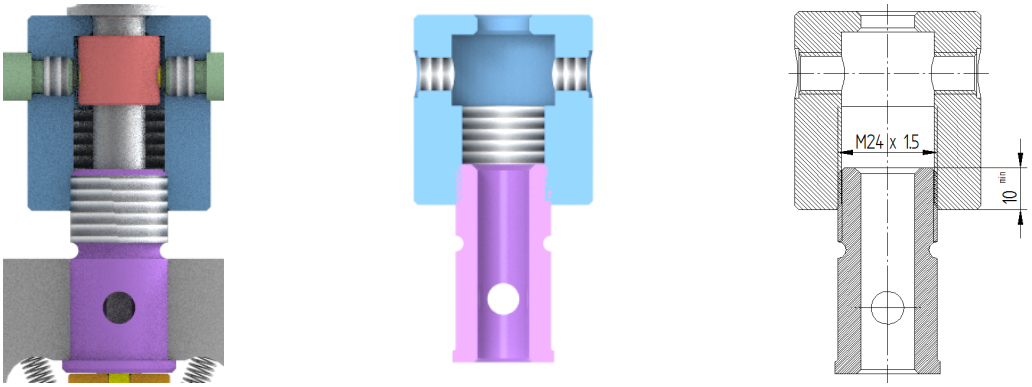

(a) General assembly (b) Component engagement (c) Dimensioning scheme

Figure 3.20: Bushing - Control Nut thread engagement

The connection was checked for shear stress, where the shear area A_τ is given by

$$A_\tau = 0.5 \cdot \pi \cdot d_p \cdot L_e \tag{3.10}$$

where L_e is the thread engagement and the pitch diameter d_p is given by

$$d_p = D - 0.75psin(60^o) \Leftrightarrow d_p = (D - 0.75 \cdot 1.5 \cdot sin(60^o) \Leftrightarrow d_p = 23\text{mm} \tag{3.11}$$

Considering the degradation of the mechanical properties, due to the temperature conditions, of

the AISI 304 stainless steel, we considered an admissible shear stress $\tau_w = 40$ MPa,

$$\frac{F}{A_\tau} \leq \tau_w \Leftrightarrow \frac{F}{0.5 \cdot \pi \cdot d_p \cdot L_e} \leq \tau_w \Leftrightarrow L_e \geq \frac{F}{0.5 \cdot \pi \cdot d_p \cdot \tau_w} \tag{3.12}$$

therefore the minimum thread engagement is

$$L_e \geq 1.8 \text{ mm} \tag{3.13}$$

As the minimum thread engagement is 10 mm, the Bushing does not risk thread striping.

(a) Isometric view

(b) Detail of Handles assembly in the Control Nut

Figure 3.21: Control Nut - Handles assembly

The Handles [Drawing GP-06 in Appendix A.1](Figure 3.21) serve, through mechanical advantage, to rotate the Control Nut. With a pitch of 1.5 mm and an equivalent vertical gripping range of approximately 9 mm, the Control Nut needs to complete six rotations to fully tighten the grip beginning at the maximum value of the gripping range.

3.1.8 Spindle

The Spindle [Drawing GP-07 in Appendix A.1] is responsible for fixing the Shoe position, which prevents the Jaw Faces from moving when the Body is drawn up, supporting the Control Nut through a Sleeve and a clevis pin, and connecting the grip to the Lower and Upper Assemblies (Figure 3.22).

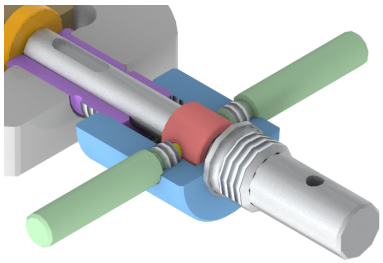

Figure 3.22: Spindle assembly

The Spindle and the Bushing have a running fit [16] allowing for an easy relative vertical movement between the components.

3.1.8.1 Set Screw

The Set Screw limits the rotation of the grip Body forcing its tightening (Figure 3.23). This is accomplished by assembling the Set Screw in the Spindle keyway.

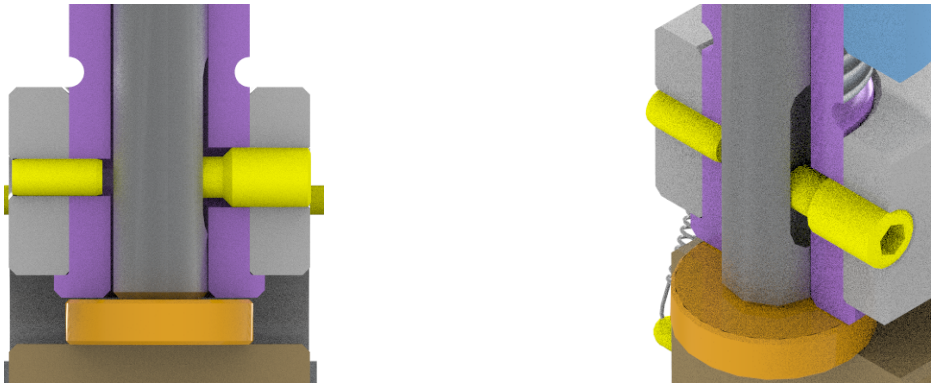

Figure 3.23: Set Screw assembly

The Set Screw prevents the grip's Body rotation. As the tip of Set Screw cannot touch the keyway, as it would lock the vertical movement of the Spindle, a nut was used to control the engagement of the Set Screw, which guarantees that the Set Screw only contacts the keyway on its sides.

3.1.8.2 Sleeve

The Sleeve [Drawing GP-08 in Appendix A.1](Figure 3.24) is the supporting component between the Control Nut and the Spindle.

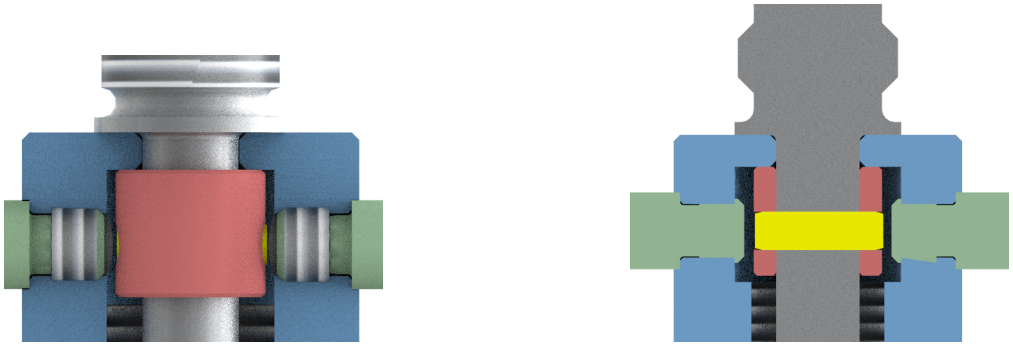

Figure 3.24: Sleeve assembly

Since double shear is acting upon this joint, the connection was checked for bearing stress and pin shearing [17]. The pin chosen was a parallel pin DIN 6325 $\phi 6 \; x \; 20$.

The stress of the connection was checked for the weakest material, which is the AISI 304 stainless steel, and for the component with the lesser contact area length with the pin. The contact area length between the Spindle and the pin is the Spindle diameter D =13 mm, and the contact area length between the Sleeve and the pin is $D_m - D = 7$ mm. The Sleeve was checked for bearing stress, shear-out stress and tear-out stress. The Sleeve has an external diameter $D_m = \phi 35$ mm, an internal diameter $D = \phi$ 20 mm, a pin hole diameter $d = \phi 6$ mm and the distance from the center of the pin hole to the top of the sleeve is $h = 10$ mm

The bearing stress is the stress acting on the hole the pin goes through and was checked to determine whether the connection might induce any deformation of the hole. The bearing area could be the contact area length $D_m - D$ multiplied by the diameter of the hole d. The bearing stress $\sigma_{bearing}$ is given by

$$\sigma_{bearing} = \frac{F}{(D_m - D)d} = 59.5 \text{ MPa} \tag{3.14}$$

The shear-out stress $\sigma_{shear-out}$

$$\tau_{shear-out} = \frac{F}{(D_m - D) \cdot h \cdot 2} = 17.9 \text{ MPa} \tag{3.15}$$

The tear-out stress $\sigma_{tear-out}$ is the stress acting in the cross section area of the Sleeve.

$$\tau_{tear-out} = \frac{F}{\frac{\pi D_m^2}{4} - \frac{\pi D^2}{4} - (D_m - D) \cdot d} = 27.3 \text{ MPa} \tag{3.16}$$

3.1.8.3 Shoe

The Shoe's [Drawing GP-02 in Appendix A.1] function during the test is to prevent the Jaw Faces from moving when the Body is being drawn up. During setup, it limits the opening of the grip, preventing the complete loosening and disassembling of the grip Body (Figure 3.25). The Shoe was fixed to the Spindle using a ISO 10642 M5 $\times$ 12.

(a) Shoe (b) Mechanical limit

Figure 3.25: Shoe assembly

3.2 Lower Assembly

The Lower Assembly [Drawing LA-00 in Appendix A.3] contains the cylinders, its connections to the Lower Beam, and the connections between the cylinders and the lower grips. Freire [3] predicted that the cylinders couldn't be close to the Climatic Chamber due to the operating temperature parameters. This limitation denied the use of a cylinder flange commercially available so a Spacer Sleeve was designed to distance the cylinder from the high temperature source. As the cylinder rod became far apart from the work area, a cylinder extension and a connection to the lower grip were also designed.

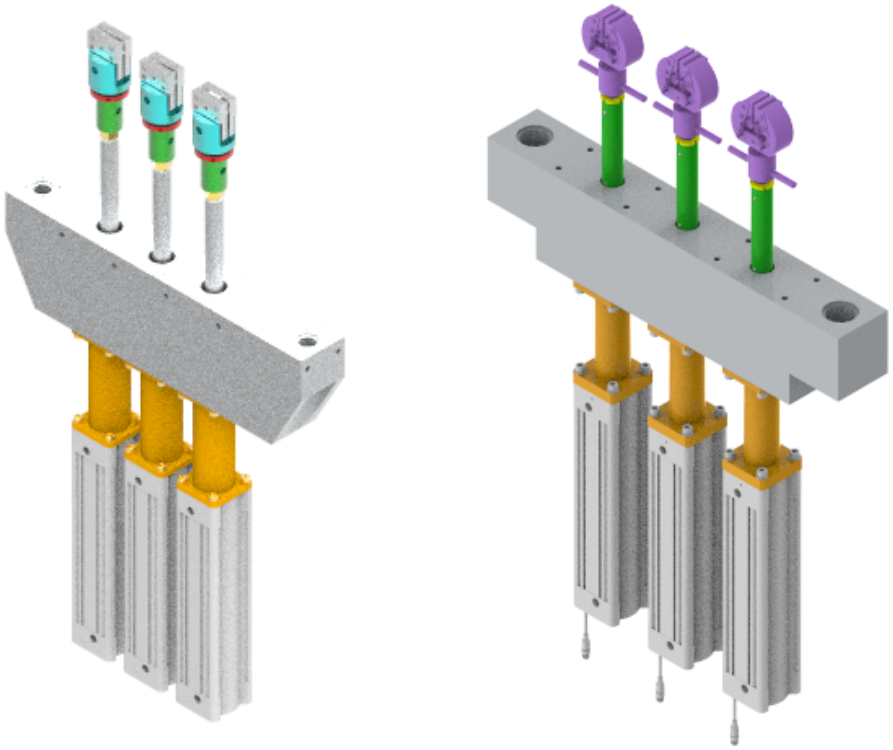

(a) Original design (b) Improved design

Figure 3.26: Lower Assembly design comparison

Freire's [3] design didn't allow for an easy exchange of the cylinder extensions , so we decided to separate the cylinder's connection to the lower grip into a fixed extension (Cylinder Extension) and a replaceable extension (Lower Coupling) which also serves as a connection to the lower grip (Figure 3.27).

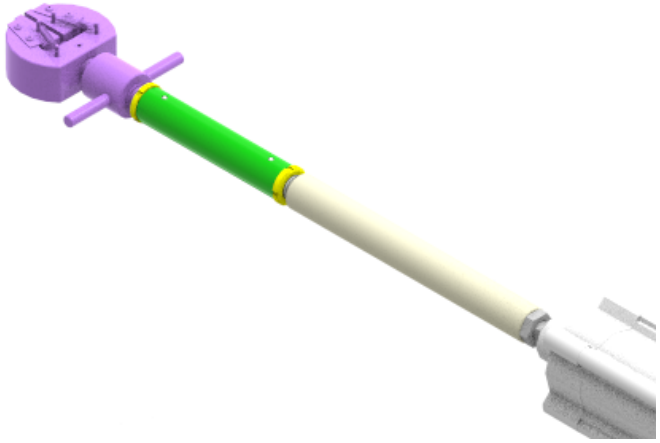

Figure 3.27: Improved Lower Grip - Cylinder Connection

3.2.1 Cylinder Rod Extension

Given that the maximum operating temperature of the cylinder, which is 80 ^{o}C, must be respected, the connection between the lower grip and the cylinder must take that requirement into account. To ensure that the tip of the cylinder, where the sealants are, stay below that temperature, the distance between the chamber and the cylinder was increased through the use of a Spacer Sleeve and a Cylinder Rod Extension, shown in Figure 3.28.

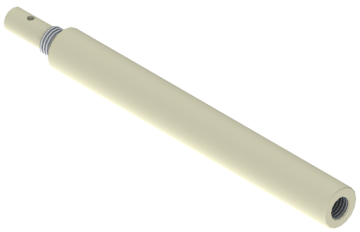

Figure 3.28: Cylinder Rod Extension

The analysis of the necessary lenght of the Cylinder Rod Extension [Drawing LA-02 in Appendix A.3], which would ensure that the tip of the cylinder stays below 80 ^{o}C, is simplified if some assumptions are made. This analysis assumes that the Lower Coupling is at 200 ^{o}C and the heat exchange occurs only in the Cylinder Extension due to natural convection with a coefficient of $h = 4.2$ W$/$(m^2.K) [calculated through ASTM C680] and an ambient temperature of $T_{amb} = 20$ ^{o}C. It also assumes, as represented in Figure 3.29, a simplified form of a ϕ 35$\times$ 350 mm rod, steady-sate conditions, one-dimensional conduction along the Cylinder Rod Extension, constant properties, negligible radiation exchange with surroundings, uniform hear transfer coefficient over the surface, and an adiabatic tip [18].

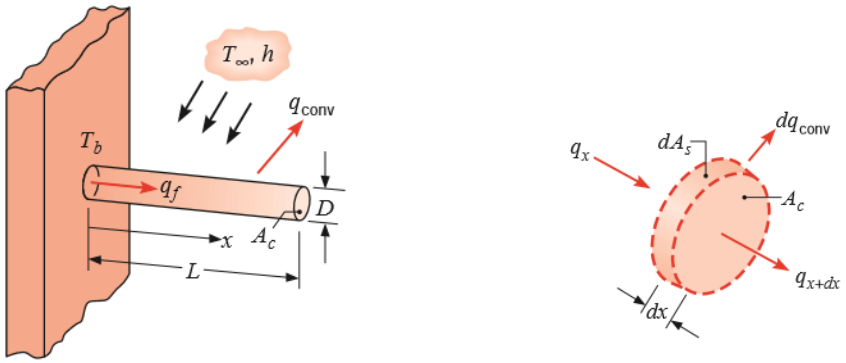

(a) Rod heating transfer scheme (b) Differential element

Figure 3.29: Thermal analysis of the Cylinder Extension [18]

Applying the conservation of energy requirement to the differential element we obtain

$$q_x = q_{x+dx} + dq_{conv} \tag{3.17}$$

Where q_x is the conduction heat rate at x, q_{x+dx} is the conduction heat rate at $x+dx$, and dq_{conv} is the convection heat transfer rate for the differential element. Fourier's law states that the conduction heat rate q_x is given by

$$q_x = -kA_c \frac{dT}{dx} \tag{3.18}$$

where A_c is the cross-sectional area. The conduction rate at $x+dx$ may be expressed as

$$q_{x+dx} = q_x + \frac{dq_x}{dx}dx = -kA_c \frac{dT}{dx} - kA_c \frac{dT}{dx} \tag{3.19}$$

and the convection heat transfer rate dq_{conv} may be expressed as

$$dq_{conv} = hdA_s(T - T_\infty) \tag{3.20}$$

where dA_s is the surface area of the differential element.
Replacing the transfer rate equations 3.18,3.19 and 3.20 into the energy balance 3.17, we obtain

$$\frac{d}{dx}\left(A_c \frac{dT}{dx}\right) - \frac{h}{k}\frac{dA_s}{dx}(T - T_\infty) = 0 \tag{3.21}$$

or

$$\frac{d^2T}{d^2x} + \left(\frac{1}{A_c}\frac{dA_c}{dx}\right)\frac{dT}{dx} - \left(\frac{1}{A_c}\frac{h}{k}\frac{dA_s}{dx}\right)(T - T_\infty) = 0 \tag{3.22}$$

For the rod, the cross-sectional area A_c is constant , $A_s = Px$ is the surface area measured from base to x, being P the rod perimeter. Therefore $\frac{dA_c}{dx} = 0$ and $\frac{dA_s}{dx} = P$. Equation 3.22 is reduced to

$$\frac{d^2T}{d^2x} - \left(\frac{hP}{kA_c}\right)(T - T_\infty) = 0 \tag{3.23}$$

To simplify the form of Equation 3.23, we transform the variable by defining $\theta(x)$ as the excess temperature

$$\theta(x) \equiv T(x) - T_\infty \tag{3.24}$$

Since T_∞ is a constant, $\frac{d\theta}{dx} = \frac{dT}{dx}$ Thus,

$$\frac{d^2\theta}{dx^2} - m^2\theta = 0 \tag{3.25}$$

where

$$m^2 \equiv \frac{hP}{kA_c} \tag{3.26}$$

Equation 3.25 is a linear, homogeneous, second-order differential equation with constant coefficients. Its general solution is

$$\theta(x) = C_1 e^{mx} + C_2 e^{-mx} \tag{3.27}$$

To determine the constants C_1 and C_2 it's necessary to specify the boundary conditions. One of such conditions may be specified as the temperature of the tip T_0

$$\theta(0) = T_0 - T_\infty = \theta_0 \tag{3.28}$$

substituting Equation 3.27 into Equation 3.28 we obtain

$$\theta_0 = C_1 + C_2 \tag{3.29}$$

The other condition corresponds to the assumption that the convective heat loss from the rod tip is negligible, in which case the tip may be treated as adiabatic

$$\left.\frac{d\theta}{dx}\right|_{x=L} = 0 \tag{3.30}$$

replacing in the derivative of Equation 3.27 and dividing by m we obtain

$$C_1 e^{mL} - C_2^{-mL} = 0 \tag{3.31}$$

Using Equation 3.29 with Equation 3.31 to solve for C_1 and C_2 and substituting into Equation 3.27 we obtain

$$\theta(x) = \frac{\theta_0}{e^{2mL}+1} e^{mx} + \frac{e^{2mL}\theta_0}{e^{2mL}+1} e^{-mx} \tag{3.32}$$

or

$$\frac{\theta(x)}{\theta_0} = \frac{e^{mx}}{e^{2mL}+1} + \frac{e^{2mL}e^{-mx}}{e^{2mL}+1} = \frac{e^{mx-mL}}{e^{mL}+e^{-mL}} + \frac{e^{mL-mx}}{e^{mL}+e^{-mL}} \tag{3.33}$$

where after multiplying both sides by e^{-mL} we can simplify with hyperbolic cosine functions

obtaining the temperature distribution $\frac{\theta(x)}{\theta_0}$

$$\frac{\theta(x)}{\theta_0} = \frac{cosh\ m(L-x)}{cosh\ mL} \tag{3.34}$$

which may also be expressed as

$$T = T_\infty + (T_0 - T_\infty)\frac{cosh\ m(L-x)}{cosh\ mL} \tag{3.35}$$

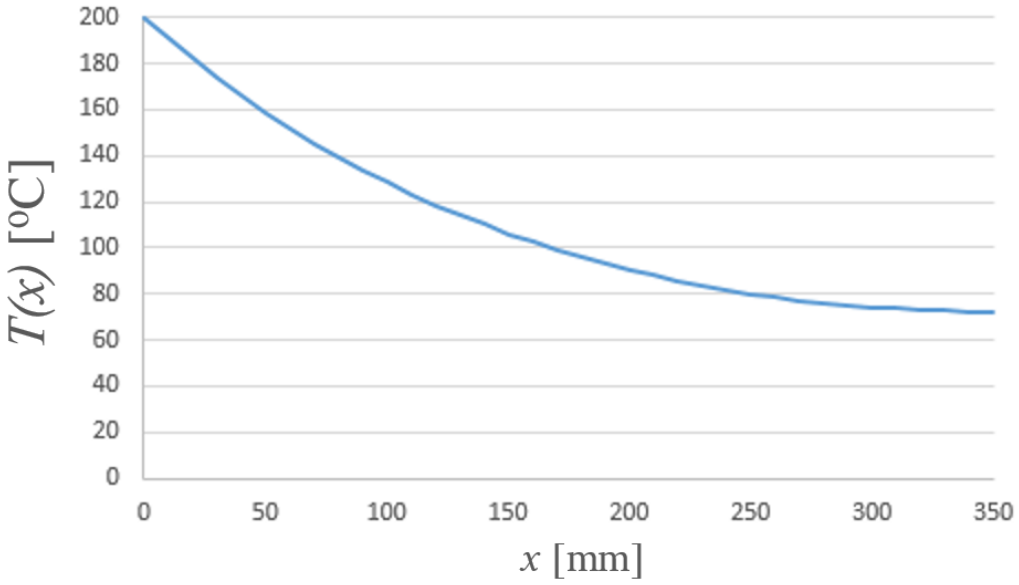

Figure 3.30: Temperature Distribution of Cylinder Extension

Figure 3.30 shows the temperature distribution of the Cylinder Extension with the tip staying within the operating temperature values.

In *SolidEdge Simulation* the Cylinder Extension is loaded with a temperature of 200 °C on its upper tip and natural convection heat transfer on its surface. The temperature on the lower tip, where it connects to the cylinder, as shown in the simulation (Figure 3.31), stays bellow the recommended value.

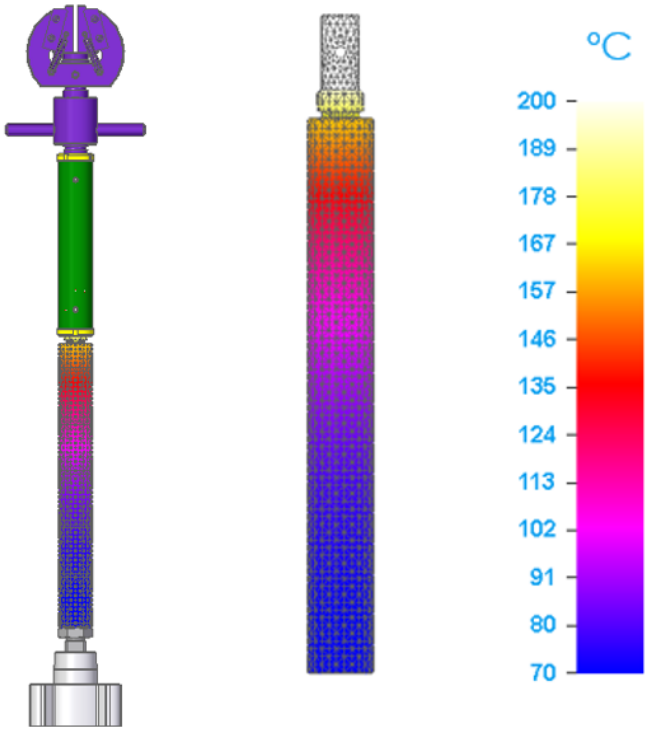

Figure 3.31: Thermal Simulation of Cylinder Extension

3.2.2 Spacer Sleeve

The idea of inserting the Spacer Sleeve [Drawing LA-01 in Appendix A.3] hoping to maintain the temperature of the cylinder within its operating range, was initially thought of as a sole component (Figure 3.32) [3]. However, the component was redesigned and became an assembly of two identical flanges [Drawing LA-012 in Appendix A.3] and a sleeve [Drawing LA-011 in Appendix A.3] through the use of disc type keys [Drawing LA-013 in Appendix A.3], thus simplifying the Spacer Sleeve manufacturing (Figure 3.33).

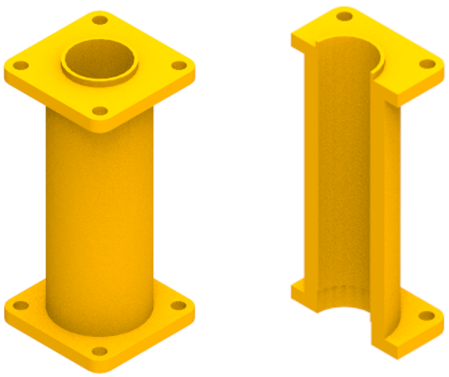

Figure 3.32: Original Spacer Sleeve

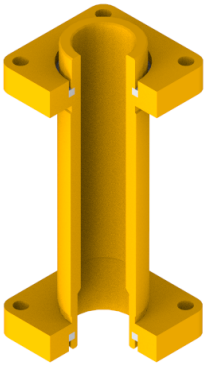

Figure 3.33: Improved Spacer Sleeve

The Spacer Sleeve is also responsible for aligning the cylinders with the Lower Beam and therefore with the machine. The cylinder alignment feature is assembled to the interior of the Spacer Sleeve and the Spacer Sleeve itself is assembled to the alignment bore of Lower Beam , as shown in Figure 3.34). By choosing an appropriate fit between the Spacer Sleeve components, its assembly on the cylinder and on the Lower Beam forces the keys to always be in tension conditions, eliminating any possible slack.

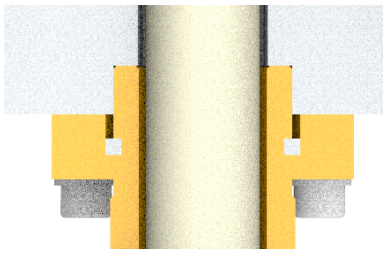

Figure 3.34: Spacer Sleeve assembly

3.2.3 Lower Coupling

The Lower Coupling [Drawing LA-03 in Appendix A.3] serves as the variable part of the extension (Figure 3.35). It was designed with two running fit pin connections, thus being easily replaced with an extension of different length.

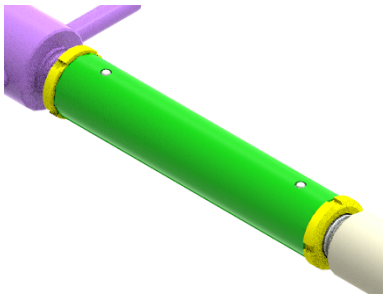

Figure 3.35: Lower Coupling assembly

The locknut has the purpose of eliminating the existing slack on the running fit pin connection of the grip assembly to the pull rods. We chose the *SKF* KM5 locknut. The thread of the Spindle and the Cylinder Extension was chosen according to the threads of the lock nuts available.

3.3 Upper Assembly

The Upper Assembly (Figure 3.36) of the machine contains the upper grip, the Upper Coupling between the Grip and the Load Cell, the Load Cell, and the Axial Spherical Plain Bearing with its necessary connections.

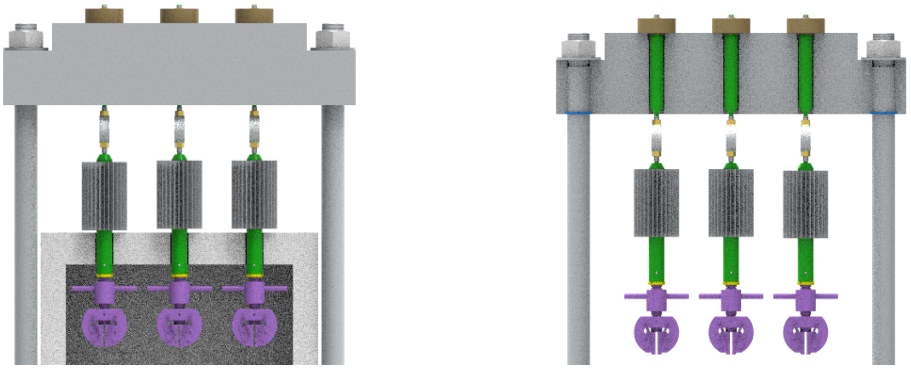

Figure 3.36: Upper Assembly

3.3.1 Upper Coupling

In the Upper Coupling (Figure 3.37), the maximum operating temperature of the load cell, which is 50 °C, must be respected.

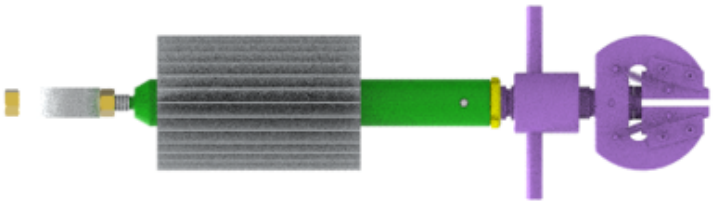

Figure 3.37: Upper Coupling

Repeating the analysis made to the Cylinder Extension [Section 3.2.1] we assumed a simplified form of a $\phi 35 \times$ 300 mm rod, steady-sate conditions, one-dimensional conduction along the Upper Coupling rod, constant properties, negligible radiation exchange with surroundings, uniform heat transfer coefficient, and an adiabatic tip. The lower tip of the component was considered to be at 200 °C and the surface of the rod, due to natural convection, was considered to have a coefficient of $h = 4.2\ W/m^2K$ [calculated through ASTM C680] and an ambient temperature of $T_{amb} = 20\,°C$. As the maximum operating temperature of the load cell was lower than that of the cylinder, the heat transfer due to natural convection on the Upper Coupling did not bring the temperature down to the operating temperature without compromising the length of the component and therefore the total height of the machine.

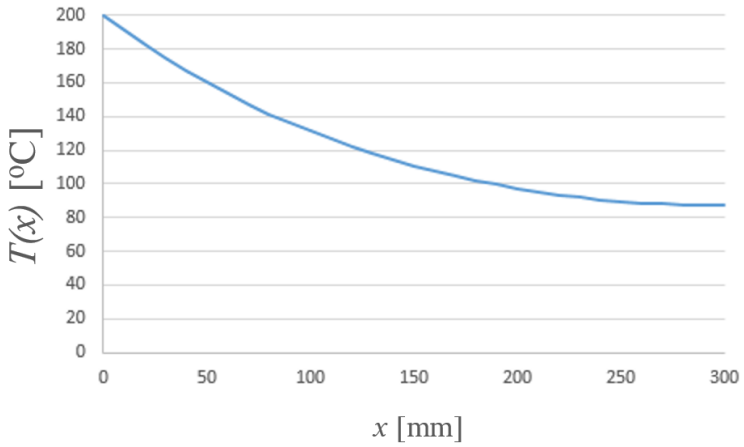

Figure 3.38: Temperature Distribution of Upper Coupling

Figure 3.38 shows the temperature distribution of the Upper Coupling with the tip staying outside the operating temperature values.

To fulfil the operating temperature requirement of the load cell, either forced convection or a heat sink should be used. The heat sink solution was the one adopted, which increases the convection area, increasing, in turn, the heat exchanged by convection. The surface area A_s of the rod measured from base to L was $A_s = PL = 32987$ mm^2

Figure 3.39: Heat Sink

We considered a heat sink, represented in Figure 3.39, with a length of 150 mm with 30 fins with a width of 25 mm. The area of convection, considering only convection on both sides of the fins, was $A_{s_{heatsink}} = 225000$ mm^2. The surface area of the heat sink was about seven times higher than the surface area of the Lower Coupling, increasing the heat exchange, and thus decreasing the temperature of the upper tip, as shown in the simulation (Figure 3.40).

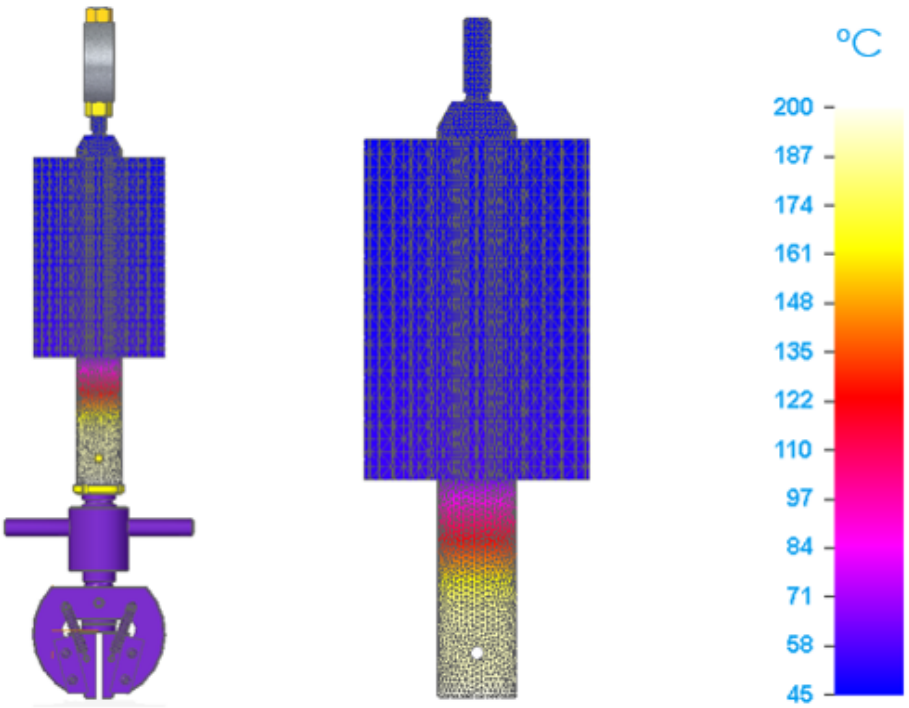

Figure 3.40: Thermal Simulation of Upper Coupling

3.3.2 Axial Spherical Plain Bearing

The alignment of the stations is crucial to perform a creep test. To ensure the alignment of the stations to prevent from inducing transversal loading to the load cell line of action, it's necessary to have an axial spherical plain bearing (Figure 3.41). Freire [3] had chosen the *INA* GE-12-AW Axial Spherical Plain Bearing due to it having a connection identical to the load cell and the necessary load capacity [19].

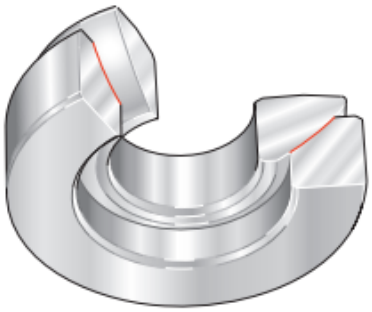

Figure 3.41: GE-12-AW Axial Spherical Plain Bearing [19]

Figure 3.42 shows the Spherical Bearing Flange supporting the Axial Spherical Bearing. It contains a ledge which is responsible for its alignment with the Upper Beam.

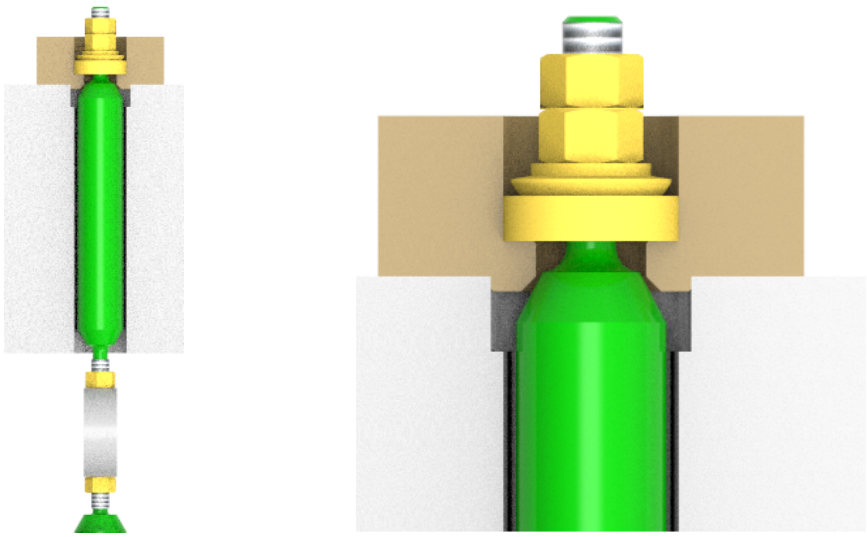

Figure 3.42: Axial Spherical Plain Bearing assembly

The upper grip, due to the load cell's connection to the Axial Spherical Plain Bearing, is articulated. If we had both grips locked in rotation, we could unintentionally induce torsional loading on the specimen. Having one of the grips articulated prevents unwanted loadings on the specimen. To prevent torsional loading in the setup, the articulated grip should be the first to be tightened, and then aligned with the other grips.

3.4 Mechanical Structure

The mechanical structure, shown in Figure 3.43, contains the Load Frame [Drawing MS-01 in Appendix A.4], which is subjected to the test conditions, and the Support Frame [Drawing MS-02 in Appendix A.4] which supports the whole machine.

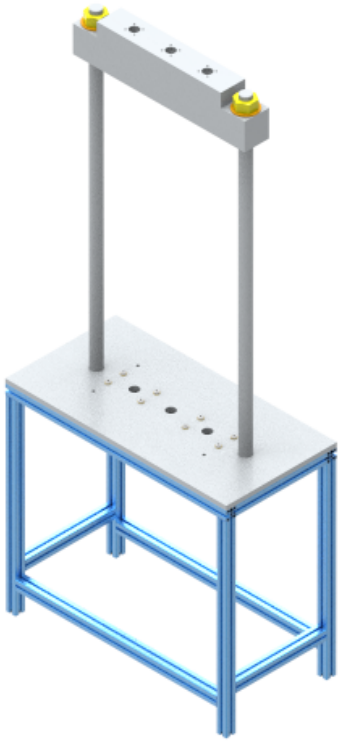

Figure 3.43: Mechanical Structure

3.4.1 Test Frame

Freire's mechanical structure [3] contained two Load Frame modules of three stations side by side with an asymmetrical design that allowed the observation of the six stations (Figure 3.44). When it was decided we should implement a Load Frame per chamber, the asymmetric design of the Upper and Lower Beams was no longer an interesting feature to include. The beams' design was also improved to allow for the direct assembly of the columns on the beams instead of using a spacer component, and therefore simplifying its manufacture (Figure 3.45).

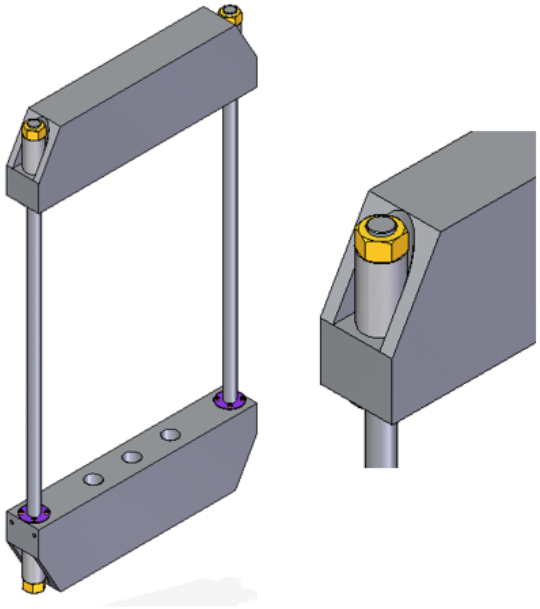

Figure 3.44: Original Load Frame

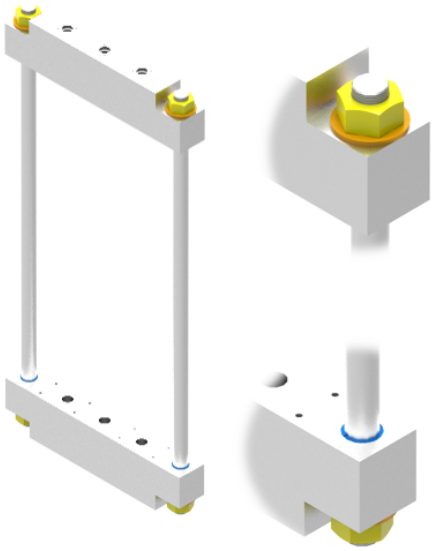

Figure 3.45: Improved Load Frame

The Upper Beam [Drawing MS-012 in Appendix A.4](Figure 3.46) is responsible for supporting the Upper Assembly intermediate the spherical bearing flange.

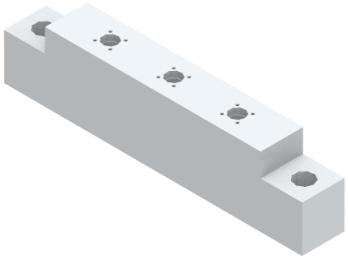

Figure 3.46: Upper Beam

The Lower Beam [Drawing MS-011 in Appendix A.4](Figure 3.47) is responsible for supporting the cylinders' intermediate Spacer Bushing and is the component that assembles the Mechanical Structure and all the components connected to the Support Frame [Drawing MS-00 in Appendix A.4].

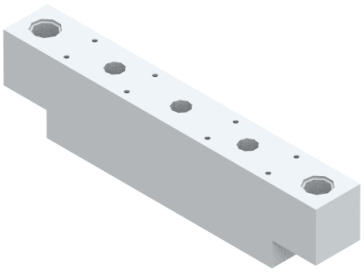

Figure 3.47: Lower Beam

The material of the beams, which was the AISI 1045 (Table 3.5), the same of the columns, was changed to a AL 7075 aluminium (Table 3.4).

Table 3.4: Properties of AL 7075 aluminium

Ultimate Tensile Strength, σ_r	$\geq$ 620 MPa
Yield Tensile Strength, σ_y	$\geq$ 340 MPa
Young's modulus, E	200 GPa

3.4.1.1 Columns

The Columns [Drawing MS-013 in Appendix A.4] connect the Lower Beam to the Upper Beam. Since these are the most susceptible components to buckling, they were under serious stress considerations.

Table 3.5: Properties of AISI 1045 steel

Ultimate Tensile Strength, σ_r	$\geq$ 620 MPa
Yield Tensile Strength, σ_y	$\geq$ 340 MPa
Young's modulus, E	200 GPa

Solving the diagram of forces acting on the structure, shown in Figure 3.48, we obtain $R_a = R_b = 3750$ N.

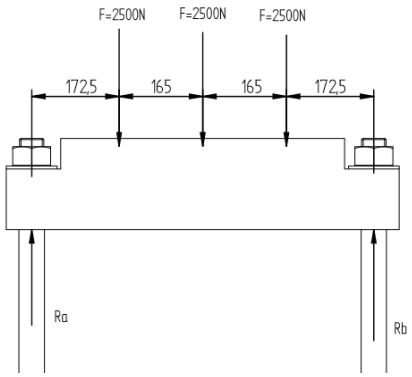

Figure 3.48: Scheme for determining the reactions on the columns (dimensions in mm)

The columns' initial diameter of ϕ 30 mm [3] was updated up to ϕ 50 mm to increase the structure's stiffness. The length of the column used in this calculation was the unsupported length L between the Lower Beam and the Upper Beam, which is 1250 mm. The columns were considered to be fixed in the Lower Beam joint and free in the Upper Beam, which is the worst case scenario, and the load was considered to be applied in its axis. The Column's effective length was $L_e = CL$ where C is the end condition length factor. For these buckling end conditions, as shown in Figure 3.49, the length factor $C = 2$, and therefore the effective length is $L_e = 2500$ mm.

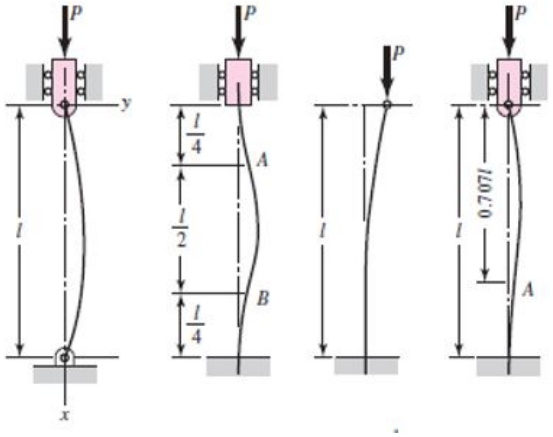

Figure 3.49: Buckling end conditions [20]

The critic load P_{cr} can be determined by Euler's formula

$$P_{cr} = \frac{\pi^2 E}{\lambda^2} \tag{3.36}$$

where the coefficient λ is the slenderness ratio. Determining the minimum area moment of inertia I of the cross section of the column

$$I = \frac{\pi \cdot r^4}{4} = 306796 \text{ mm}^4 \tag{3.37}$$

and the cross sectional area of the column

$$A = \pi \cdot r^2 = 1963,5 \text{ mm}^2 \tag{3.38}$$

we can obtain

$$i = \sqrt{\frac{I}{A}} = 12,5 \text{ mm} \tag{3.39}$$

and therefore the slenderness ratio λ

$$\lambda = \frac{L}{i} = 100 \tag{3.40}$$

the transition slenderness (Figure 3.50) λ_T ratio, such that $P_{cr}/A = \sigma_y/2$, is given by

$$\lambda_T = \sqrt{\frac{2\pi^2 E}{\sigma_y}} = 108 \tag{3.41}$$

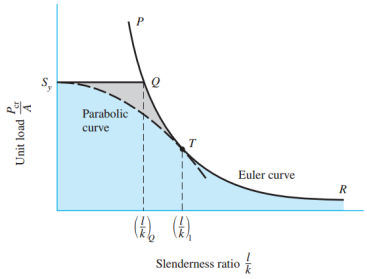

Figure 3.50: Critical tension vs. slenderness ratio [20]

As $\lambda \leq \lambda_T$, the critical load P_{cr} can be determined by Euler's formula (Equation 3.36), obtaining

$$\frac{P_{cr}}{A} = \frac{C \cdot \pi^2 \cdot E}{\lambda^2} = 51,82 \text{ MPa} \tag{3.42}$$

The effective load applied in each column is

$$\frac{P}{A} = 1,91 \text{ MPa} \tag{3.43}$$

and therefore the safety factor is given by

$$c_s = \frac{P_{cr}}{P} = 26 \tag{3.44}$$

It was not enough to ensure each column wouldn't undergo buckling when loaded individually. Taking advantage of the *SolidWorks Simulation* tools, and defining the right fixtures and loads to the Load Frame assembly, we obtained a safety factor of 20. As expected, the safety factor was slightly lower than the one determined for each column individually (Figure 3.51).

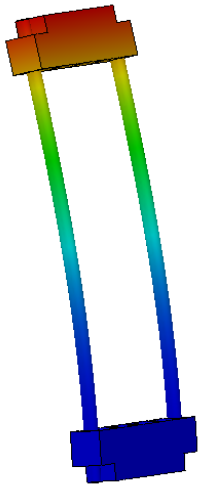

Figure 3.51: Buckling Simulation - first mode of failure

3.4.1.2 Keys

The assembly of the Columns to the upper and lower beams, as shown in Figure 3.52, is done through a disc type Key [Drawing MS-014 in Appendix A.4].

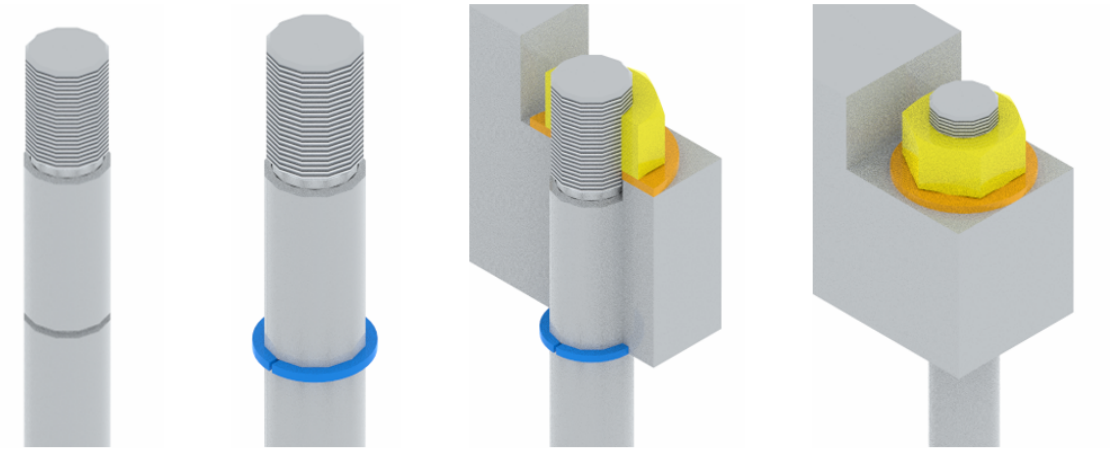

Figure 3.52: Assembly of the Columns on the Upper Beam

The connection was checked for shear stress and compression stress. The keys were made with AISI 1045 steel so we considered an admissible tensile stress $\sigma_w = 170$ MPa , and therefore an admissible shear stress $\tau_w = 100$ MPa

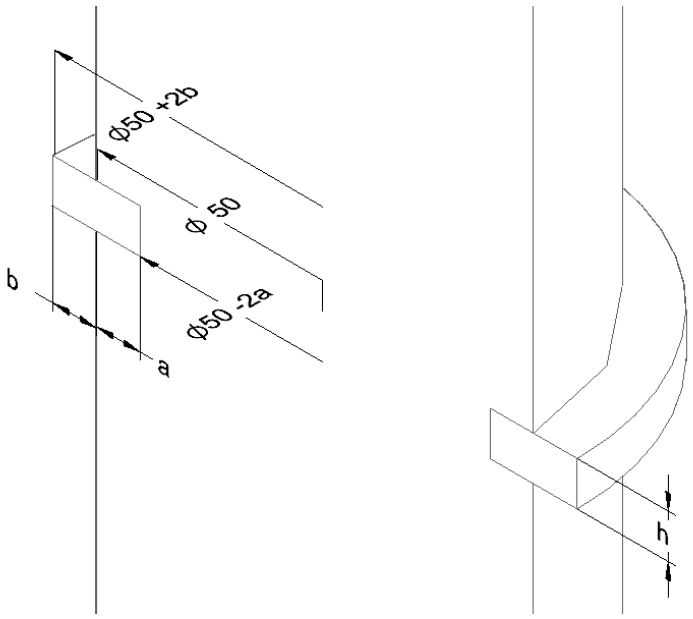

Figure 3.53: Key dimensioning scheme

The shear stress A_τ area is given by

$$A_\tau = \pi Dh = \pi \cdot 0,050 \cdot h \tag{3.45}$$

replacing (Figure 3.53) and assuming a worst case scenario in which the entire load of the three stations lies in one column

$$\frac{7500}{\pi \cdot 0,050 \cdot h} \leq \tau_w \tag{3.46}$$

we obtain the keys' minimum height

$$h \geq 0.478 \text{ mm} \tag{3.47}$$

For the compression component of the stress suffered by the keys we have

$$\sigma \leq \sigma_{adm} \tag{3.48}$$

$$A_{comp} = \frac{\pi}{4} \cdot (0,050^2 - (0,050 - 2a)^2) \tag{3.49}$$

$$\frac{7500}{\frac{\pi}{4} \cdot (0,050^2 - (0,050 - 2a)^2)} \leq 170 \tag{3.50}$$

obtaining a keyway depth of

$$a \geq 0.050 \, mm \tag{3.51}$$

obtaining the necessary dimensions for the key assembly on the Columns (Figure 3.54).

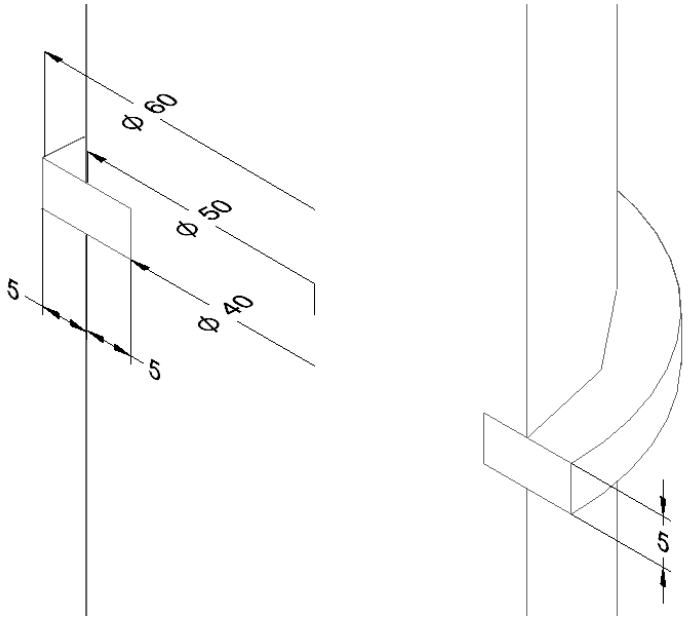

Figure 3.54: Key - dimensions in [mm]

3.4.2 Support Frame

The Support Frame (Figure 3.55) has to carry the weight of the mechanical structure. The test loads were internal to the Load Frame.

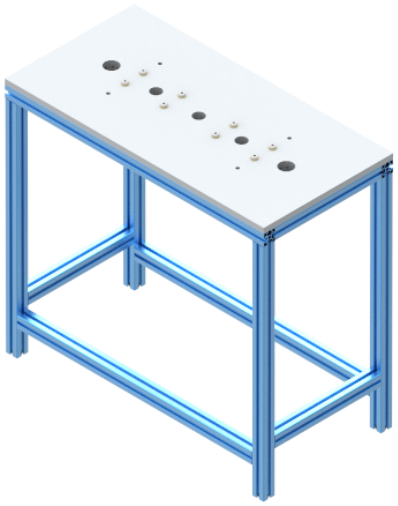

Figure 3.55: Support Frame

The Aluminium Board [Drawing MS-01 in Appendix A.4] is part of the load frame through assembly to the Lower Beam with eight M12 x 45 screws. The structure is attached to the bottom of the Aluminium Board instead of attaching its sides to the profile assembly as was designed by Freire [3]. The Aluminium Plate has, on its bottom, two L profiles bonded in the largest side, which fit and can be fastened against the Support Frame. To assemble the Support Frame, some of the profiles [Drawing MS-021,MS-022 in Appendix A.4] needed to be machined and connected as shown in Figure 3.56.

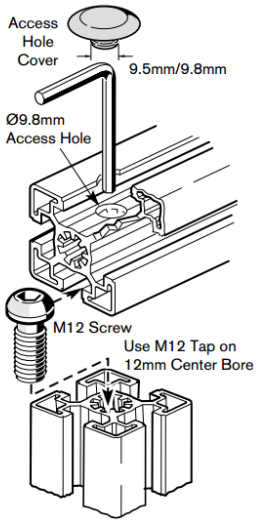

Figure 3.56: Profile Frame assembly

3.5 Displacement Analysis

Measuring the deformation of each specimen is the main focus of this machine, and those measurements should be acquired as near to the joint being tested as possible. Through the developed machine, we will be reading the displacement of each cylinder assuming that it will equal the deformation of each specimen. However, the elasticity of the structure and the mechanical chain will influence the measurement of the cylinder integrated displacement encoder. Using *Solidworks Simulation* to perform a static analysis with the work load of 2500 N applied on each of the three stations and the test frame fixed on the Lower Beam, we obtained a maximum resultant displacement of the Upper Beam of 0.036 mm (Figure 3.57).

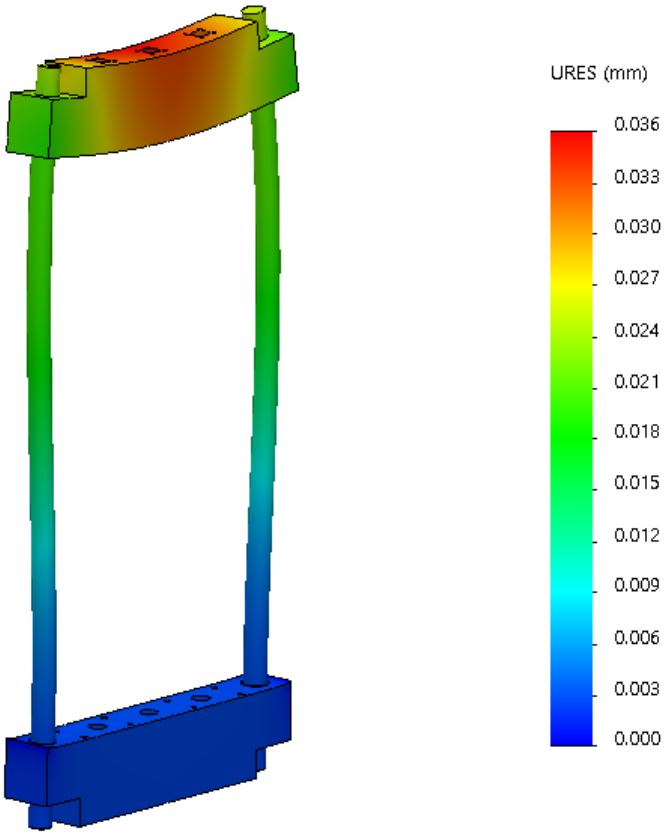

Figure 3.57: Resultant Displacement of the test frame

Also taking in consideration the deformation of the Cylinder Extension, the Upper Coupling and the Load Cell Extension, Hooke's law states

$$\sigma = E\varepsilon \Leftrightarrow \frac{F}{A_s} = E\frac{\triangle l}{l} \Leftrightarrow \triangle l = \frac{Fl}{AE} \tag{3.52}$$

where

- σ - tensile stress applied to the component

- E - Young's modulus of the component's material
- ε - strain of the component
- F - load applied to the component
- A_s - component cross sectional area
- l - component initial length
- $\triangle l$ - component displacement

Considering Young's modulus at 200 ^{o}C of AISI 304 stainless stell is E =182 GPa and adopting a simplified rod form for the components, the deformation of the Cylinder Extension is 0.0043 mm ,the deformation of the Upper Coupling is 0.0022 mm, and for the load cell extension the deformation estimated is 0.0025 mm. Adding together the deformation of the Test Frame and the deformation of the elastic chain, the total displacement inherent to the machine is 0.045 mm. We can, via software or result analysis neglect this deformation inherent to the machine to obtain a more reliable deformation of the specimen.

3.6 Conclusions

The mechanical project suffered various iterations according to the requirements of the AD-FEUP group and the FEUP workshop limitations, so although some of the components could not exist or be simplified in some other design, we had to take in consideration making every component possible and easy to manufacture in the FEUP workshop. As the material in rod form from the local supplier was already grounded, we tried adapting each component's dimensions to a rod dimension available through the supplier. Some of the components were modified or even replaced after ordering the material, and we then adapted their dimensions to the rod dimensions already ordered.

The body of the Grip and the Bushing should be a unique component. The fact that it had to be separated brought worries about the assembly. We choose the AISI 304 stainless steel because of its balance between thermal and mechanical properties. For some components of the grip, we could trade some of the thermals properties for an increase of the mechanical properties. The use of AISI P20, as it has a higher surface hardness comparing to the AISI 304 steel, would have better prevented galling of the components [21].

The operating temperature range of both the load cell and the cylinder was taken into account upon the design of the components, assuming only heat transfer by natural convection. The existence of heat transfer by radiation increases the temperature safety factor of the component. The Upper Coupling was left with enough space for a heat sink, and the heat sink itself was a representation of the ones available in the market. Some assembly adaptations may be needed, as well as the use of a thermal mass to optimize the heat transfer between the Upper Coupling rod and the heat sink.

The designed components were all manufactured by the FEUP workshop which reduced the cost of the mechanical parts to just the cost of acquisition of the material and normalized elements, which are detailed in the Table 3.6.

Table 3.6: Cost of acquisition of components and material

Component	**Cost without VAT**
Load Frame Columns	285 €
Load Frame Beams	516 €
Support Frame Plate	201 €
Support Frame Profiles	163 €
Steel and Aluminium	483 €
Normalized Components	350 €
Total	**1998 €**

Chapter 4

Climatic Chamber

A creep test aims to study the behaviour of a material when subjected to a constant temperature. To subject the specimens to the temperature conditions, the creep testing machine needs a climatic chamber whose project will be addressed in this chapter.

As the great majority of the commercial models (Figure 4.1) of machines able to perform creep tests have a single station, the commercial models of climatic chambers, that are usually from the same supplier as the universal test machines, are also designed for one station. The absence of a standard solution to a multi-station climatic chamber left us with the choice of either ordering a customized construction, which would be expensive and surpass this thesis' budget, or designing and assembling a chamber matching the ADFEUP specifications. It was decided that designing the climatic chamber was the best option, and to accomplish that, the chamber design, insulation and temperature control needed to be defined. The chamber dimensions are limited by the Load Frame dimensions [Chapter 3], which are, in turn, subjected to the workshop limitations in manufacturing parts, so both projects were developed simultaneously.

(a) *MTS* chamber [6]

(b) *CARBOLITE GERO* furnace [22]

Figure 4.1: Commercial Solutions

4.1 Design

Most commercial models feature a removable wedge port, which allows the chamber to be easily removed from the test area without the need for dismantling the gripping system (Figure 4.2) .

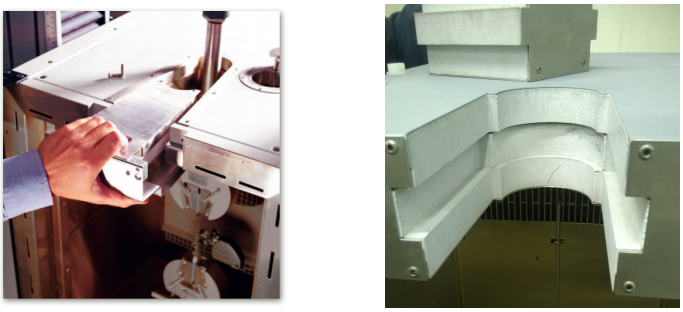

Figure 4.2: *INSTRON* wedge port feature [6]

Although the removable wedge port design is an interesting solution, when adapting it for three stations, the chamber would need either three removable wedge ports, which would compromise the structure, or a sole removable wedge port for all three stations (Figure 4.3).

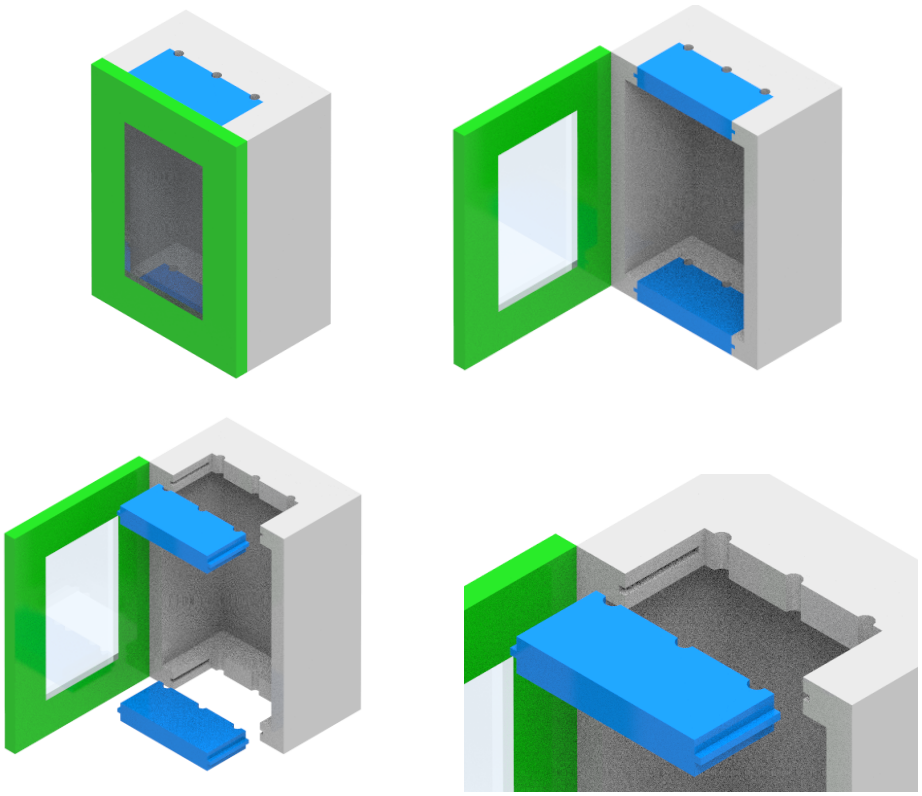

Figure 4.3: Wedge Port Solution

Figure 4.4 shows another possible solution, that is a vertically split design, vastly used in high temperature furnaces, which would split the chamber in two halves. With this design, the front half of the chamber can't be hinged with the other half, as the Test Frame columns would limit the opening of the chamber to less than 90^{o}. Each half of the chamber would have to move away from each other either with a track system, pivoting around each column, or a combination of both.

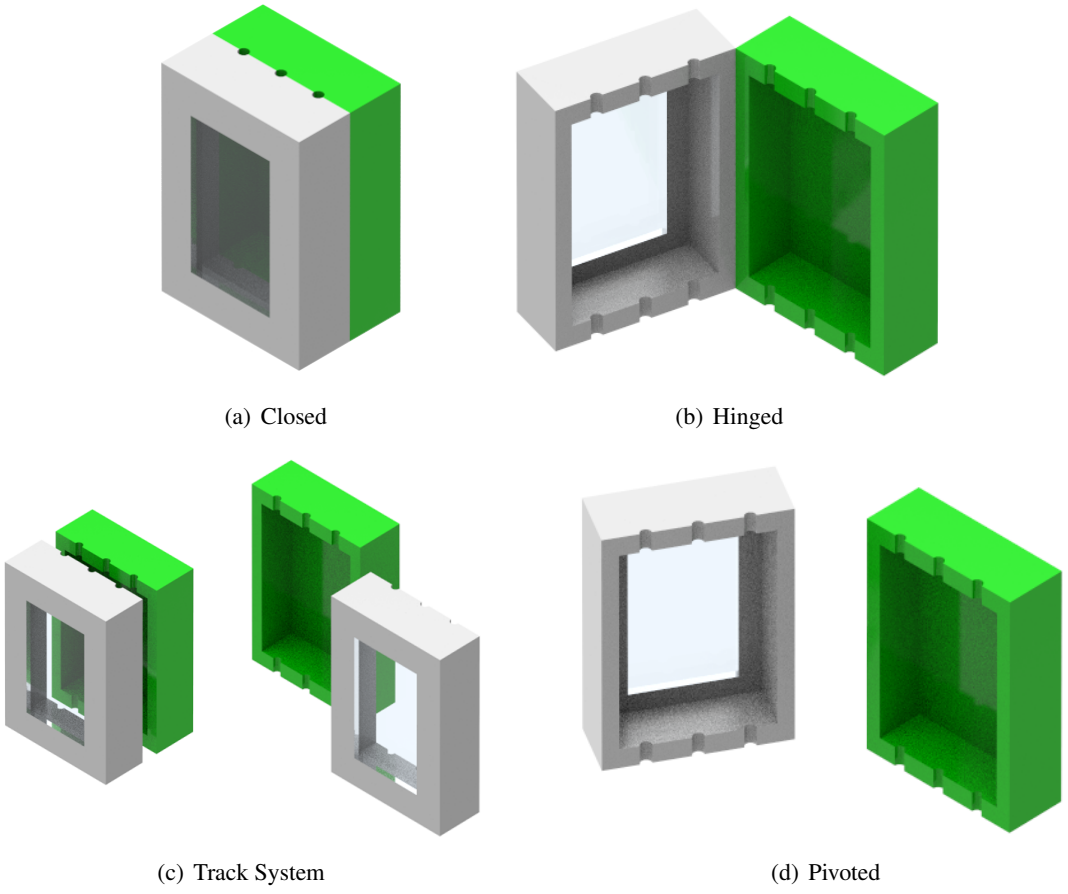

(a) Closed (b) Hinged

(c) Track System (d) Pivoted

Figure 4.4: Vertical Split Solution

The ADFEUP decided to adopt the vertically split design. The opening of the chamber should allow for a reasonable work space in order to have an easy setup of the specimens, so each half of the chamber will be attached and pivot around each one of the columns of the Load Frame (Figure 4.5). The support arms of the chamber will each contain a self lubricated bushing assembled in the columns, allowing for its rotation and therefore the pivoting of the chamber.

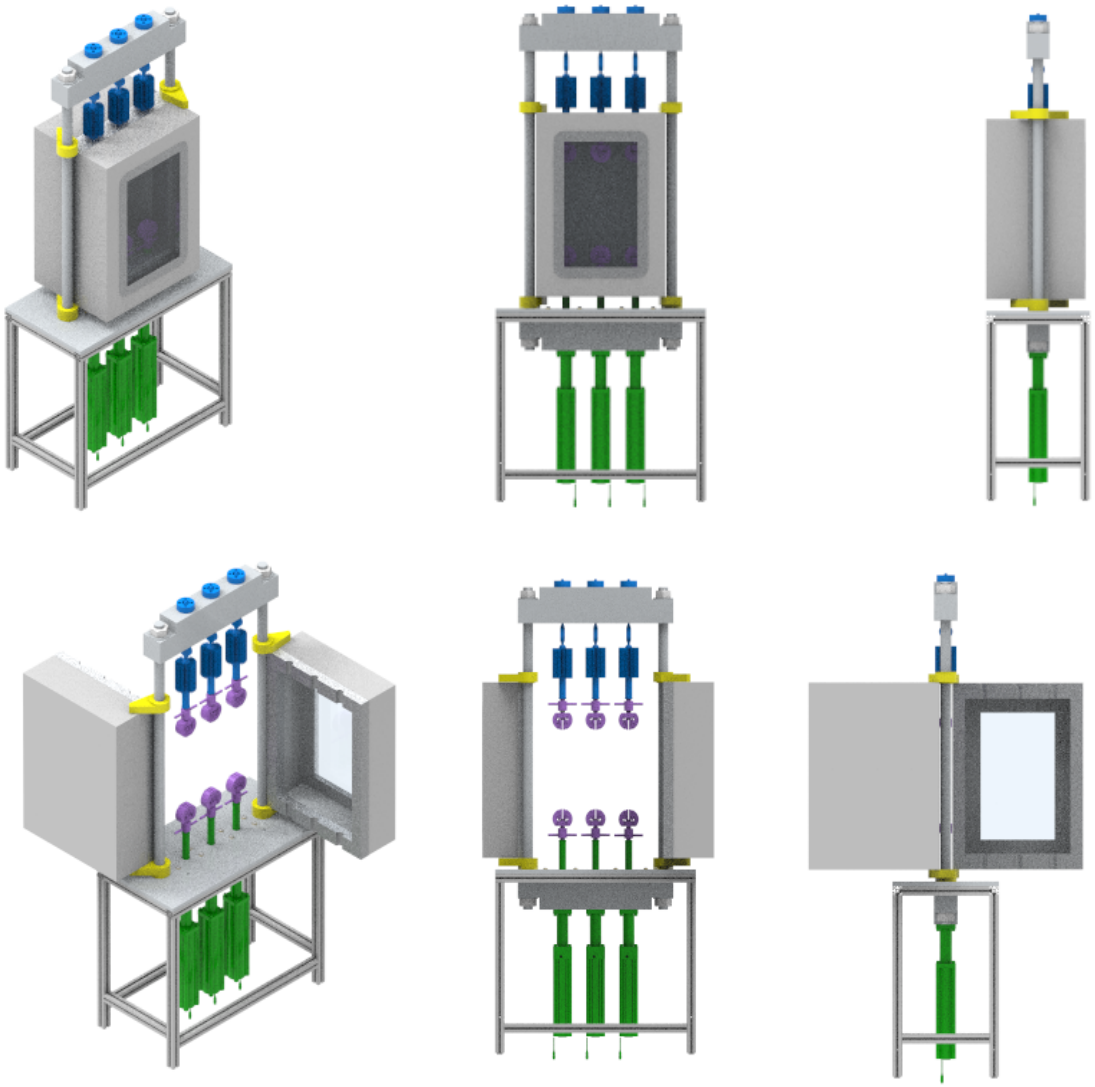

Figure 4.5: Vertically Split pivoting design

The rear half of the chamber, instead of pivoting, can be attached to a rail mount, which will allow it to roll out of the work space (Figure 4.6). As the heating, cooling and control elements will be attached to the rear half of the machine, it will be heavier than the front one.

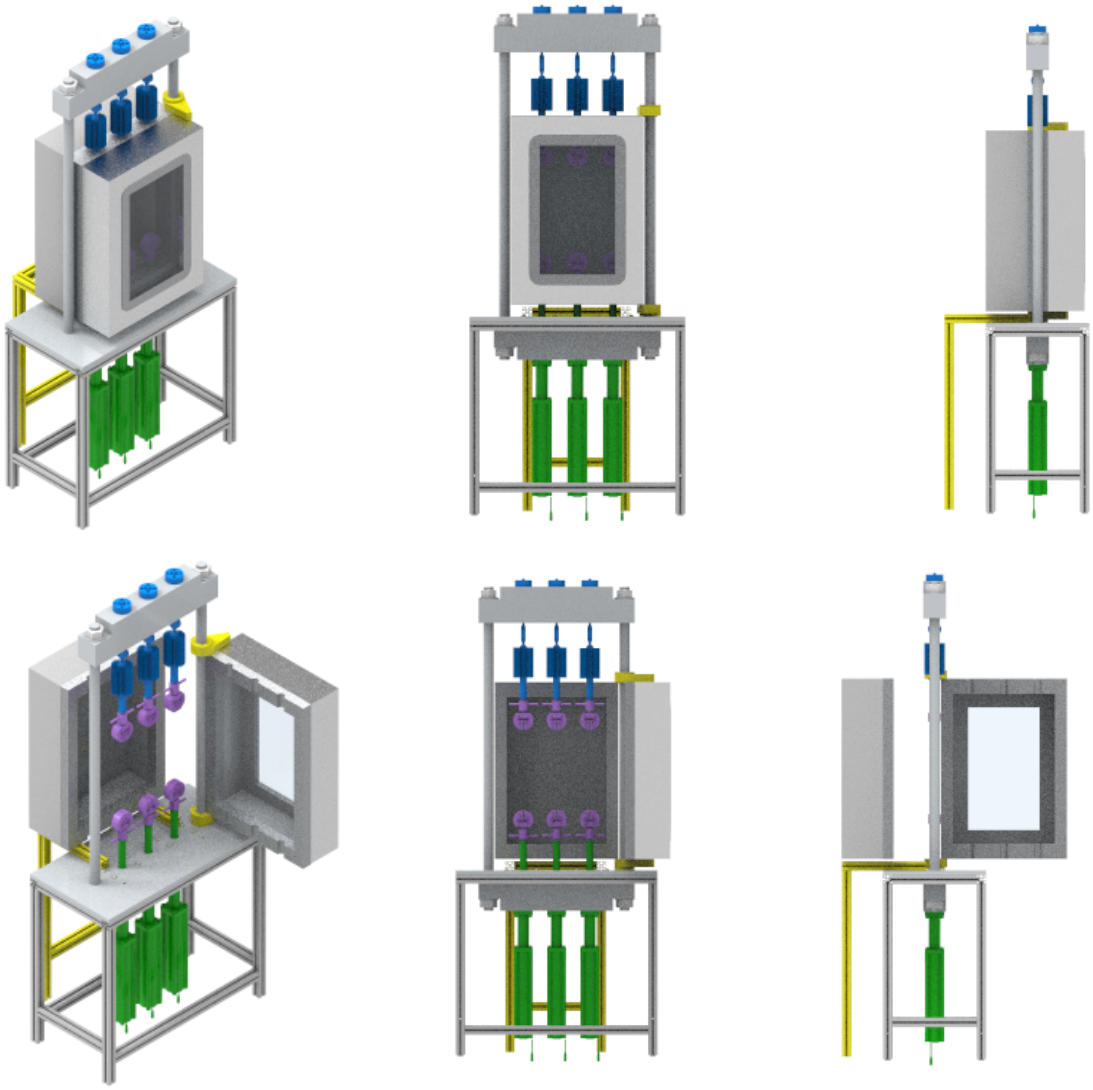

Figure 4.6: Vertically Split pivoting and roller mount design

To allow both options to be further implemented, enough space was left for both the rail mount and the pivoting support to be assembled.

Each half of the chamber has an internal case, an insulation layer, an external case and a partition frame, which will provide the partition surface, and will be assembled to both internal and external cases of each half of the chamber (Figure 4.7). The partition frame surface will have insulation strips creating a thermal labyrinth. To maintain the chamber closed, toggle latches will be used to compress each half of the chamber together, improving the thermal labyrinth created by the insulation strips. The rear half will contain the heating, cooling and temperature control elements, and the front half will contain the window opening to allow the visualization of the specimen during the test. The window opening should be layered, to improve insulation.

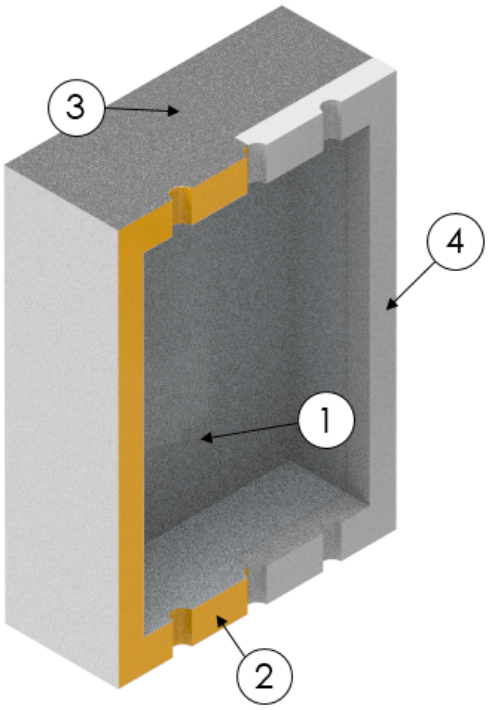

Figure 4.7: Half of the chamber layers
1 - internal case 2 - insulation layer 3 - external case 4 - partition frame

The manufacturing of the Lower and Upper Beam of the Test Frame in the local workshop brought a restriction of their maximum width and therefore a maximum space available between the two columns. As the chamber has to fit between the columns of the structure, the chamber's internal and external dimensions are a compromise between the ADFEUP specifications of the chamber's internal area and the wall thickness necessary for insulation (Figure 4.8).

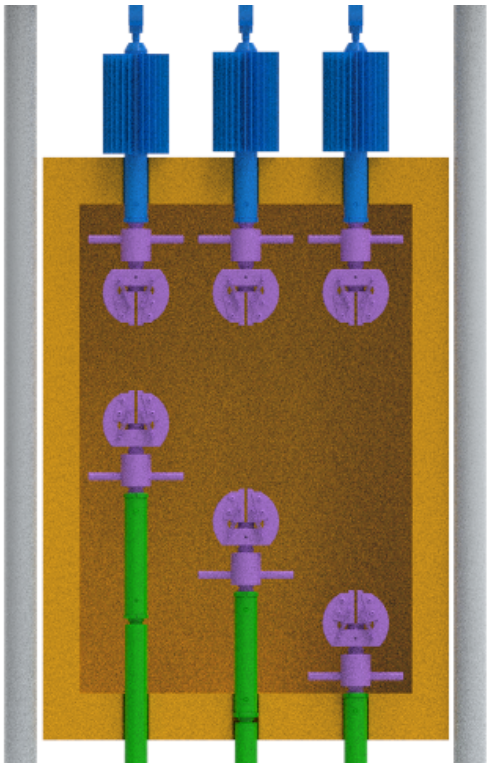

Figure 4.8: Representation of the chamber

The dimensions, after the manufacturing of the beams of the structure, are limited to

- 165 mm between stations
- 85 mm between the side stations and the inner wall of the chamber
- 735 mm of internal height
- 150 mm depth for each half of the chamber

This internal area leaves space for a 55 mm insulation layer in the chamber's sides. As the front, back, top and bottom of the chamber aren't compromised, their insulation thickness can increase. The internal area of the chamber, and therefore the remaining space for the insulation layer, was planned with knowledge of the dimensions and insulation material of commercial solutions with the same temperature range.

The upper and lower grips will occupy about 335 mm of the internal heigh leaving the chamber with a work height of 400 mm. As the cylinder has a work stroke of 300 mm, different Lower Couplings need to be used according to the specimen dimensions, allowing us to work in the full vertical range of the climatic chamber.

4.2 Insulation

As the inside of the climatic chamber will be at extreme conditions, choosing the right insulation method, material and thickness is essential. The creep test for the adhesive joints will occur at a constant temperature during long periods of time, so a climatic chamber with a high thermal inertia is advisable. The chamber needs an insulation material able to operate within a range of temperatures between -100 ^{o}C and +200 ^{o}C and with low conductivity in order to decrease the necessary thickness of the climatic chamber walls.

Most of the commercial models of climatic chambers, within the same temperature range as the one that is being designed, use rigid boards of Alkaline Earth Silicate (AES) fiber insulation wool. These insulation boards have a very low conductivity and the board shape provides self-support. *MORGAN ADVANCED MATERIALS* offers the *Superwool*, an AES fiber insulation material, which is used by most of the commercial models of climatic chambers, and has, as shown on Table 4.1, a low conductivity for the chamber's maximum operating temperature.

Table 4.1: Properties of Superwool insulation

Thermal Conductivity λ	
Temperature	200
$\lambda(W/m.^{o}C)$	0.05

The commercial models of climatic chambers operating in the same temperature range do not specify any type of insulation for negative temperatures, and the insulation materials are not fully tested in the temperature range required. We can assume that either it's not needed, or the insulation boards also insulate the negative temperature from the ambient temperature. This detail needs further investigation. There are however, solutions for negative temperature insulation. A cryogel blanket operates between -200 ^{o}C and +100 ^{o}C with very low conductivity coefficients (Table 4.2). The blanket does not support itself though, and as the chamber will work up to 200 ^{o}C, the cryogel foam would have to be included in a layered solution with ceramic fiber wool, preventing it from performing above its operating temperature range.

Table 4.2: Properties of Cryogel insulation

Thermal Conductivity λ				
Temperature	-100	-50	0	100
$\lambda(W/m.^{o}C)$	0.039	0.042	0.049	0.055

Some commercial models feature a supplementary fan and a gap between the insulation and the external wall to decrease, through forced convection, the external wall temperature. As the chamber is vertically split, we would need to create an air passage between each half, allowing for the air to circulate in both halves to implement such solution.

4.3 Heating, Cooling and Temperature Control

To enforce the temperature conditions inside the chamber certain components, which are capable of doing so, are necessary. The chamber will use a forced convection method to allow the hot or cold air to circulate around the specimen and the chamber, providing reduced thermal gradients and thermal stability. Forced convection provides a rapid heat transfer, and will be implemented by an electric motor driven fan. Heating is achieved by passing air over a heating element, and cooling is achieved by blowing cryogenic gas into the chamber.

As the chamber is using similar temperatures and volumes to those of a domestic oven, we can consider acquiring a 2000 W heating element from an oven replacement parts shop. A fan baffle, as shown in Figure 4.9, will shield the specimen from direct radiant heat from the heating element.

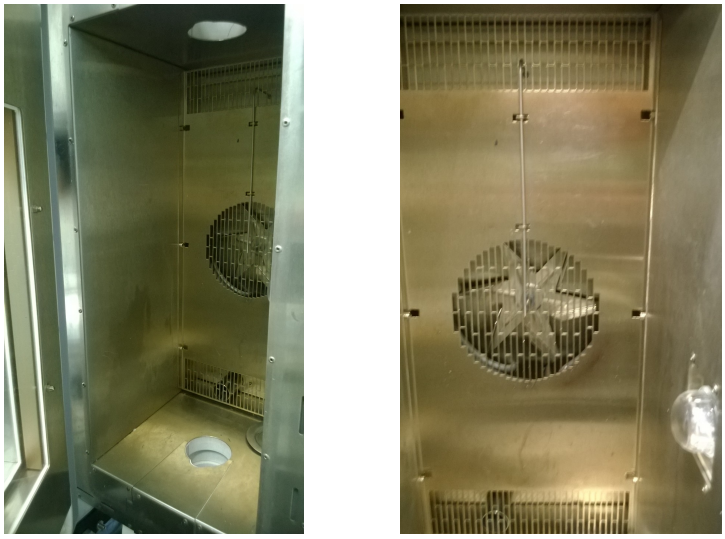

Figure 4.9: Interior view of INSTRON climatic chamber [6]

The cooling solution to the climatic chamber is based on nitrogen's properties. We will use pressurized nitrogen and inject it near the convector to homogenize the temperature in the chamber. To control the flux of nitrogen, the chamber needs a cryogenic valve to be able to withstand the negative temperatures. The chamber should also feature, as shown in Figure 4.9, an exhaust port for the waste nitrogen.

There are three basic types of temperature controllers that we could use in the chamber: an on-off controller, a proportional controller and a PID controller. The on-off controller is the simplest as its output is either *on* or *off* and will switch when the temperature crosses the setpoint. As the output only changes when the temperature crosses the setpoint, it will be cycling continuously. A proportional control aims to eliminate the cycling associated with on-off control. A proportional controller decreases its output value as the temperature approaches the setpoint, eliminating the overshooting. The third controller type provides proportional control with integral and derivative control, or PID, which automatically compensates for changes in the system.

4.4 Conclusions

The brief project of the climatic chamber aimed to acknowledge its assembly requirements and limitations. A vertical split design was chosen over a wedge port design

The insulation materials and techniques of the commercial solutions were analysed and discussed with specialized technicians of local available suppliers of insulation solutions. The use of a insulation material for negative temperature is advised, but as the commercial solutions don't specify any solution in consideration to the negative temperatures, it should be further studied.

The temperature control will be implemented by a PID controller, which is the only controller type that can maintain a stable temperature. The controller will be defined and ordered, as well as the temperature sensor. As we have a heating process and a cooling process, we will need two PID controllers for each process.

Chapter 5

Actuation and Instrumentation

Creep tests strive to enforce a constant load and obtain the resulting displacement. Relaxation tests, on the other hand, strive to enforce a displacement and acquire the load applied. To accomplish those conditions, the machine must have a loading system and a control circuit to maintain the load (when performing creep tests) or the displacement (when performing relaxation tests) constant. To acquire the measurements needed for the test, a displacement acquisition system and a load acquisition system are needed.

5.1 Overview

Freire's thesis [3] studied and defined the type of actuation system of the creep testing machine. Various aspects were analysed, among which the advantages and disadvantages of different solutions, namely an electromechanical solution; a mechanical solution; and a pneumatic solution. The electromechanical loading system was studied by Freire [3] as a solution to one station within the creep testing machine that would load the specimens up to 30 kN. This loading solution is the one used by most of the universal test machines. Although having found this option interesting, the ADFEUP group opted to give up the electromechanical station due to its cost and decided to adopt a creep test machine with only 2500 N stations. The mechanical solution, using a lever advantageous mechanism, would not only take up a lot of space, but it would also only be possible to load the specimen with a combination of calibrated weights. Freire [3] ended up choosing a pneumatic system because of its simplicity and reduced cost.

5.2 Loading System

According to the requirements of 2500 N load capacity and 300 mm (updated from 200 mm) of stroke, a FESTO servo pneumatic cylinder was chosen (Figure 5.1). The FESTO cylinder has an integrated displacement encoder, making it possible for us to acquire its piston rod relative displacement.

Figure 5.1: FESTO DDPC-Q-80-300-QA [23]

Although the cost of a pneumatic solution is reduced when compared to an electromechanical solution due to its lower load capacities, it was still the most expensive part of the designed creep test machine, so we tried to find some other alternatives to the FESTO solution.

These alternative solutions would need to have the same work length and load, and also have a displacement encoder. An AVENTICS [24] and a SMC [25] solution were considered, but they either didn't have the necessary load capacity or didn't respect the measurements requirements.

Table 5.1: DDPC cylinder technical data [23]

Piston	ϕ 80 mm
Stroke	300 mm
Operating pressure	4 bar ...12 bar
Pneumatic Port	G3/8
Ambient temperature	-20 °C ...+80 °C
Theoretical force at 6 bar, retracting	2721 N

The *FESTO* DDPC cylinder can operate between 4 bar and 12 bar and within a range of temperature from -20 °C to + 80 °C (Table 5.1), which was a requisite analysed in the Cylinder Extension project. It also has a square piston rod for protection against rotation, which will prevent the rotation of the lower grip.

5.2.1 Control Circuit

To control the pneumatic loading system the pneumatic circuit must have a pressure regulator valve to control the pressure in the cylinder's working chamber, and therefore the load applied by it on the specimen. The *FESTO* VPPX-8L-8-1-G14-0L10H-S1 is a 3-way proportional pressure

Table 5.2: VPPX technical data [26]

Pressure regulation range	0.1...10 bar
Supply pressure (port 1)	0...11 bar
FS linearity error	$\pm$ 0.5 %
FS repetition Accuracy	0.5 %
Setpoint input signal	0...10 V
Pneumatic ports	G 1/8
Operating voltage	24 V

regulator valve with piloted diaphragm design and a pressure regulation range from 0.1 bar to 10 bar (Table 5.2).

The VPPX proportional pressure regulator valve (Figure 5.2) (which will be referred to from now on as [VPPX]) has a closed-loop control system. It includes a comparator that receives both the reference variable (w) defined by the user via software and the feedback of the controlled variable (r). During a creep test, we want to control the load applied, so the reference variable (w) is the test load chosen by the user, and the controlled variable (r) is the measured signal of the load cell. The control element detects the system deviation (e), and attempts to compensate for the difference between the reference variable (w) and the controlled variable (r). The process runs continuously so the system always detect changes either on the reference variable (w) or on the controlled variable (r). These deviations will happen when the flow through the valve changes due to specimen deformation and consequential cylinder movement [26].

Figure 5.2: VPPX [26]

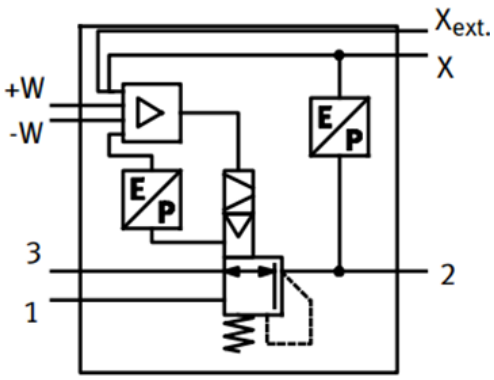

Figure 5.3: VPPX scheme [26]

The VPPX is designed to control pressure or an external value proportionately to a specified setpoint value. If the valve is operated in the internal control mode, the integrated pressure sensor measures the pressure at the working port and compares it to the setpoint value (Figure 5.3). If there is a deviation between the setpoint value and the actual value, the valve regulates it until the setpoint value is reached at the output. In the external control mode, the additional external sensor measures the value and feedbacks it to the proportional valve. This value is compared to the setpoint one. If there is a deviation between the setpoint value and actual value, the valve regulates

the output pressure until the value of the external sensor reaches the setpoint value (Figure5.4) [26]. As we want to force the external value to equal the setpoint, we will use the external control mode.

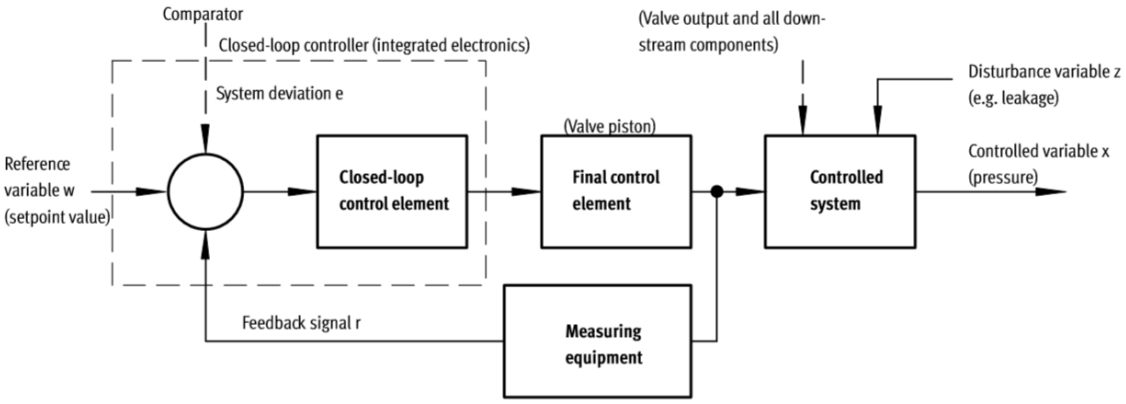

Figure 5.4: Control Circuit of VPPX [26]

For each VPPX, pin 2 and pin 7 is used for the power supply, pin 4 is the setpoint value and pin 8 the feedback signal of the load cell. The setpoint signal is applied to contacts 3 and 4, where the lower potential must be connected to contact 3 and the higher potential to contact 4. Contact 3 (– setpoint value) can and will be connected to contact 7 (GND) (Table 5.3).

Table 5.3: VPPX pin arrangement [26]

Pin	Terminal	Channel in the DAQ
1	Digital communication (do not connect!)	–
2	+24 V DC power supply	–
3	Analogue input W- (- setpoint value)	–
4	Analogue input W+ (+ setpoint value)	Analogue Output
5	Digital communication (do not connect!)	–
6	Analogue output X (actual value)	–
7	0 V DC or GND	–
8	Analogue input Xext (external actual value)	Analogue Output

As the 10 V of the feedback signal of load cell represents its maximum load capacity of 3000 N and the pressure regulation range of the VPPX is between 0.1 bar and 10 bar corresponding to 1 % and 100 % of the setpoint signal, the analogue reference *Setpoint* of a load F to send to the VPPX is

$$S = \frac{F}{3000 - 30} \cdot (10 - 0.1)\text{V} \tag{5.1}$$

5.2.2 Pneumatic Circuit

The pneumatic circuit was built keeping in mind both the normal and abnormal situations that might occur during the functioning of the machine. It includes a filter regulator unit and three cylinders, each counting with a proportional pressure regulator valve, a directional valve, two flow control valves and two proximity sensors. On the pneumatic circuit scheme, shown in Figure 5.5, we only see one of the stations represented, since the other two have identical circuits in parallel after the filter regulator unit, which is common to the three cylinders.

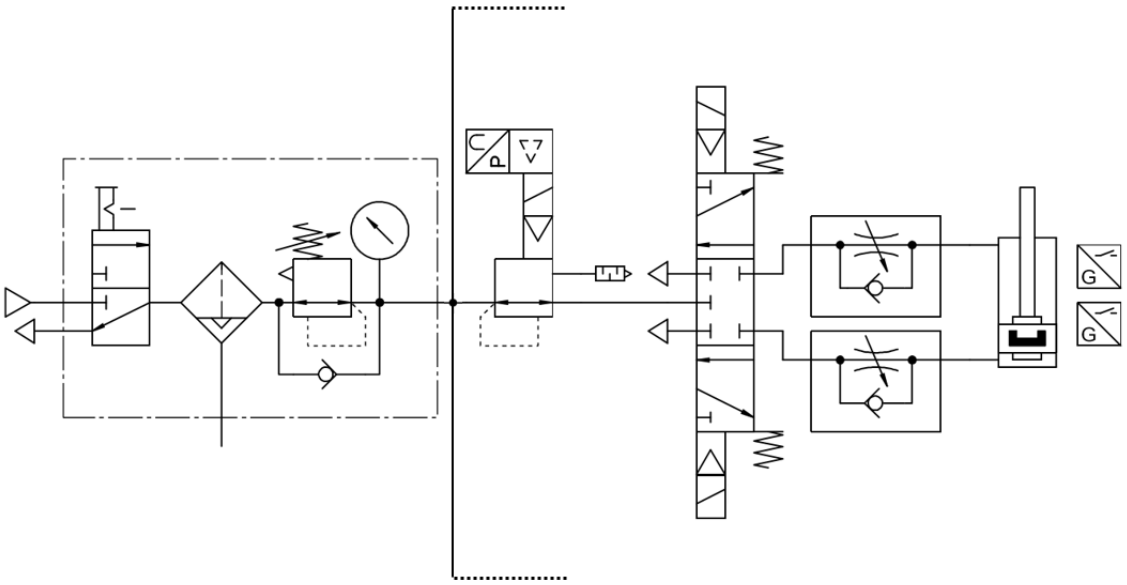

Figure 5.5: Pneumatic Circuit

5.2.2.1 Filter Regulator Unit

The FESTO MSB4-1/4:C3J3-WP filter regulator unit (Figure 5.6) chosen includes an on-off valve manually actuated with a silencer, and the filter regulator. The filter has a pressure regulation range between 0.5 bar and 12 bar, a grade of filtration of 5 μm (which is recommended for the good functioning of the cylinders), a plastic bowl guard, a manual condensate drain, an integrated pressure gauge and a rotary knob [27].

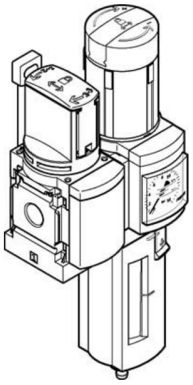

Figure 5.6: Filter Regulator Unit [26]

5.2.2.2 Directional Valve

Freire [3] suggested the use of a directional valve 5/2 normally exhausted. With this kind of valve, the specimen setup would be done by manually moving the rod from the cylinder. However, after testing the suggested procedure, we reached the conclusion that it would be better to have the positioning of the cylinders built-in the pneumatic circuit. To achieve that, we changed the directional valve to a solenoid-actuated 5/2 normally closed directional valve (Figure 5.7) with mechanical spring return whose solenoids can be activated via Command Panel or via Graphical User Interface.

Figure 5.7: VUVS Directional Valve [26]

5.2.2.3 Flow Control Valve

The one-way flow control valve (Figure 5.8) in each chamber controls the flow of the exhaust air. The meter-out design helps reduce the stick slip, improving the motion of the piston and allowing the user to position the cylinder via pneumatic circuit [28]. The flow control valve on the cylinder's main chamber also serves to reduce the impact force of the piston when specimen rupture occurs. Speed adjustment is done through exhaust air flow control.

Figure 5.8: Flow Control Valve [28]

5.2.2.4 Travel Limit Switch

The circuit has two FESTO SMT magneto-resistive proximity sensors (Figure 5.9) for each cylinder with a normally open contact that switches when it senses the piston rod. The proximity sensors will be part of the command and control circuit of the machine. The operating voltage of the proximity sensors is 24 V.

Figure 5.9: SMT Proximity Sensor [29]

5.3 Displacement Acquisition System

The FESTO cylinder chosen has an integrated relative displacement encoder that allows us to obtain the relative position of the cylinder. Via software, we will compare the values of displacement along the test with the one before the test started.

Table 5.4: DADE converter technical data [23]

Output Signal	Analogue 0 - 10 V
Linearity error	$<\pm$ 0.08 mm
Resolution	$\leq \pm$ 0.025 %
Repetition Accuracy	$<\pm$ 0.1 mm
Operating Voltage	24 V

As the maximum stroke is 300 mm, the minimum resolution should be of 0.075 mm (Table 5.4). The displacement encoder (Figure 5.10) uses both limits of the analogue signal for

troubleshooting, so the effective analogue output of the DADE measured value converter is between 0.1 V and 9.9 V. The relative displacement x [mm], within the work stroke of 300 mm, for a measured voltage U [V] is given by

$$x = \frac{9.9 - U}{9.9 - 0.1} \times 300 \tag{5.2}$$

Figure 5.10: DADE converter [23]

Table 5.5: DADE pin arrangement

Pin	Terminal	Channel in the DAQ
1	+24 V power supply	–
2	Measured signal (analogue)	Analogue Output
3	Reference output	Digital Input
4	0 V measured signal	Analogue GND
5	Reference input	Digital Output
6	Calibration input	Digital Output
7	Ready output	Digital Input
8	0V DC or GND	–

5.4 Load Acquisition System

To measure the load applied on the specimen we need a load cell and an amplifier. Freire [3] suggested using an S-Beam type load cell due to its low cost when compared to other solutions within the desired characteristics. We tried to look for something other than the S-beam type of load cell because of the possible advantages it could bring in terms of structure assembly. The excessive cost of all the other solutions though, had us ending up following Freire's recommendation [3]. The suggested load cell from Freire [3] was from *Tedea Huntleigh* and an Signal Conditioning Module by *Honeywell* but due to problems with acquisition we opted for a cheaper solution We analysed some other options in the market and chose a pack of a load cell (Figure 5.11) and an

amplifier (Figure 5.12) of the same supplier with the lowest cost within the necessary characteristics. For the load measurement (Table 5.6) (Table 5.7) we will use a pack from *AEP Transducers*. The measured signal of the load cell is our reference of control to maintain the load applied to the specimen constant.

Figure 5.11: TS Load Cell [30]

Figure 5.12: TA 4/2 Transmitter [31]

Table 5.6: Load Cell and Transmitter technical data [30] [31]

Nominal Load	3000 N
Linearity error	<± 0.08 mm
Resolution	≤ ± 0.025 %
Repetition Accuracy	<± 0.1 mm
Operating Voltage	24 V DC

Table 5.7: TS Load Cell and Transmitter pin arrangement

Pin	Terminal	Channel in the DAQ
1	+24 V power supply	–
2	0 V power supply	–
3	Vout	Analogue Input
4	mAout	–

5.5 Data Acquisition System

The DAQ system is the interface between the computer and the machine. Its primary function is to digitize the incoming analogue signals so that the computer can interpret them. It also has analogue inputs, analogue outputs and digital I/O, and the hardware is responsible for converting the signals of and to the machine. The DAQ system was defined through studying of the necessary analogue inputs, analogue outputs and digital I/O. For the DAQ dimension we considered the necessary connections for each station to the load cell and its transmitter, the cylinder and its

transducer, the pressure regulator proportional valve, the proximity sensors, the directional valves and some signals necessary for the machine operation (Table 5.8).

Table 5.8: Channels necessary of the DAQ system

	AO	**AI**	**DO**	**DI**
VPPX	6	–	–	–
DDPC + DADE	–	3	3	3
Load Cell + Transmitter	–	3	–	–
VULV	–	–	6	–
SMT	–	–	–	3
Others	–	–	1	2
Total	6	6	7	8

As the ADFEUP group expects to assemble a second module in the future, acquiring a DAQ board capable of controlling the two modules was an option under consideration. However, such combination of channels would require a board with excessive connections available which would be both unnecessary and expensive at this point in time. The analogue inputs and analogue outputs are the expensive features of the DAQ boards, so instead of an overload board, a combination of boards with the necessary analogue outputs and analogue inputs for the two machines, but with digital I/0 necessary for one module only was acquired. Upon the assembly of the second machine, a board with enough digital I/0 will be needed.

The boards acquired were the NI-PCI-6010 (Figure 5.13) and the NI-PCI-6703 (Figure 5.14) from *National Instruments*. who also offers the graphical user interface design software *LabView*, used in this thesis.

Figure 5.13: NI-PCI-6010 board

Figure 5.14: NI-PCI-6703 board

As the NI-PCI-6010 board has a measuring range between -5 V and +5 V and the signals it will be acquiring are between 0 V and 10 V, an input offset voltage amplifier is needed to transform the analogue signal of 0-10 V coming from the load cell and DADE into a signal between -5 V and +5 V.

Another option would be to use a voltage divisor to convert the 0-10 V analogue signal into a 0-5 V analogue signal. This however would reduce the resolution in half. The resolution of a 16 bit acquisition board, for a analogue signal between 0 and 10 V, corresponding to a stroke between 0 and 300 mm is given by

$$\frac{300}{2^{16}} = 0.00458 \text{ mm} \tag{5.3}$$

As half of the resolution of the DAQ system would still be greater than the available resolution from the displacement encoder, both measuring range adapting options can be implemented without altering the measurement characteristics.

5.6 Conclusions

The actuation and instrumentation components have taken a big part of the available budget. The actuation system with displacement encoder by *FESTO* was the only reliable option of those analysed, making it mandatory. The load cell was chosen due to being the cheapest solution within the requisites defined. We could obtain an easier assembly and even remove the necessity of having an Axial Spherical Bearing by having a load cell other than the S-beam type. However, that would increase its cost of acquisition.

Instead of the NI-PCI-6010 board, the NI-PCI-6013 one, which has a measuring range from -10 V to +10 V, could have been ordered, negating the need for the offset amplifier or the tension divisor. However, that solution would have presented a greater cost of acquisition.

Table 5.9 details the cost of the instrumentation components, and were, as expected, the most expensive part of the machine. We sought for alternatives for the cylinders with a displacement encoder, load cell and DAQ system, but the ones chosen were either the only viable option or the cheaper option within the requirements or desired characteristics. Some of the pneumatic accessories were not purchased during this thesis, so an estimated price was considered for the "pneumatic circuit" parcel.

Table 5.9: Cost of acquisition of actuation and instrumentation components

Component	**Cost without VAT**
DDPC cylinders	1799 €
VPPX	1450 €
DADE converters	540 €
Pneumatic circuit	$\leq$ 500 €
Load Cell and Transmitter	945 €
DAQ system	2215 €
Total	**7449 €**

Chapter 6

Command and Control

To ensure the machine works properly, it's necessary to create and implement a command logic and control system which will put the machine through a logic sequence of well defined stages and transitions. Most of the transitions between the stages include user interference, so the user will have available a command panel and a graphical user interface (GUI), created using *LABView*, which will have different action windows in the machine's normal functioning. This command and control system also includes the electric switchboard, which will power the actuation and instrumentation components and implement the command and control logic.

6.1 State Diagram

The creep testing machine operates between five macro states as shown in Figure 6.1.
The *Initialization* routine is a referencing routine that occurs every time that the machine is powered on, after leaving an emergency state or by user choice in the graphical user interface.
The *Manual* state is the state where the user is allowed to control the pneumatic circuit via command panel, positioning the cylinder piston and therefore the lower grips. *PC* is a state where the user can either start the initialization routine, change to manual mode or setup the conditions of the next test. The *Test* state includes the command and control of the pneumatic and electrical circuit to apply the test conditions and acquire the desired measurements.

As the cylinder has a relative displacement encoder, the DADE must run a *Calibration* routine in its first commissioning to acknowledge the stroke in which the cylinder will work.

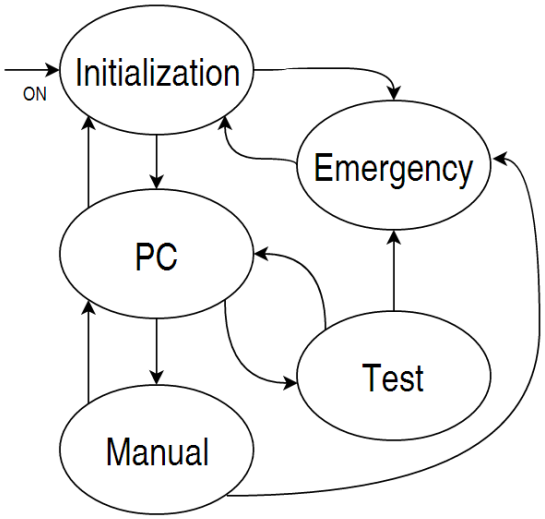

Figure 6.1: Creep Test Machine State Diagram

6.1.1 Calibration

The *Calibration* routine of the DADE must force the cylinder piston to both ends of the work stroke (Figure 6.2). The VPPX Setpoint is set to 10V and the VPPX External Value is set to 0V to allow maximum air flow to the Cylinders. The Directional Valve's solenoid is activated to allow the air to flow to the primary chamber of the cylinder, beginning an ascending movement. When the cylinder reaches its upper position and the Upper Limit Proximity Sensor emits a signal, we activate DADE Reference Input during 0.5 s. The DADE Reference Output switches on when the Cylinder saves the referencing point. Then, the Directional Valves switch the orientation of the cylinder's movement and when the Lower Limit Proximity Sensor emits a signal, the DADE Calibration Input is activated during 0.5 s. When the DADE acknowledge its position and ends the calibration, a signal appears on DADE Ready Output. The Directional Valves return to its normal position and the VPPX are turned off to prevent movement of the piston rod.

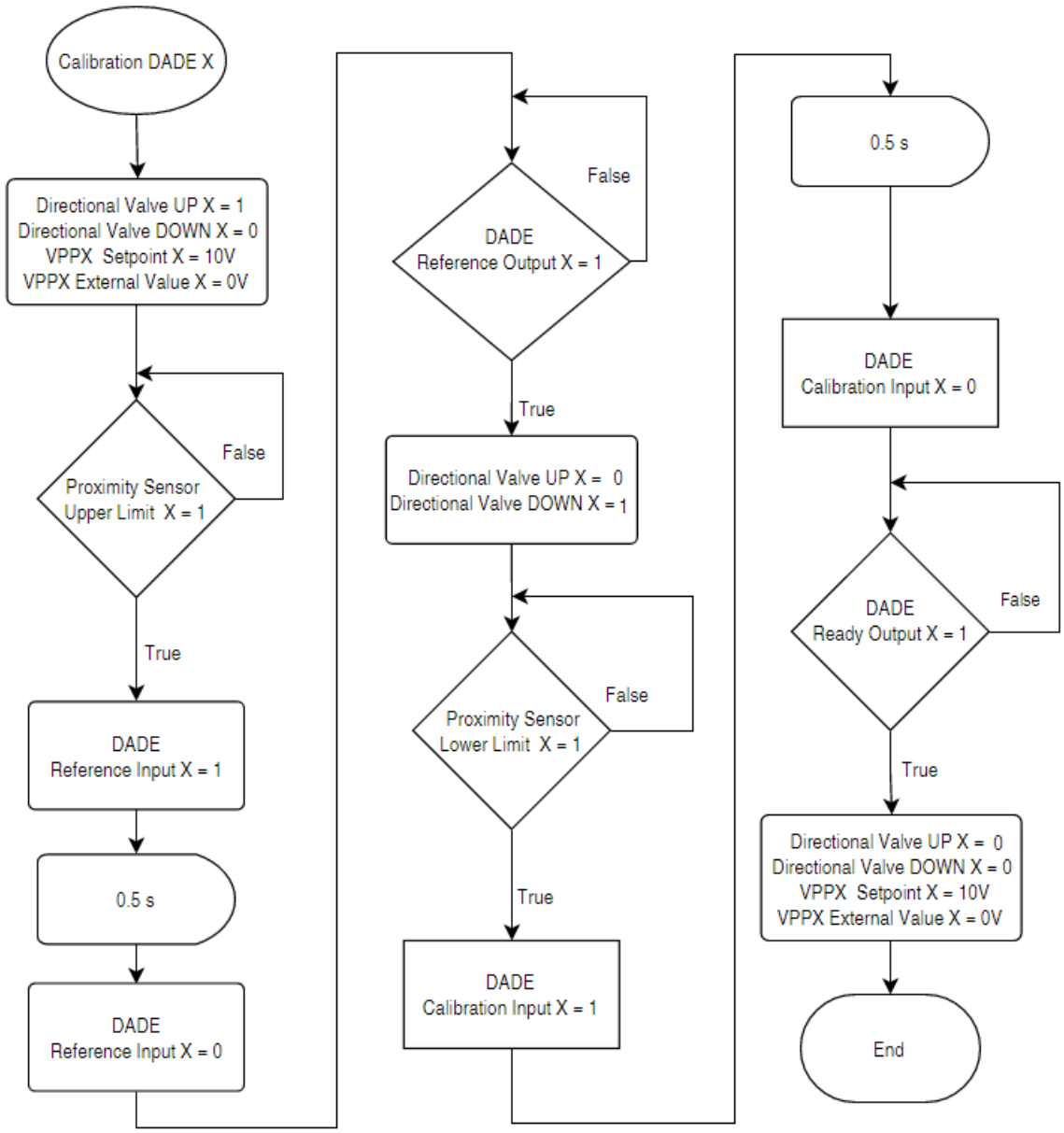

Figure 6.2: Calibration of DADE X routine flowchart

This calibration routine commands the cylinder to its both travel limits to acknowledge the cylinder stroke.

6.1.2 Initialization

The initialization routine aims to give a reference of the cylinder's position (Figure 6.3). After the calibration, the encoder only saves the work stroke. When powering up the machine, the encoder, which works with relative displacements, needs to get its reference. We will use one of the travel limits of the cylinder.

The *Initialization* routine of the DADE must force the cylinder piston to one end of the work stroke. The VPPX Setpoint is set to 10V and the VPPX External Value is set to 0V to allow the maximum air flow to the Cylinders. The Directional Valve solenoid is activated to send air to the secondary chamber of the cylinder, beginning an descending movement. When the Upper Limit Proximity Sensor emits signal, we activate the DADE Reference Input during 0.5 s. The DADE Reference Output switches on when the Cylinder saves the referencing point, switching on the DADE Ready Output ending the *Initialization* routine. The Directional Valves return to its normal position and the VPPX are turned off to prevent movement of the piston rod.

When the user runs the *Calibration* routine, they receive a message informing the routine started and after all stations are calibrated, they are informed that the *Calibration* is complete. The *Calibration* routine of the three cylinders is identical and happens in parallel to each other. The *Calibration* of the Cylinder X (being X equal to 1, 2 or 3) is shown in the following flowchart.

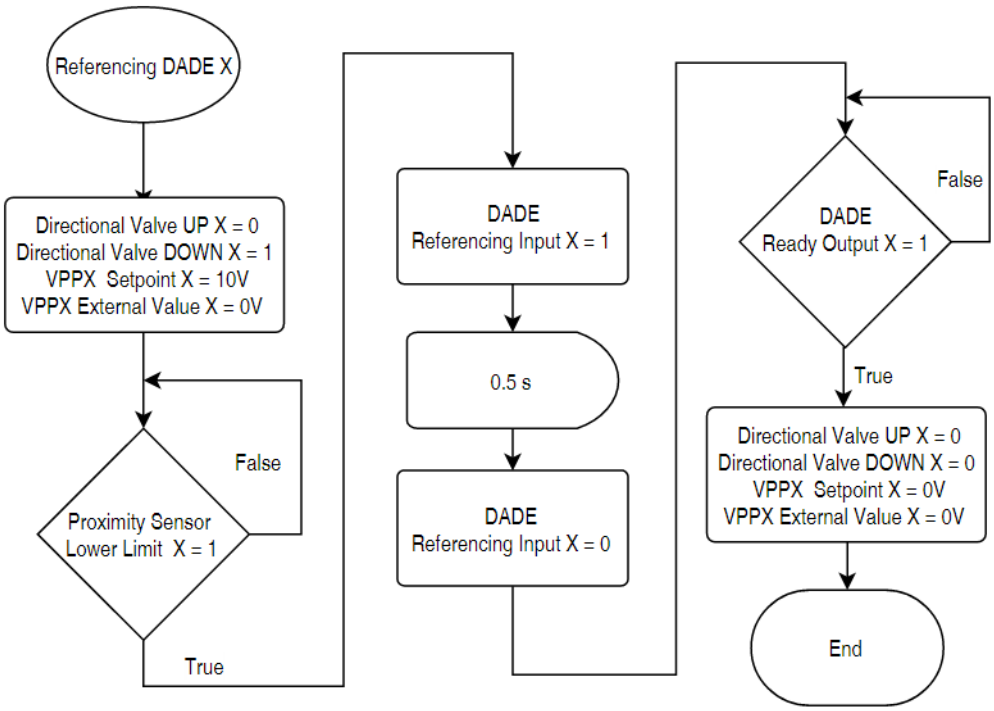

Figure 6.3: Referencing DADE X routine flowchart

6.1.3 Manual

In the *Manual* state the user can begin an ascending or descending movement of the selected station of the cam switch in the Command Panel (Figure 6.4).

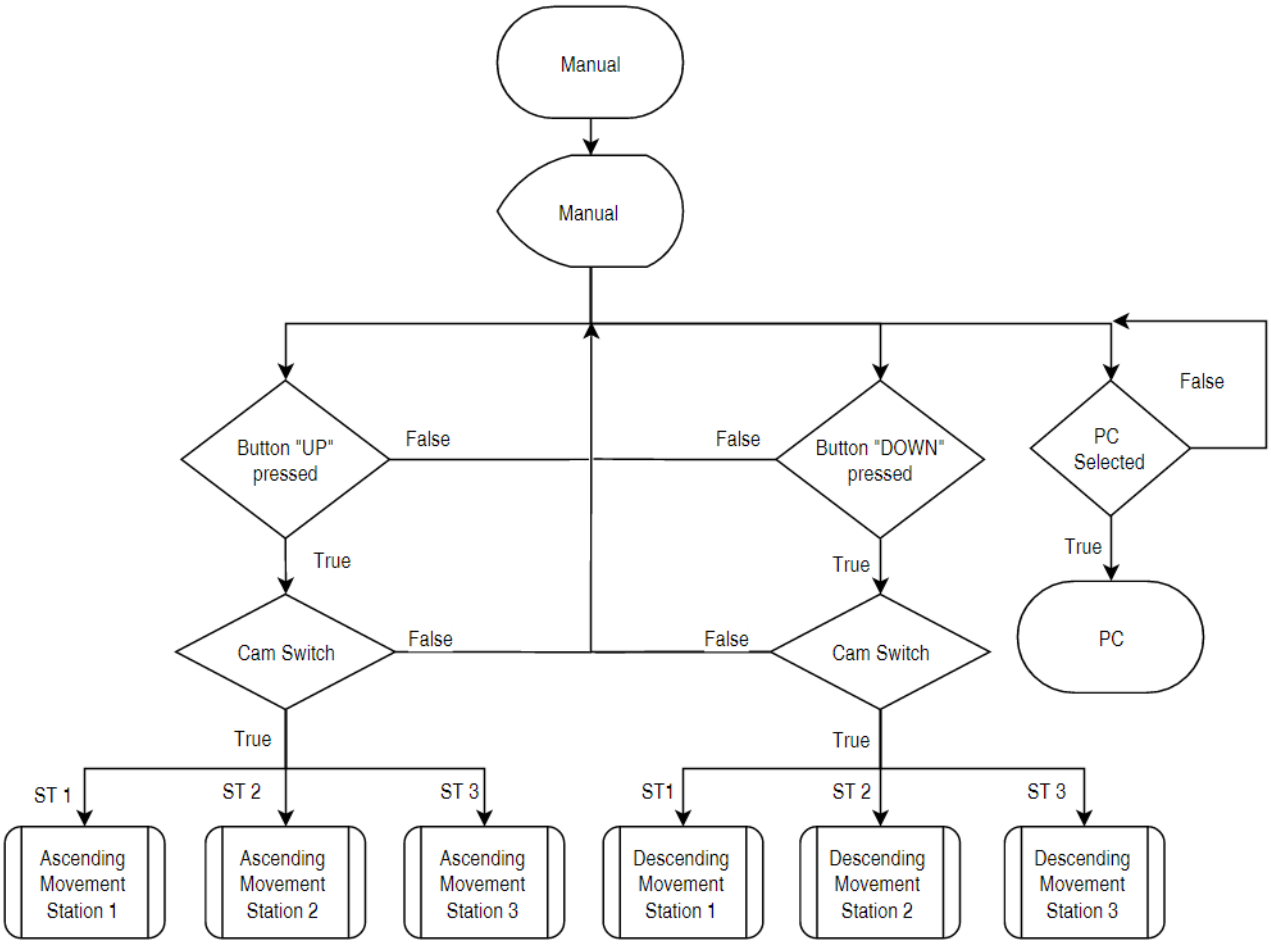

Figure 6.4: Manual routine flowchart

The ascending (Figure 6.5) or descending (Figure 6.6) movement of each station occurs either until the user stops pressing the "Up" or "Down" button or the cylinder reaches its upper or lower limit.

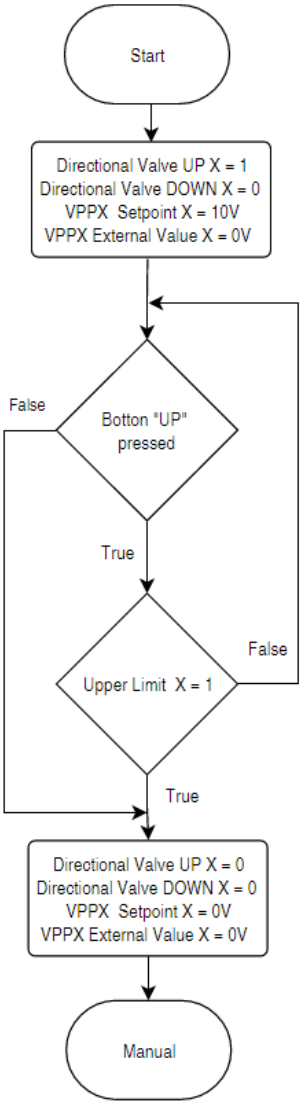

Figure 6.5: Ascending Movement of Station X

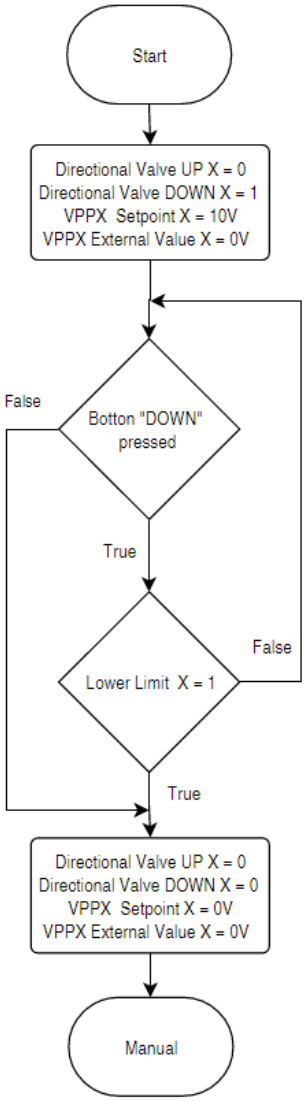

Figure 6.6: Descending Movement of Station X

6.1.4 PC

The *PC* state occurs in the graphical user interface. In this state the user has the option to setup the parameters of the test, begin the *Initialization* routine or change to *Manual* mode. This state occurs mainly on the Graphical User Interface.

6.1.5 Test

During the *Test* state, the computer is sending the analogue references defined in the previous state and also the load cells signal, acquired by the DAQ system, to the VPPX. Each VPPX will operate based on the reference value and the actual value. In parallel, the DAQ system is also acquiring the displacement of the cylinder and the GUI is plotting the creep curve of each station.

6.1.6 Emergency

The user enters the *Emergency* state after either the physical emergency button or the virtual emergency button in the GUI is pressed. This states resets the directional valves to its normal position and set the VPPX setpoint to 0 V to cutting the cylinder's air supply.

6.2 Electric Circuit

To install the instrumentation and actuation components in the machine, a power supply and therefore an electric switchboard is needed for signal conditioning. The electric switchboard also contains a command logic of the machine to ensure its correct functioning, protection and safety. As most of the DAQ signals need to be conditioned, the DAQ boards will be inside the electrical switchboard enclosure. The electrical switchboard [Electrical Scheme in Appendix B] contains:

- a signal conditioning board for the outputs and inputs of the instrumentation, as they all operate with 24 V and the DAQ boards read and send a 5V signal;
- a signal conditioning board that operates as a voltage divisor or an offset amplifier to allow the NI-6010 DAQ board with $\pm$ 5 V analogue input range to acquire the 0-10 V analogue signals of the load cell's transmitters and of the DADE;
- power supply (**PS1**) to power the directional valves, proximity sensors, VPPX and the command logic of the machine;
- a rectified and filtered power supply (**PS2**) to power the transmitters off the load cells preventing the noise of a regular power supply;
- a common circuit breaker (**D1**) and one for each power supply (**D2**,**D3**).
- differential circuit breaker (**ID1**);
- relays with the poles necessary for the command and control logic.

After defining the components of the electrical switchboard, the enclosure to be chosen must have spare space to assemble future necessary components.

The transmitters for the load cell as well as the DADE converters, will be assembled on a stainless steel plate fastened to the Support Frame. This plate will also contain the components of the pneumatic circuit.

The command logic [Electrical Scheme in Appendix B] of the machine is implemented by various circuit of relays.

6.3 User Interface

The interface between the user and the machine is provided by a Command Panel and a Graphical User Interface (GUI). The Command Panel contains the components necessary for the cylinder positioning in the *Manual* state, and an Emergency Button. The GUI contains a defined sequence of menus to aid and allow the user to setup the test parameters, and once the test begins, the visualization of the creep curve.

6.3.1 Command Panel

The command panel will be attached to the machine, for an easy user access, and will contain

- "UP" and "DOWN" buttons to command the directional valves and therefore the direction of the cylinders movement
- a cam switch to select the station which the user wants to position;
- indicators to show the state of each station;
- a power switch to turn on or off the power supply line of the actuation and instrumentation components;
- an indicator to show the machine's power supply state
- an emergency button

6.3.2 Graphical User Interface

The GUI is divided into three panes. The measurement pane contains the readings of the load cells, the displacement encoder and the temperature of the chamber. The control pane contains the main controls of the interface, like the virtual emergency button, home, back and forth and help buttons. The largest pane is the menu, and it's the only one that changes as the user progresses in the setup of the test. The first menu gives the option to either start a creep test or a relaxation test (Figure 6.7).

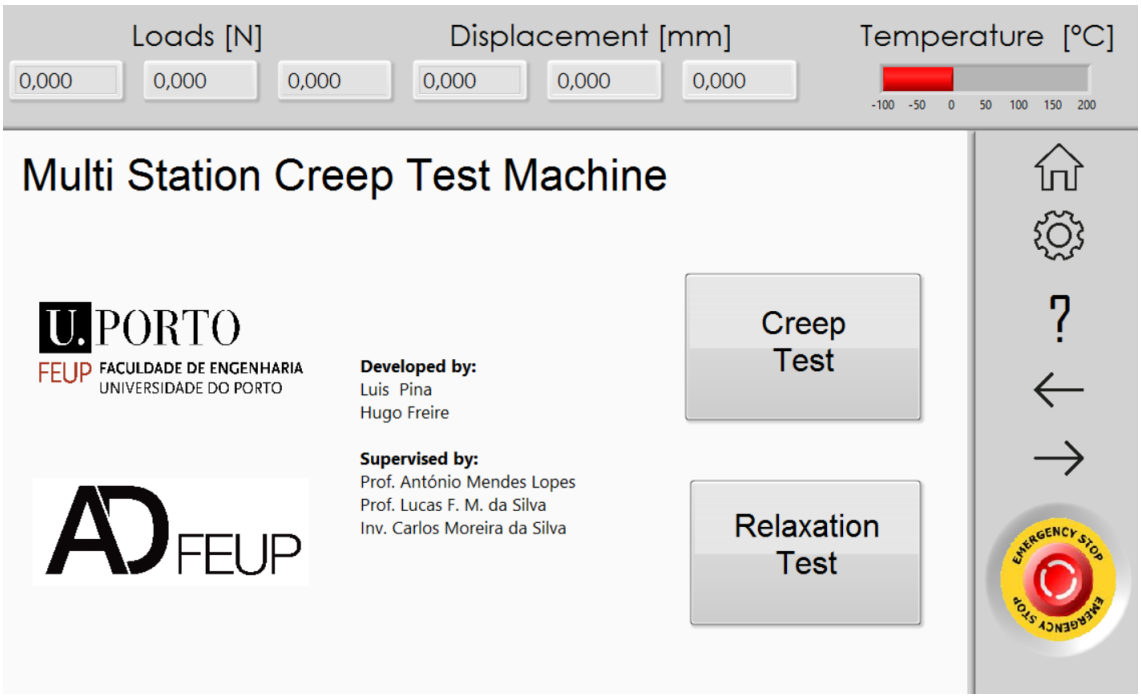

Figure 6.7: GUI Home

Beginning a test, the GUI presents a *Specimen Geometry* menu where the user may input the label, dimensions and some annotations about the specimen to be tested (Figure 6.8).

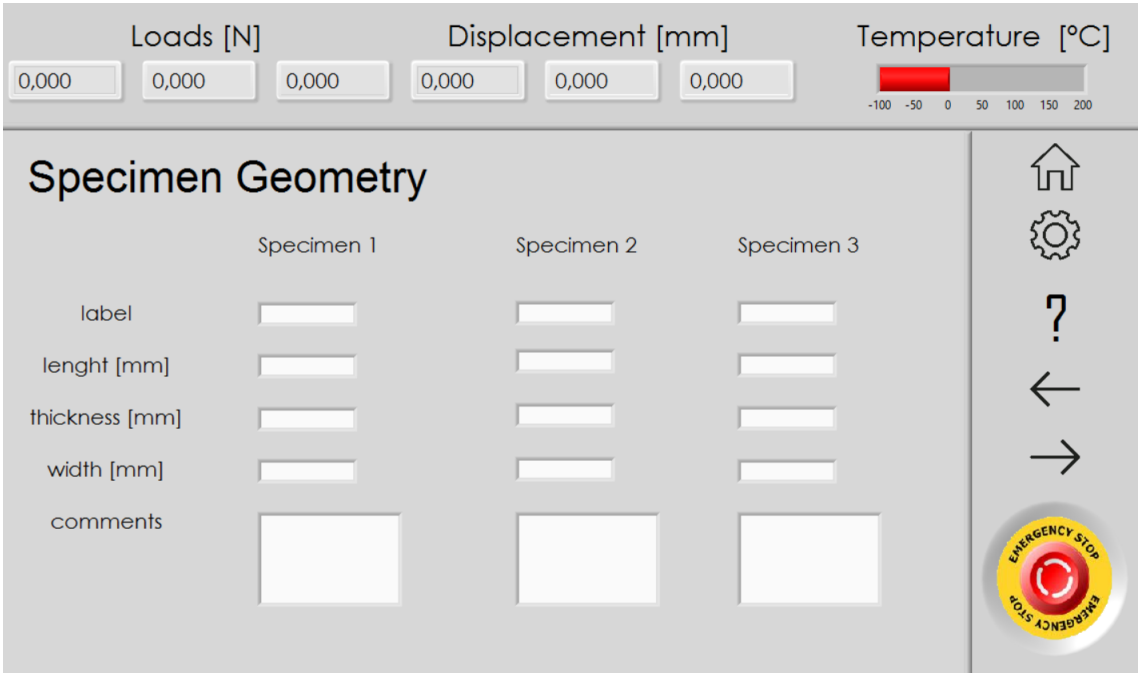

Figure 6.8: GUI Specimen Geometry

The GUI then forwards to the *Test Condition* menu where the user must choose either to test the three specimens under the same load conditions, or under different ones. The temperature

is defined for the tests occurring simultaneously. Once the user inputs the conditions for one individual station or for all three stations, a dropdown menu appears allowing the user to choose the end condition of the test. The user can decide between an "elapsed time" condition or an "until rupture" condition. The "until rutpure" condition will allow the test to run for an undefined time, only stopping it when rupture of the specimen occurs. The "elapsed time" condition will run the test during a user defined time, along which specimen rupture may or may not happen, causing or not the end of the test before the defined time elapses (Figure 6.9).

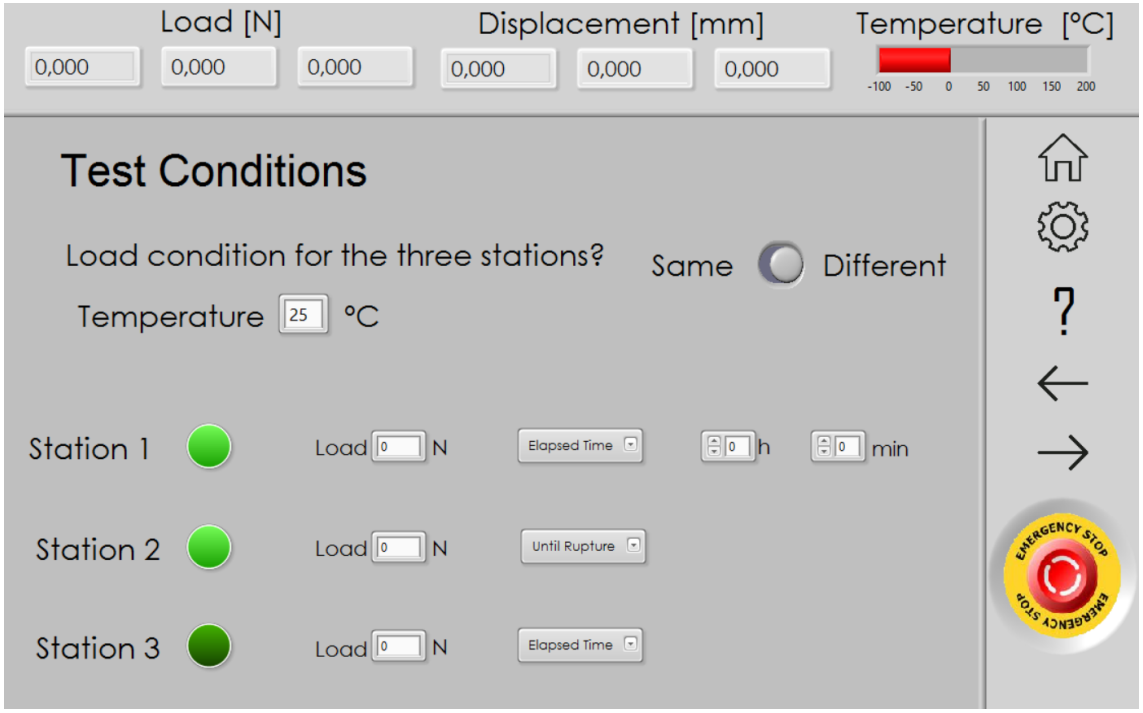

Figure 6.9: GUI Conditions

If the user chooses the "until rupture" condition, the prompt window will require the load at which the test will occur.If the user chooses the "elapsed time" condition, they are given the option to choose between a stepped load solicitation, or a constant load solicitation. The GUI asks the user for the number of steps, and then, for each step, the load and time. This allows ADFEUP the possibility of more flexible tests. After defining the last step of the load solicitation, the GUI presents a chart of the load solicitation to be applied on the specimen and the user can confirm or redefine the steps from the beginning.When the parameters are ready, the GUI presents a menu with a "Start" button that the user needs to press to begin the test.

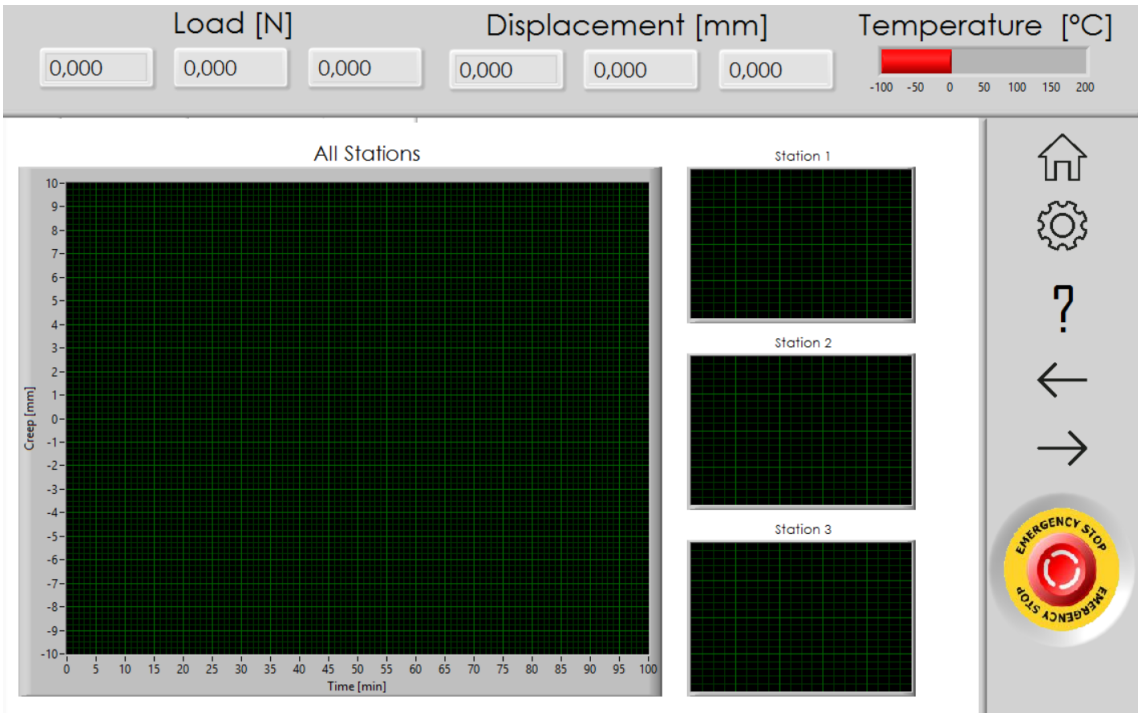

Figure 6.10: GUI Results

During the test, the user will have the option to present the three creep curves in the same plot, or see each specimen individually (Figure 6.10). They can also change the plot between a deformation versus time to a load versus time or load versus deformation. When the test ends, the GUI presents a window with the main data of the test and the option to save the results.

6.4 Conclusions

The Graphical User Interface needs to be finished and validated with simulations of the work conditions. The command and control logic circuit should be revised according to possible changes ADFEUP desires to make to the planned logic functioning of the machine.

Chapter 7

Conclusions

This chapter summarizes the main conclusions of the thesis, reporting the achieved initial objectives and addressing the possible future improvements to be implemented in the machine.

7.1 Conclusions

In a first stage, we wished to understand the possible assembly requirements of the climatic chamber to be further implemented. Therefore, the commercial solutions were analysed and a brief design of its structure, including insulation and components.

Sequentially, the mechanical components were improved and checked for thermal and stress limitations. The deformation of the structure, as it influences the reading of the cylinders, was studied under several conditions. The design of the structure and sub-assemblies suffered several iterations, to simplify its manufacturing,

The actuation and instrumentation components were revised, defined and ordered. Some of them were the only viable option within the available solutions, and other were chosen for economical reasons.

The command and control logic was defined through the electrical circuit, commanding the machine in a defined sequence of states.

The cost of the machine is currently on 10000 €without VAT. The 10000 € (without VAT)for three stations is substantially lower than acquiring another single station UTM for 45000 € . The current machine, without taking in account man hours in the workshop and in the development of the thesis, costs about one third of what a UTM would while tripling the stations, and therefore the machine throughput.

7.2 Future Development

The climatic chamber designed must be improved and its temperature control must be studied and implemented. The mechanical components are being assembled, and we are waiting for the extension springs for the grips and the heat sink for the Lower Coupling, which must be defined

and ordered. The pneumatic circuit must be assembled on an aluminium plate, which will be fastened to the Support Frame. The DAQ system channels are already defined and must be connected to the electric switchboard. The electric circuit is designed, but the components must be defined, ordered and implemented.

As the machine will run relaxation tests, where it applies a displacement on the specimen, a system to maintain the displacement constant must be implemented. As the VPPX control circuit may not be robust enough to control a position, a cylinder locking device to lock the Cylinder Extension Rod should be analysed.

The machine also needs experimental validation of the pneumatic circuit, control logic circuit and software.

Appendix A

Technical Drawings

A.1 Mechanical Wedge Action Grip

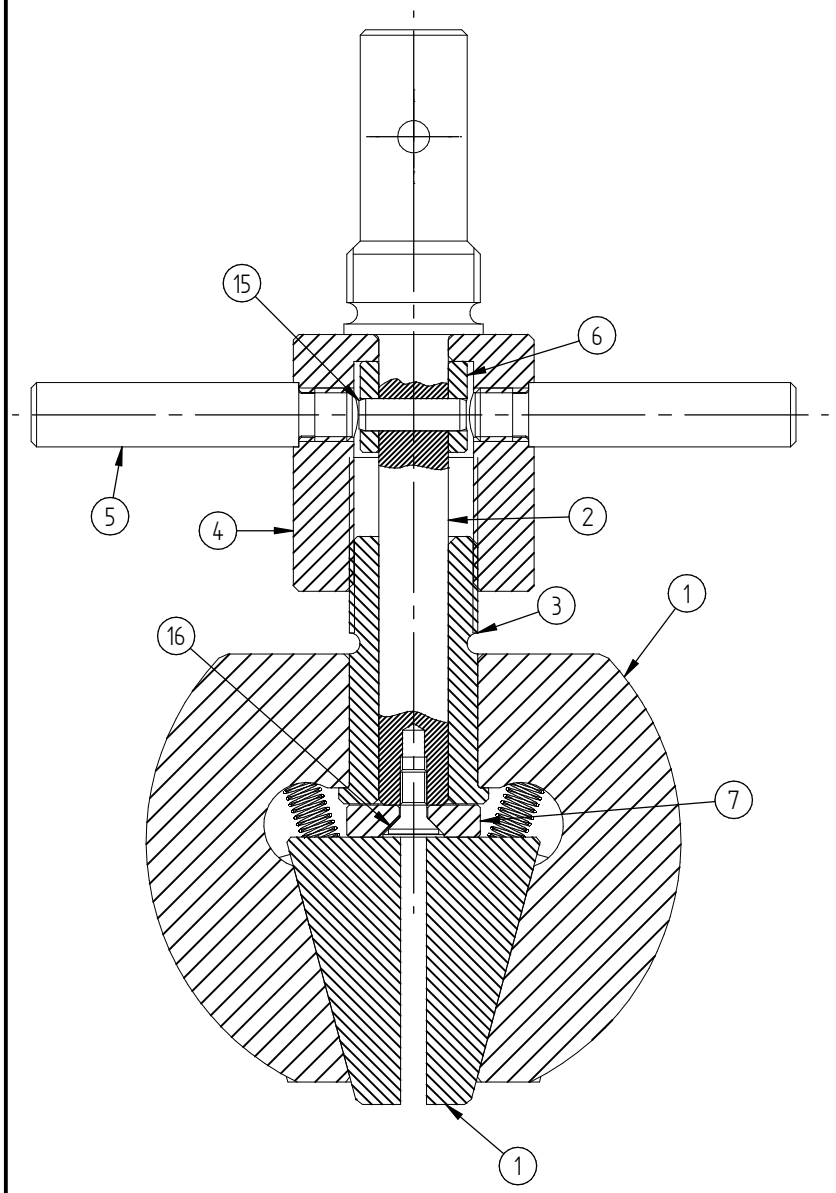

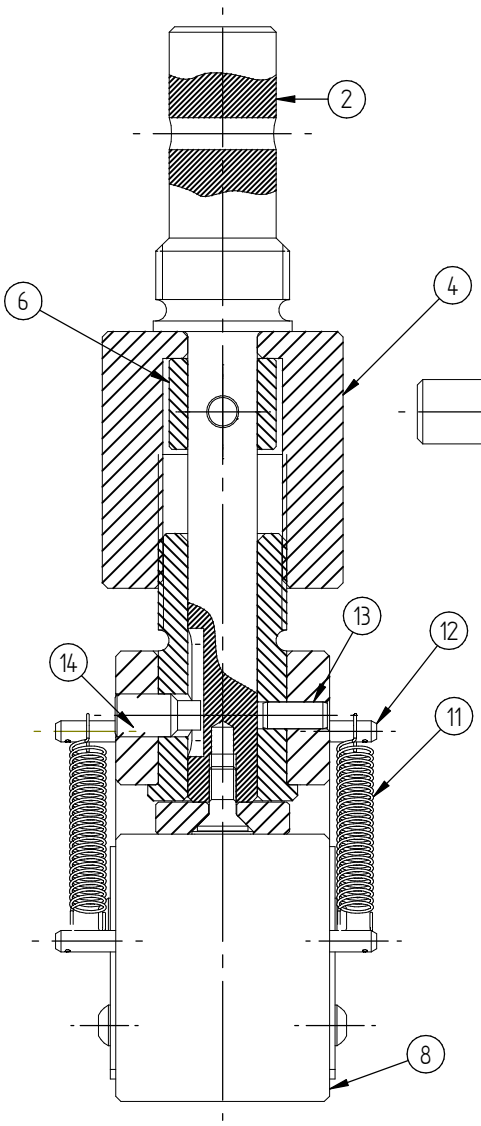

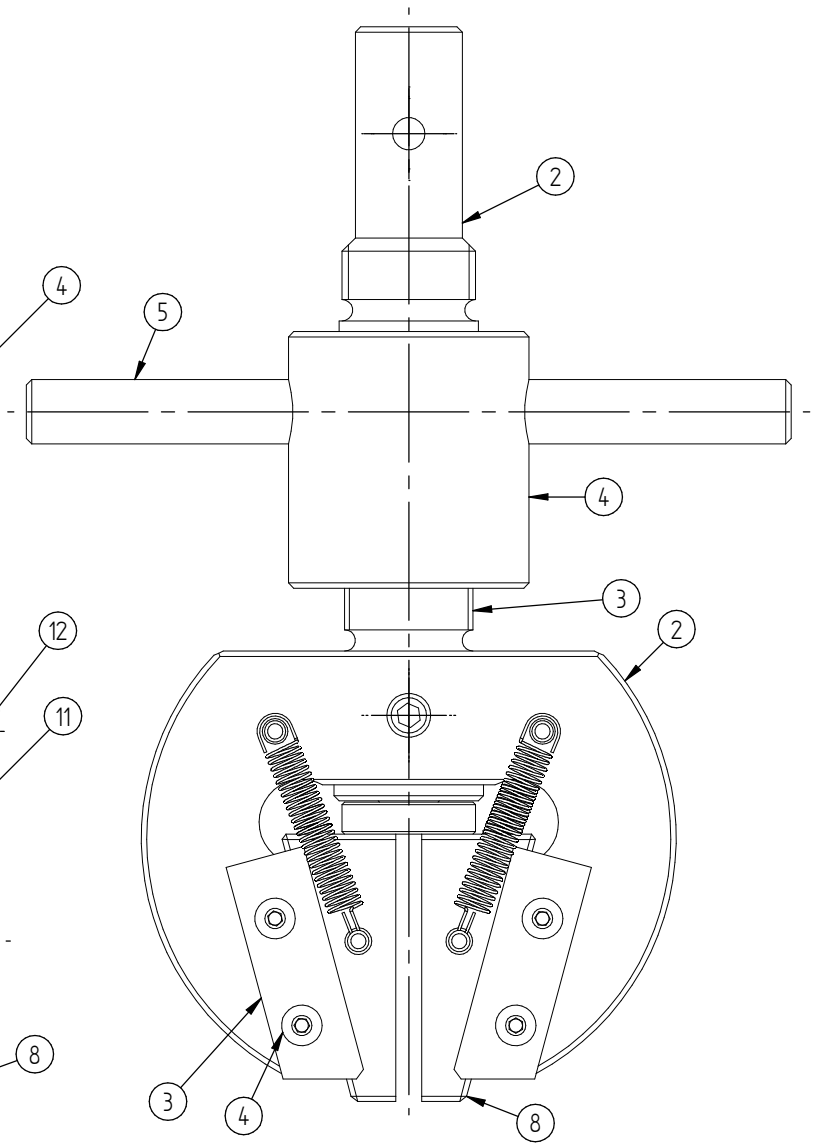

SCALE: 1:1	Toleranciamento ISO 8015 Tolerâncias gerais ISO 2768 – mH ISO 13920 Rugosidades Gerais ISO 1302 Cantos e Chanfros ISO 13715		MATERIAL:		
	NAME	DATE	TITLE: Mechanical Wedge Action Grip		DWG NO GP-00
DRAWN	Luis Pina				
CHECKED	Luis Pina		FEUP	SIZE A3	WEIGHT: / REV
ENG APPR	CM Silva				
MGR APPR					QUANTITY: / SHEET 1 OF 1

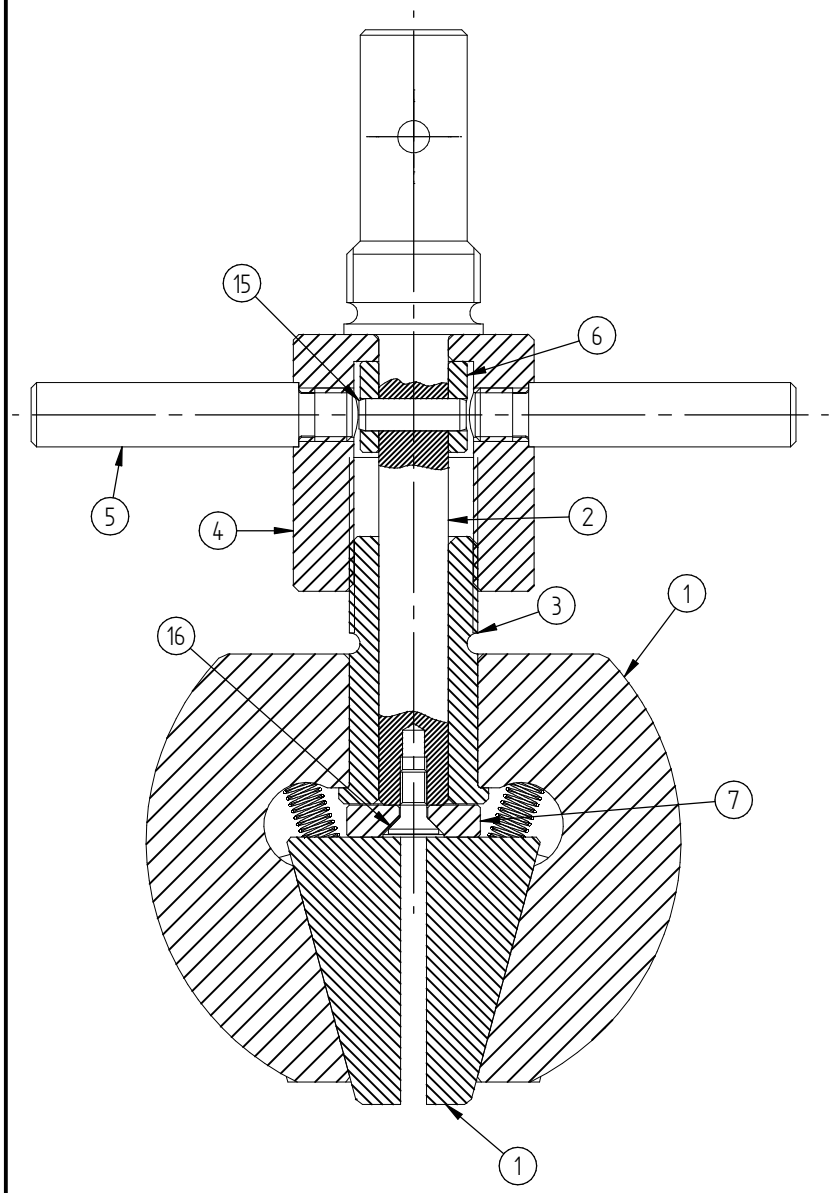

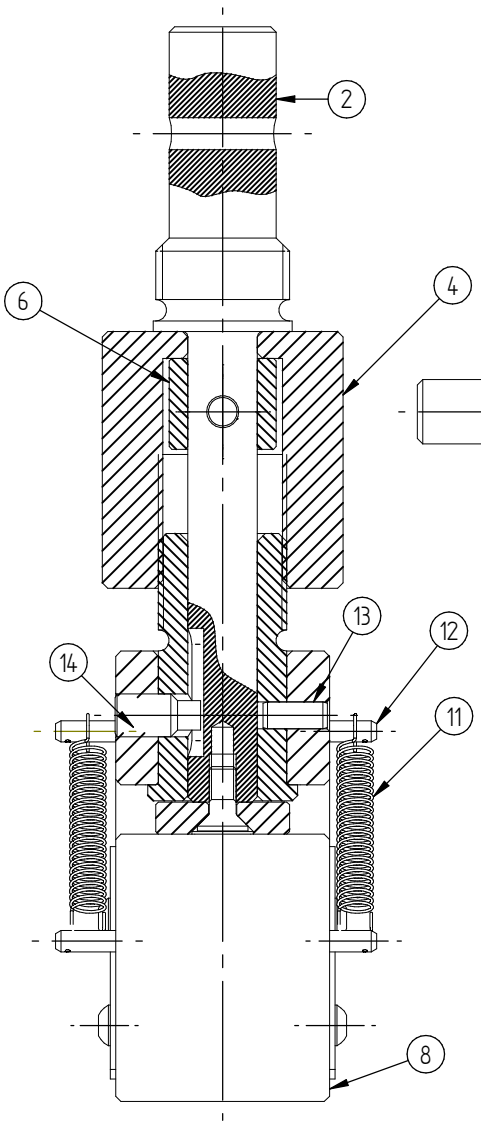

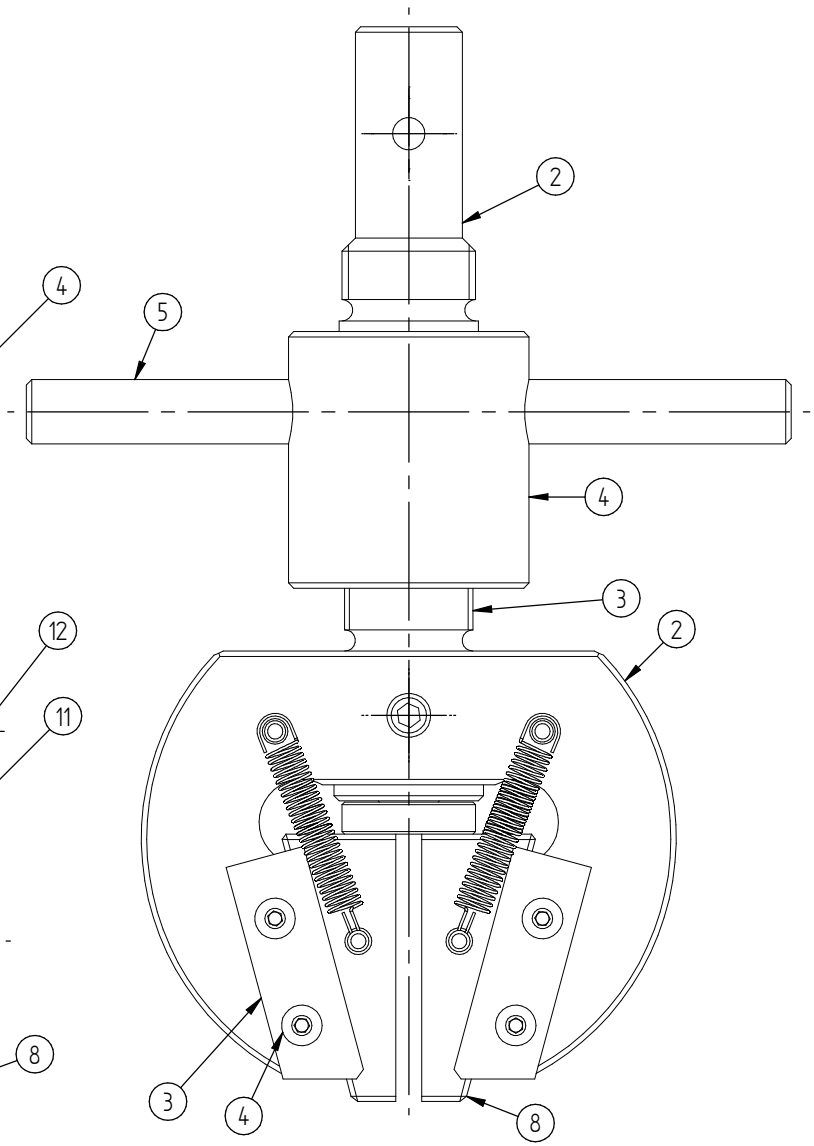

SCALE: 1:1	Toleranciamento ISO 8015 Tolerâncias gerais ISO 2768 – mH ISO 13920 Rugosidades Gerais ISO 1302 Cantos e Chanfros ISO 13715		MATERIAL:		
	NAME	DATE	TITLE: Mechanical Wedge Action Grip		DWG NO GP-00
DRAWN	Luis Pina				
CHECKED	Luis Pina		FEUP	SIZE A3	WEIGHT: / REV
ENG APPR	CM Silva				
MGR APPR					QUANTITY: / SHEET 1 OF 1

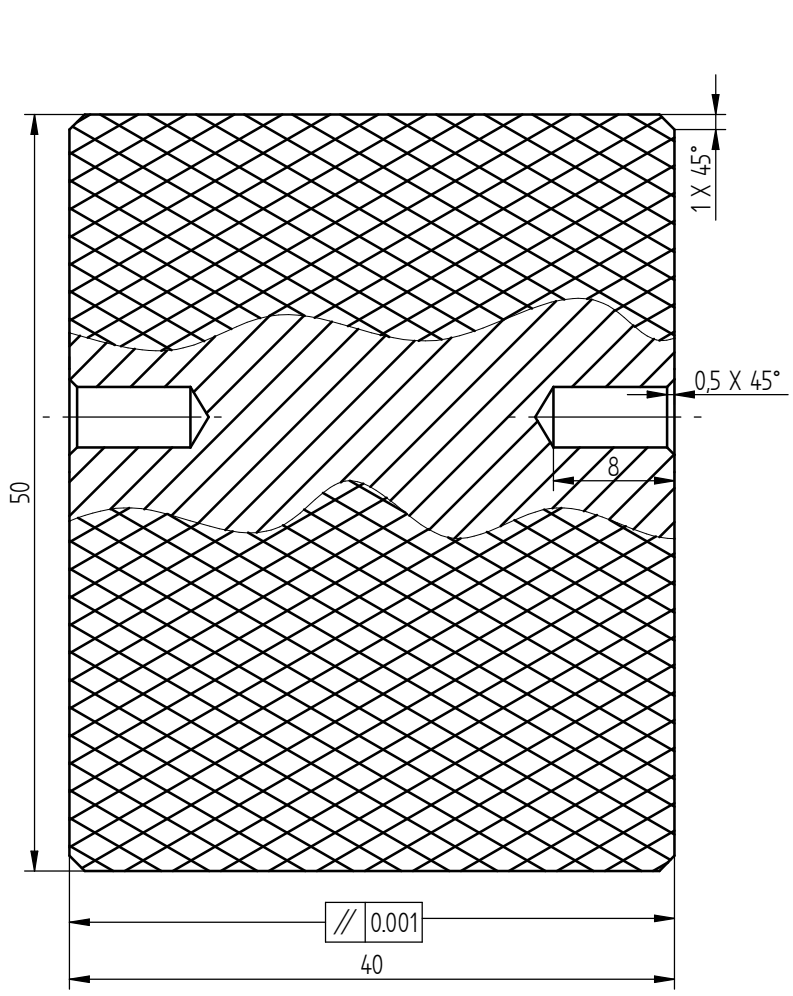

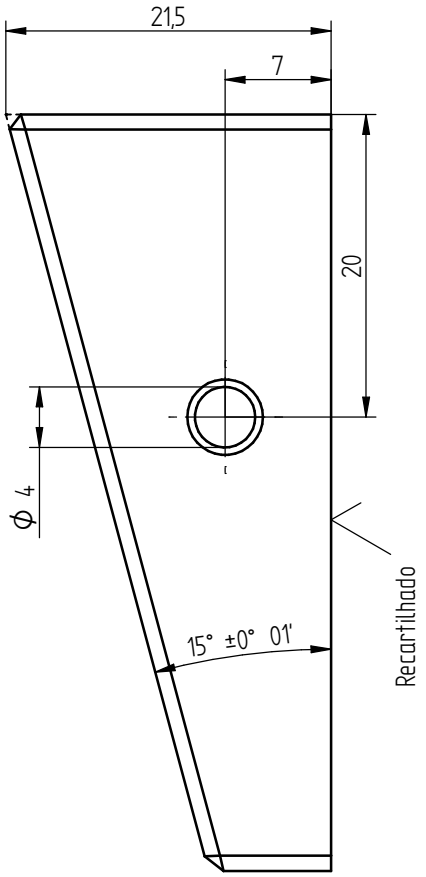

Recartilhado:
profundidade 0.5mm
passo 1mm
ângulo 60°

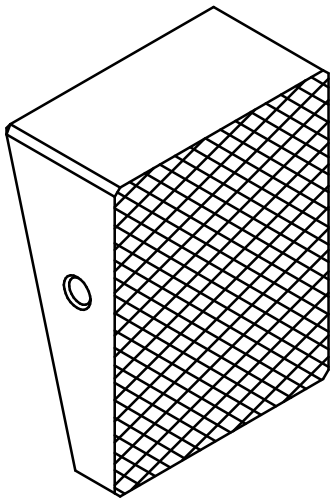

SCALE: 2:1	Toleranciamento ISO 8015 Tolerâncias gerais ISO 2768 – mH ISO 13920 Rugosidades Gerais ISO 1302 Cantos e Chanfros ISO 13715		MATERIAL: RMC20		
	NAME	DATE	TITLE: Jaw Face		DWG NO GP-01
DRAWN	Luis Pina				
CHECKED	Luis Pina		FEUP	SIZE A4	WEIGHT: / REV
ENG APPR	CM Silva				
MGR APPR					QUANTITY: 12 / SHEET 1 OF 1

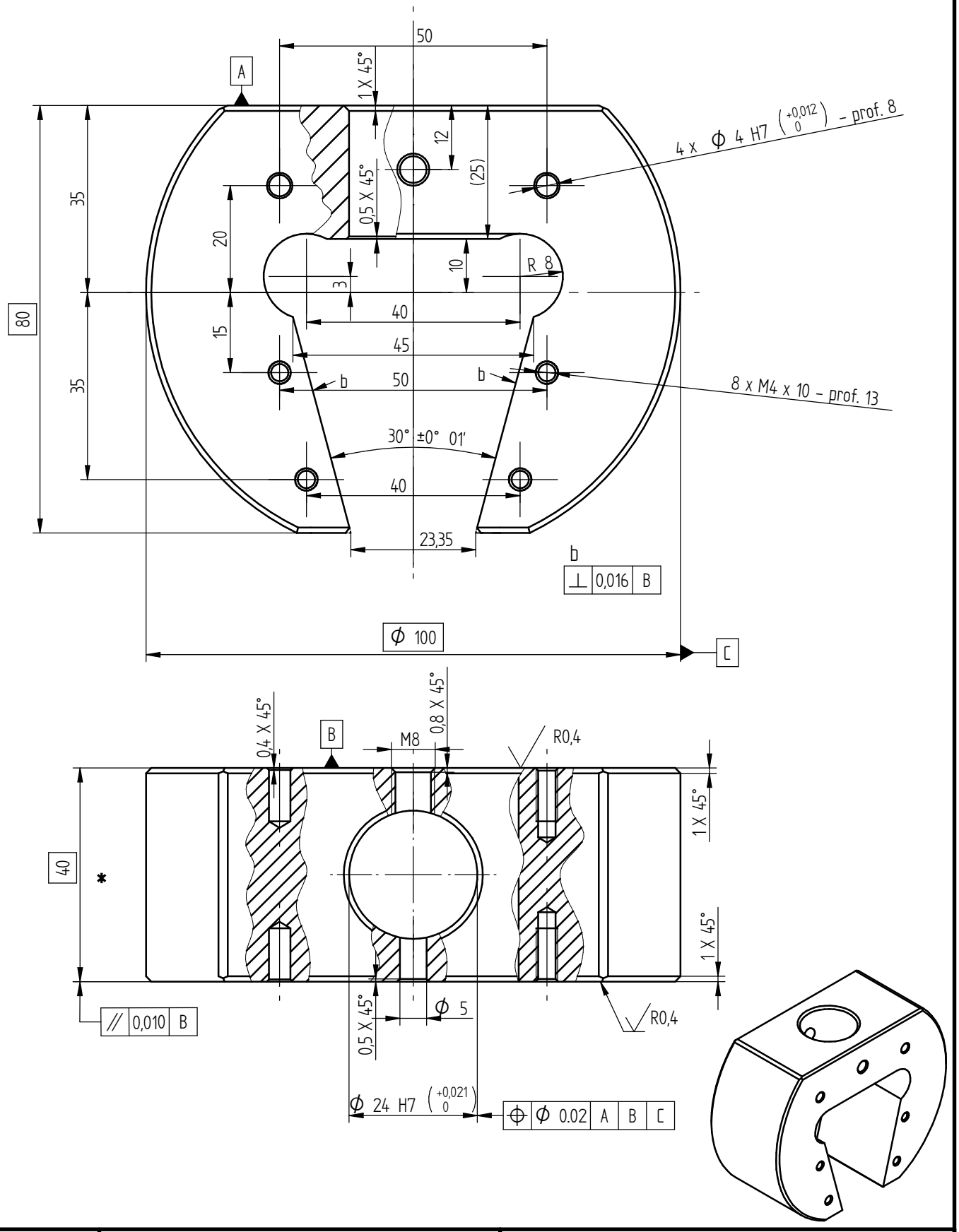

SCALE: 1:1	Toleranciamento ISO 8015 Tolerâncias gerais ISO 2768 – mH ISO 13920 Rugosidades Gerais ISO 1302 Cantos e Chanfros ISO 13715		MATERIAL: AISI 431		PERFIL RED100
			NOTAS: * Rectificar com Cunhas cementadas		
	NAME	DATE	TITLE: Body		DWG NO GP-02
DRAWN	Luis Pina				
CHECKED	Luis Pina		FEUP	SIZE A4	WEIGHT: REV
ENG APPR	CM Silva				QUANTITY: 6 SHEET 1 OF 1
MGR APPR					

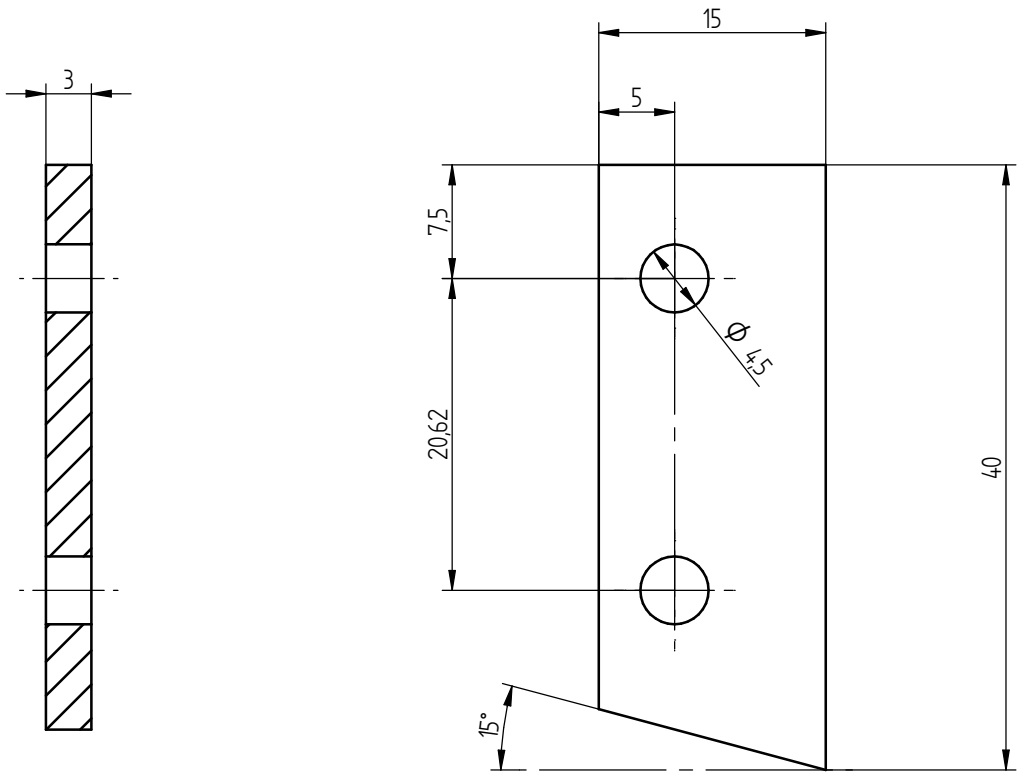

SCALE: 1:5	Toleranciamento ISO 8015 Tolerâncias gerais ISO 2768 – mH ISO 13920 Rugosidades Gerais ISO 1302 Cantos e Chanfros ISO 13715		MATERIAL: Barra Inox 15mm x 3mm		
			NOTAS: Ajustar cantos		
	NAME	DATE	TITLE: Retaining Plates		DWG NO GP-03
DRAWN	Luis Pina				
CHECKED	Luis Pina		FEUP	SIZE A4	WEIGHT: / REV
ENG APPR	CM Silva				QUANTITY: 24 / SHEET 1 OF 1
MGR APPR					

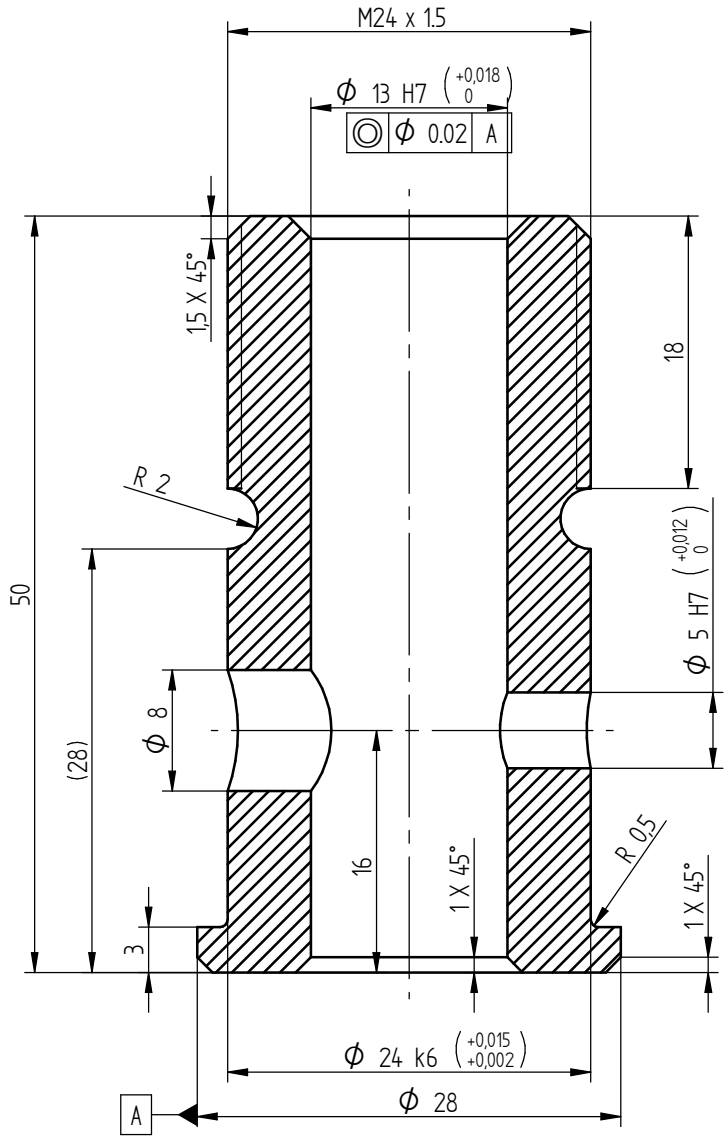

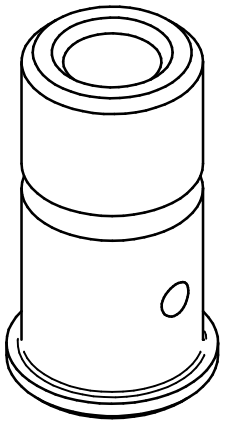

SCALE: 2:1	Toleranciamento ISO 8015 Tolerâncias gerais ISO 2768 – mH ISO 13920 Rugosidades Gerais ISO 1302 Cantos e Chanfros ISO 13715		MATERIAL: AISI 304 PERFIL RED28			
	NAME	DATE	TITLE: Bushing			DWG NO GP-04
DRAWN	Luis Pina					
CHECKED	Luis Pina		FEUP	SIZE A4	WEIGHT:	REV
ENG APPR	CM Silva					
MGR APPR					QUANTITY: 6	SHEET 1 OF 1

DETAIL A

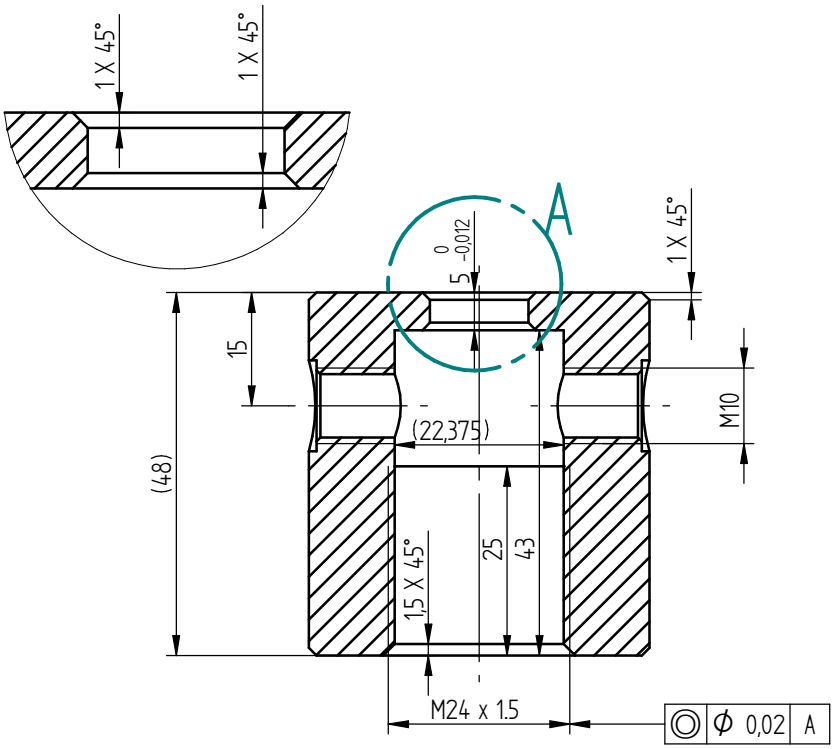

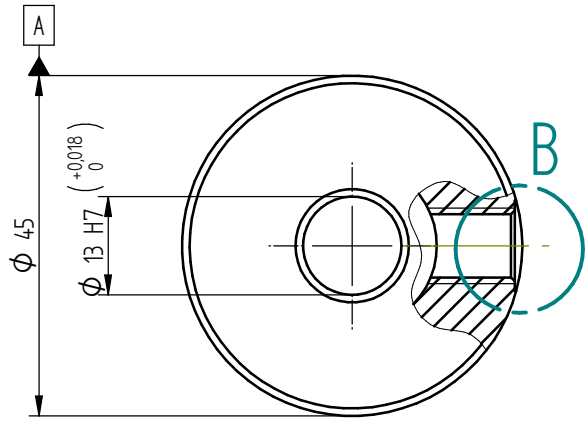

DETAIL B

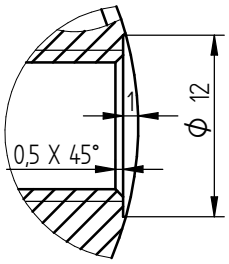

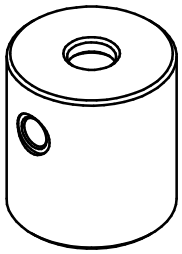

SCALE: 1:1	Toleranciamento ISO 8015 Tolerâncias gerais ISO 2768 – mH ISO 13920 Rugosidades Gerais ISO 1302 Cantos e Chanfros ISO 13715		MATERIAL: AISI 304 PERFIL RED45		
	NAME	DATE	TITLE: Control Nut		DWG NO GP-05
DRAWN	Luis Pina				
CHECKED	Luis Pina		FEUP	SIZE A4	WEIGHT: REV
ENG APPR	CM Silva				QUANTITY: 6 SHEET 1 OF 1
MGR APPR					

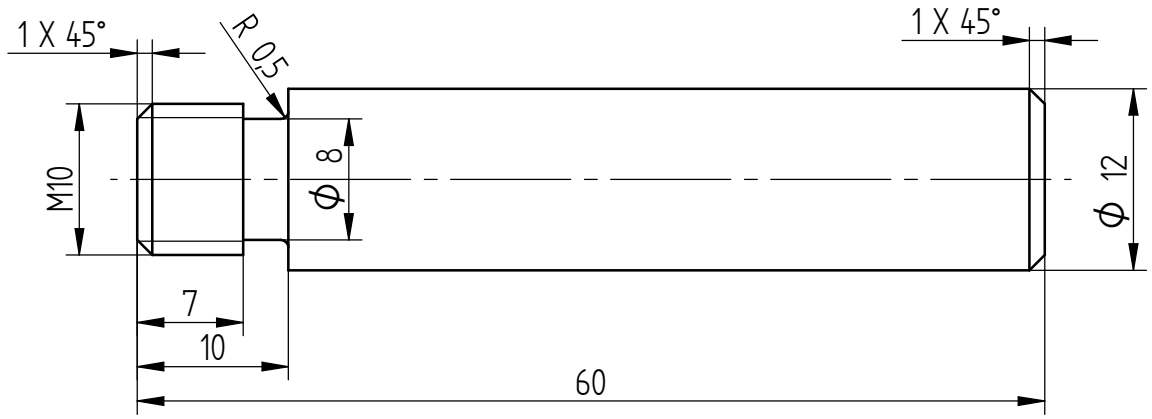

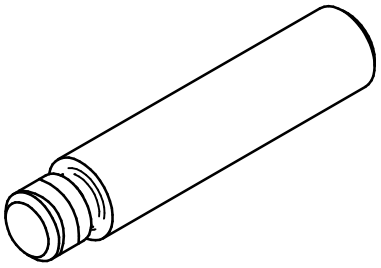

SCALE: 2:1	Toleranciamento ISO 8015 Tolerâncias gerais ISO 2768 – mH ISO 13920 Rugosidades Gerais ISO 1302 Cantos e Chanfros ISO 13715		MATERIAL: AISI 304	PERFIL RED12	
	NAME	DATE	TITLE: Handle		DWG NO GP-06
DRAWN	Luis Pina				
CHECKED	Luis Pina		FEUP	SIZE A4	WEIGHT: / REV
ENG APPR	CM Silva				QUANTITY: 12 / SHEET 1 OF 1
MGR APPR					

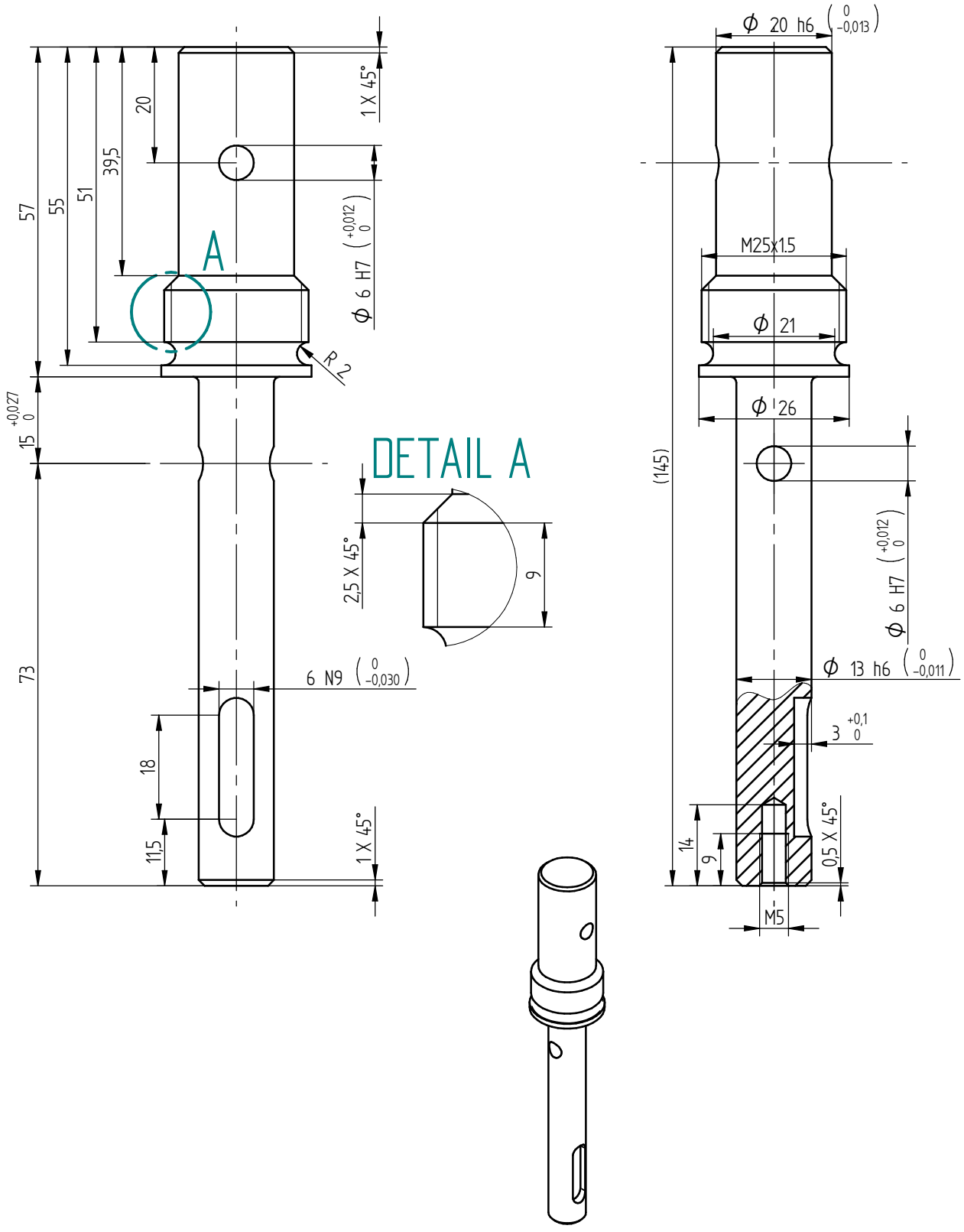

SCALE: 1:1	Toleranciamento ISO 8015 Tolerâncias gerais ISO 2768 – mH ISO 13920 Rugosidades Gerais ISO 1302 Cantos e Chanfros ISO 13715		MATERIAL: AISI 304 PERFIL RED28		
			MATERIAL: Quebrar arestas dos furos		
	NAME	DATE	TITLE: Spindle		DWG NO GP-07
DRAWN	Luis Pina				
CHECKED	Luis Pina		FEUP	SIZE A4	WEIGHT: REV
ENG APPR	CM Silva				
MGR APPR					QUANTITY: 6 SHEET 1 OF 1

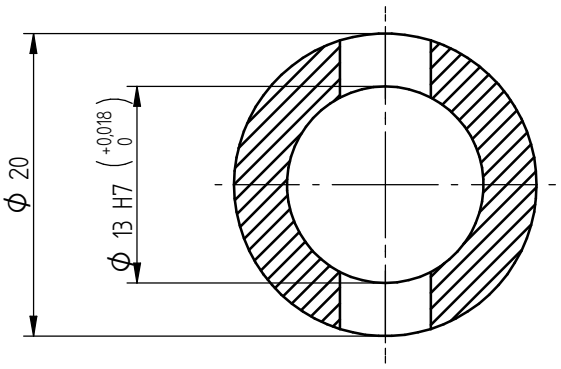

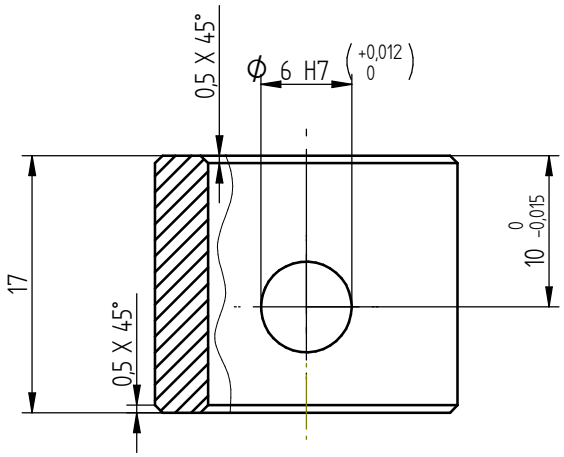

SCALE: 2:1	Tolerancimento ISO 8015 Tolerâncias gerais ISO 2768 – mH ISO 13920 Rugosidades Gerais ISO 1302 Cantos e Chanfros ISO 13715		MATERIAL: AISI 304 PERFIL RED28		
	NAME	DATE	TITLE: Sleeve		DWG NO GP-08
DRAWN	Luis Pina				
CHECKED	Luis Pina		FEUP	SIZE A4	WEIGHT: REV
ENG APPR	CM Silva				QUANTITY: 6 SHEET 1 OF 1
MGR APPR					

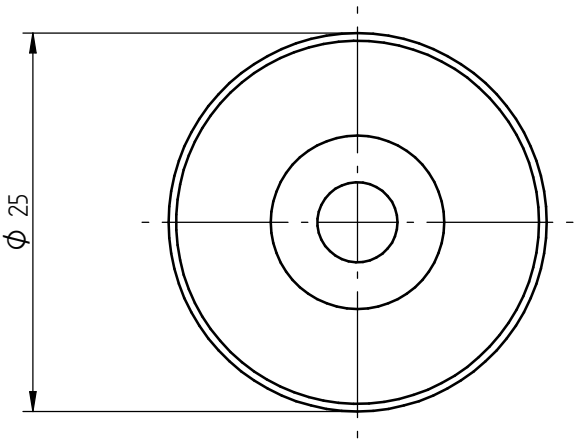

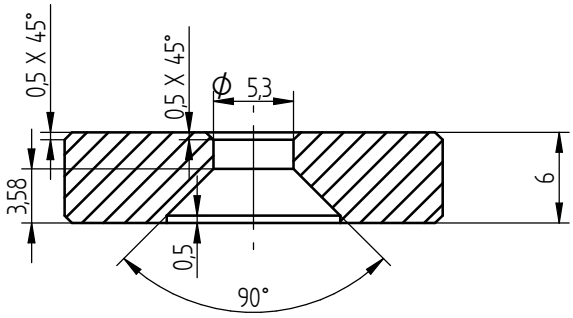

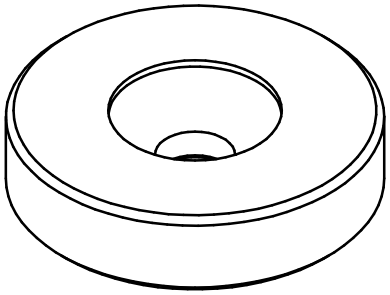

SCALE: 1:5	Toleranciamento ISO 8015 Tolerâncias gerais ISO 2768 – mH ISO 13920 Rugosidades Gerais ISO 1302 Cantos e Chanfros ISO 13715		MATERIAL: AISI 304 PERFIL RED28			
			NOTAS:			
	NAME	DATE	TITLE: Shoe			DWG NO GP-09
DRAWN	Luis Pina					
CHECKED	Luis Pina				WEIGHT:	REV
ENG APPR	CM Silva		FEUP	SIZE A4		
MGR APPR					QUANTITY: 6	SHEET 1 OF 1

A.2 Lower Assembly

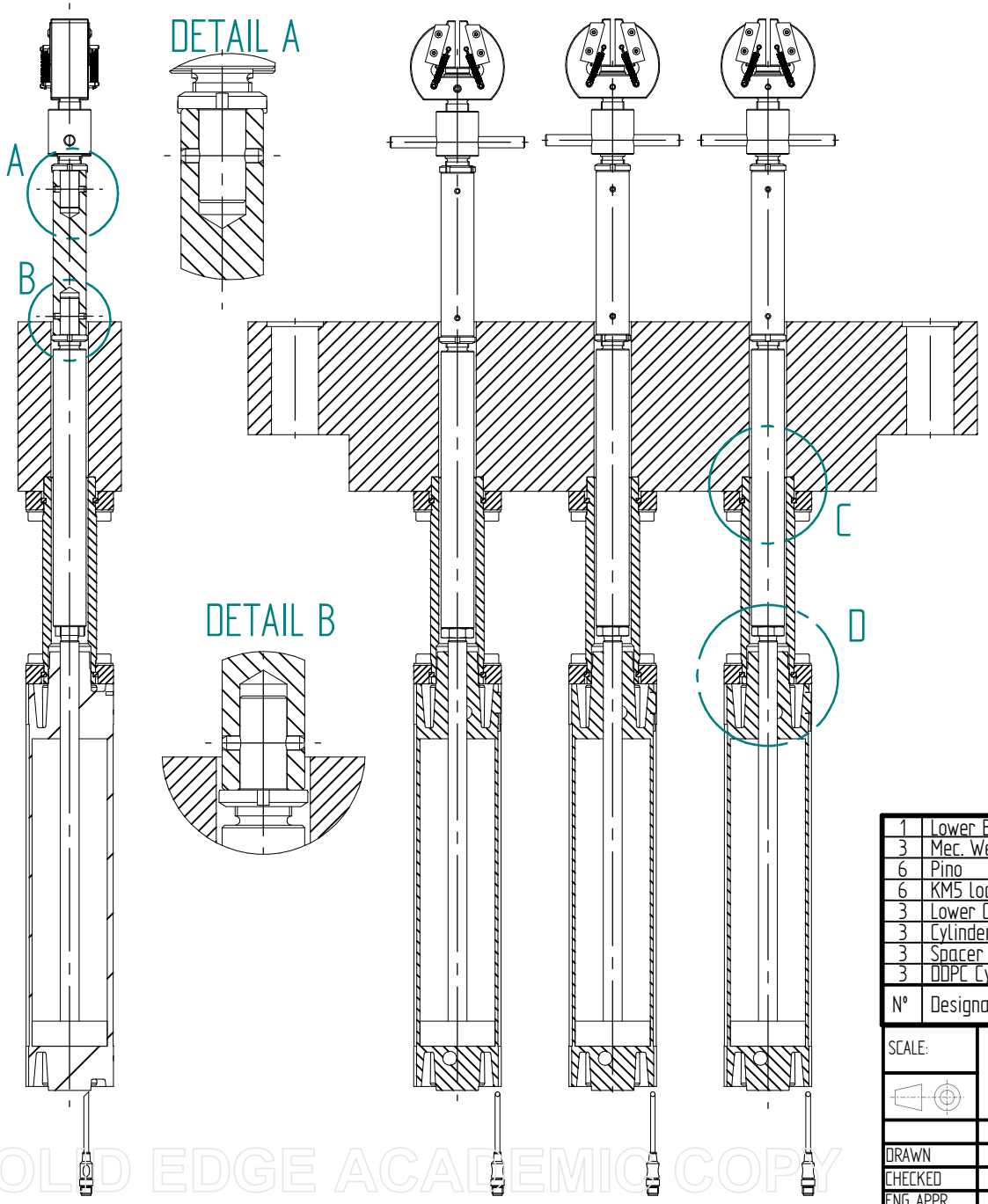

DETAIL A

DETAIL B

DETAIL C

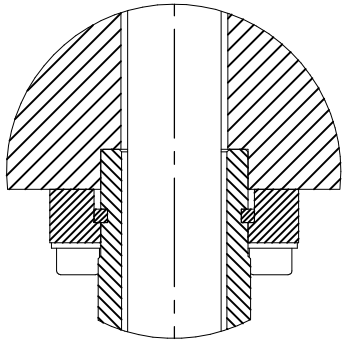

DETAIL D

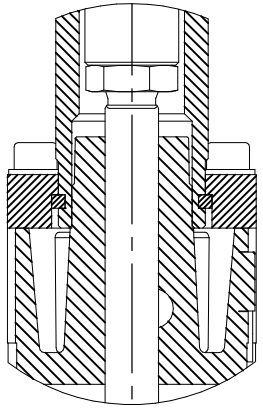

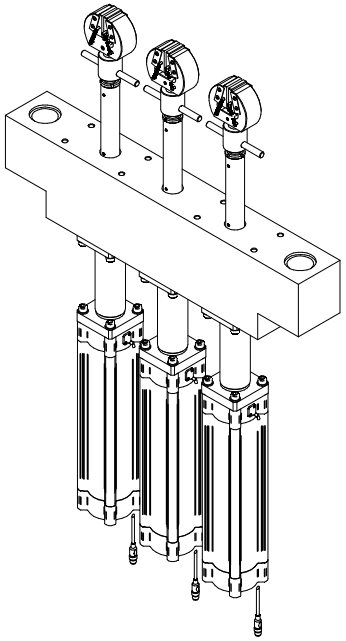

N°	Designação	Norma ou Desenho N°	Material	Rf	MOLDE n°-MATRIZ | PROD. SEMI-ACAB	MASSA	OBSERVAÇÕES
1	Lower Beam	MS-01		8			
3	Mec. Wedge Action Grip	GP-00		7			
6	Pino			6			
6	KM5 locknut			5			
3	Lower Coupling	LA-03		4			
3	Cylinder Extension	LA-02		3			
3	Spacer Bushing	LA-01		2			
3	DDPC Cylinder			1			

SCALE:	Toleranciamento ISO 8015 Tolerâncias gerais ISO 2768 - mH ISO 13920 Rugosidades Gerais ISO 1302 Cantos e Chanfros ISO 13715	OBSERVAÇÕES:

	NAME	DATE		
DRAWN	Luis Pina		TITLE: Lower Assembly	DWG NO LA-00
CHECKED	Luis Pina		FEUP SIZE A4	REV
ENG APPR	CM Silva		WEIGHT:	SHEET 1 OF 1
MGR APPR			QUANTITY:	

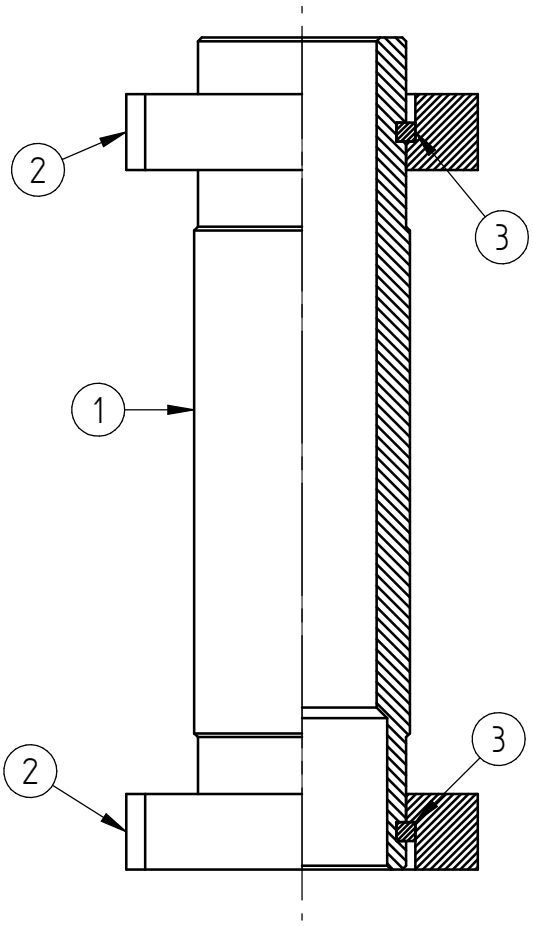

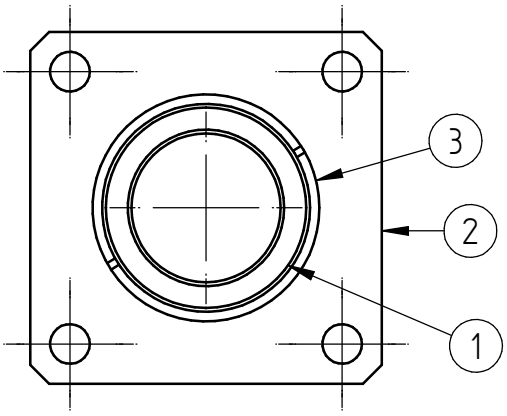

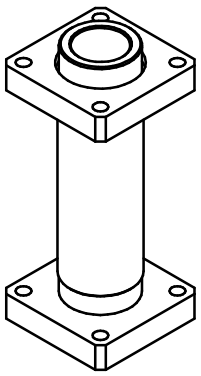

Nº	Designação	Norma ou Desenho Nº	Material	Rf	MOLDE nº-MATRIZ I PROD. SEMI-ACAB	MASSA	OBSERVAÇÕES
2	Chaveta Meio Disco	LA-013	RK442	3			
2	Flange	LA-012	CK45	2			
1	Tubo	LA-011	RK442	1			

SCALE:	Toleranciamento ISO 8015 Tolerâncias gerais ISO 2768 – mH ISO 13920 Rugosidades Gerais ISO 1302 Cantos e Chanfros ISO 13715		MATERIAL:		
	NAME	DATE	TITLE: Spacer Bushing		DWG NO LA-01
DRAWN	Luis Pina				
CHECKED	Luis Pina		FEUP	SIZE A4	WEIGHT: / REV
ENG APPR	CM Silva				
MGR APPR					QUANTITY: / SHEET 1 OF 1

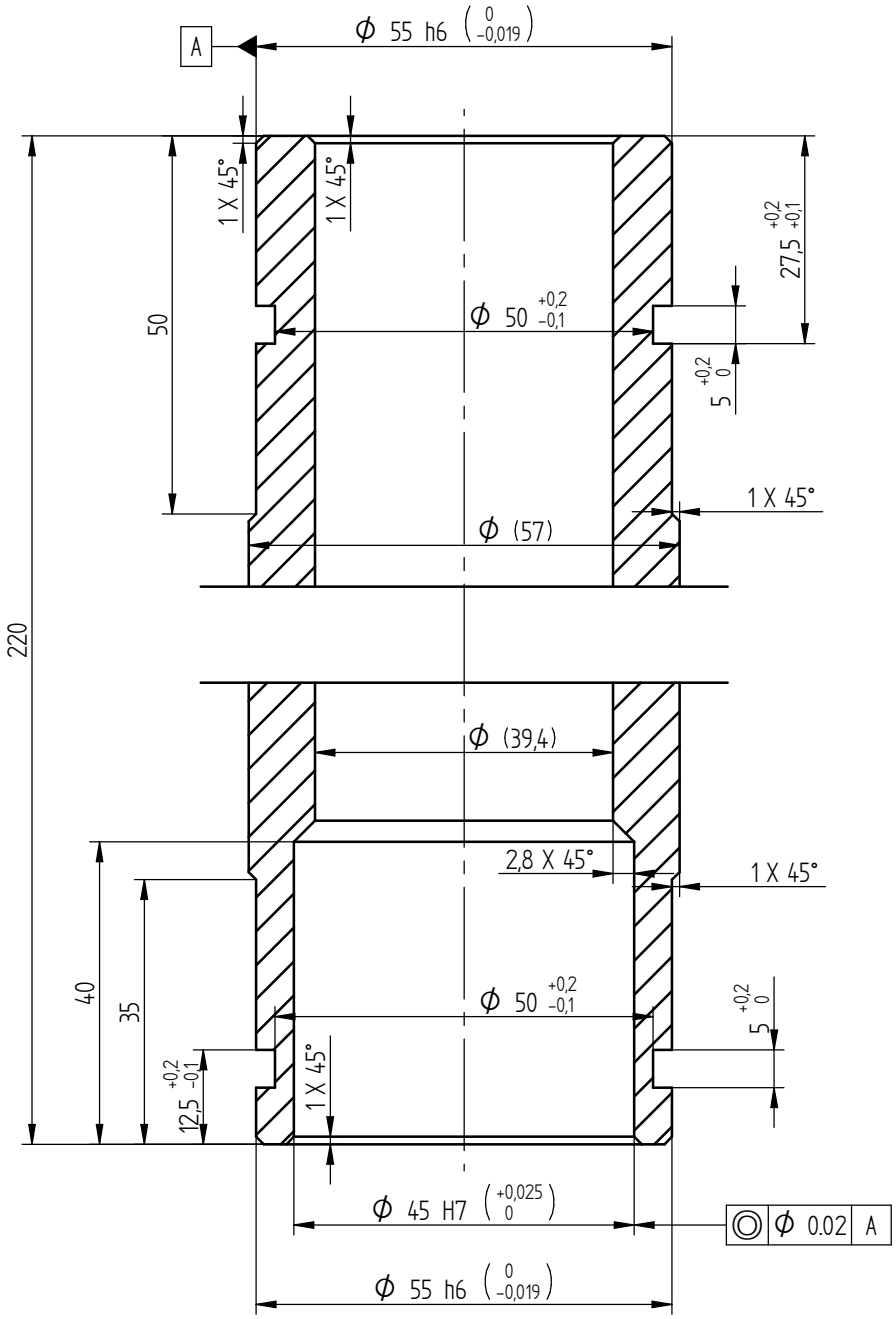

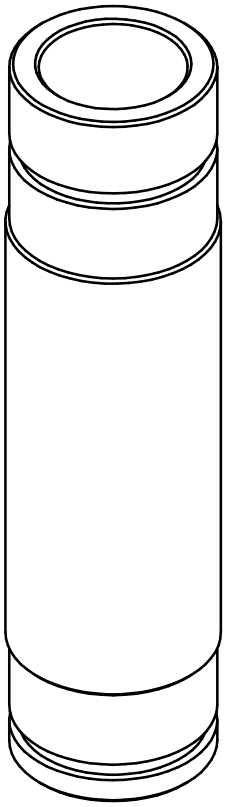

SCALE: 1:1	Toleranciamento ISO 8015 Tolerâncias gerais ISO 2768 – mH ISO 13920 Rugosidades Gerais ISO 1302 Cantos e Chanfros ISO 13715		MATERIAL: RK442		
	NAME	DATE	TITLE: SPACER		DWG NO LA-011
DRAWN					
CHECKED			FEUP	SIZE A4	WEIGHT: / REV
ENG APPR					
MGR APPR					QUANTITY: 3 / SHEET 1 OF 1

SECTION A-A

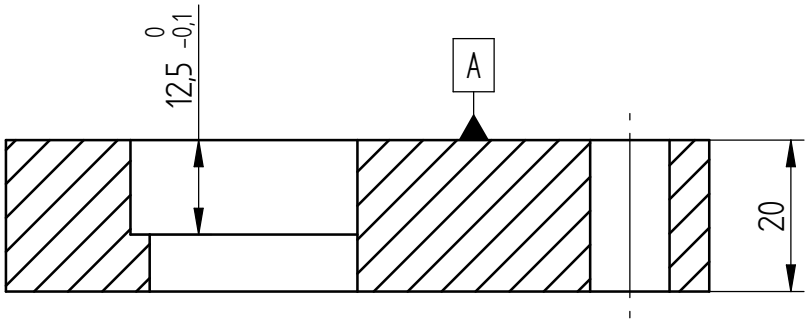

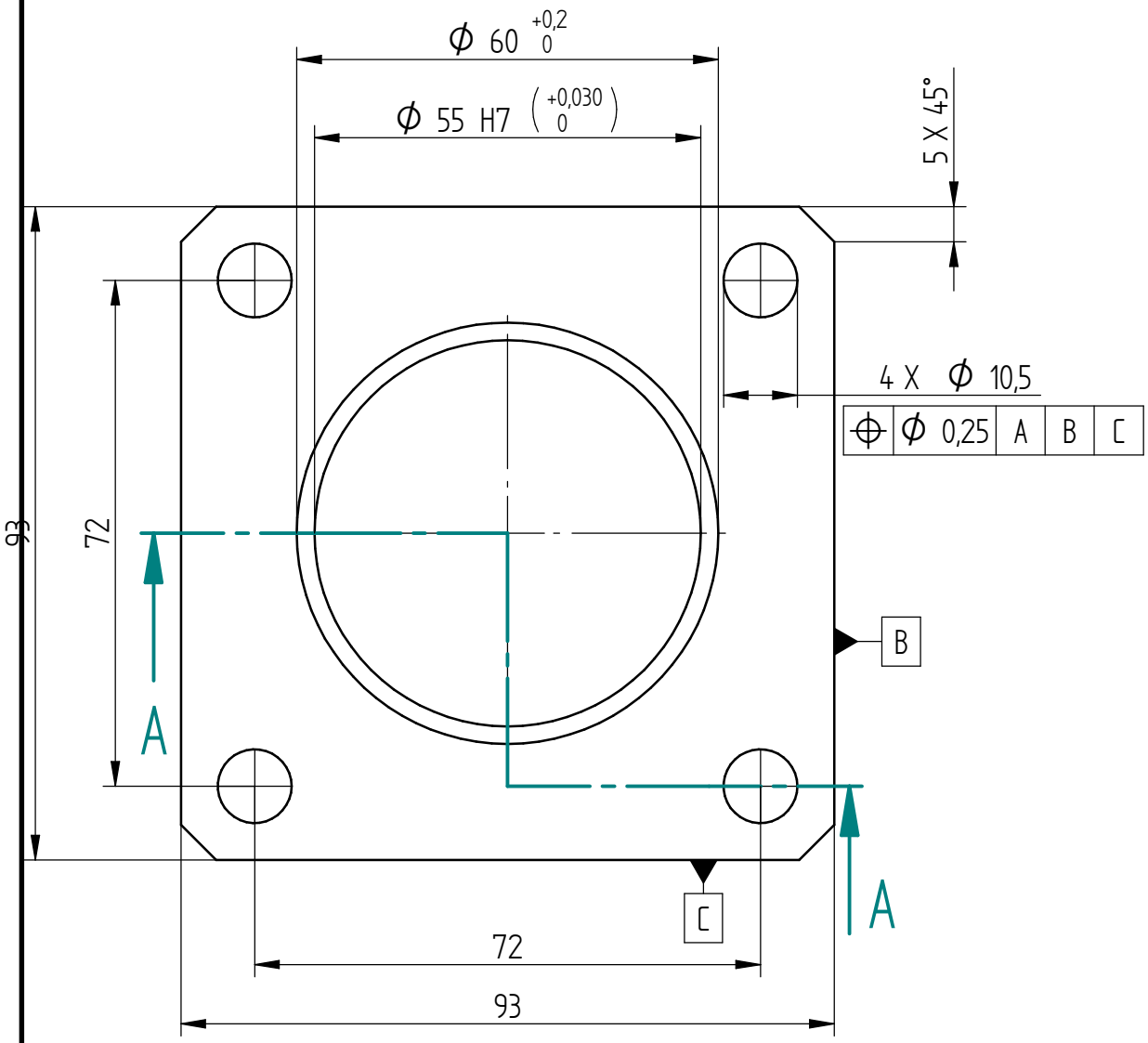

SCALE:	Toleranciamento ISO 8015 Tolerâncias gerais ISO 2768 - mH ISO 13920 Rugosidades Gerais ISO 1302 Cantos e Chanfros ISO 13715		MATERIAL: CK45		
	NAME	DATE	TITLE: FLANGE		DWG NO LA-012
DRAWN	Luis Pina	21/02/2016			
CHECKED	Luis Pina	21/02/2016	FEUP	SIZE A4	WEIGHT: / REV
ENG APPR	CM Silva				
MGR APPR					QUANTITY: 6 / SHEET 1 OF 1

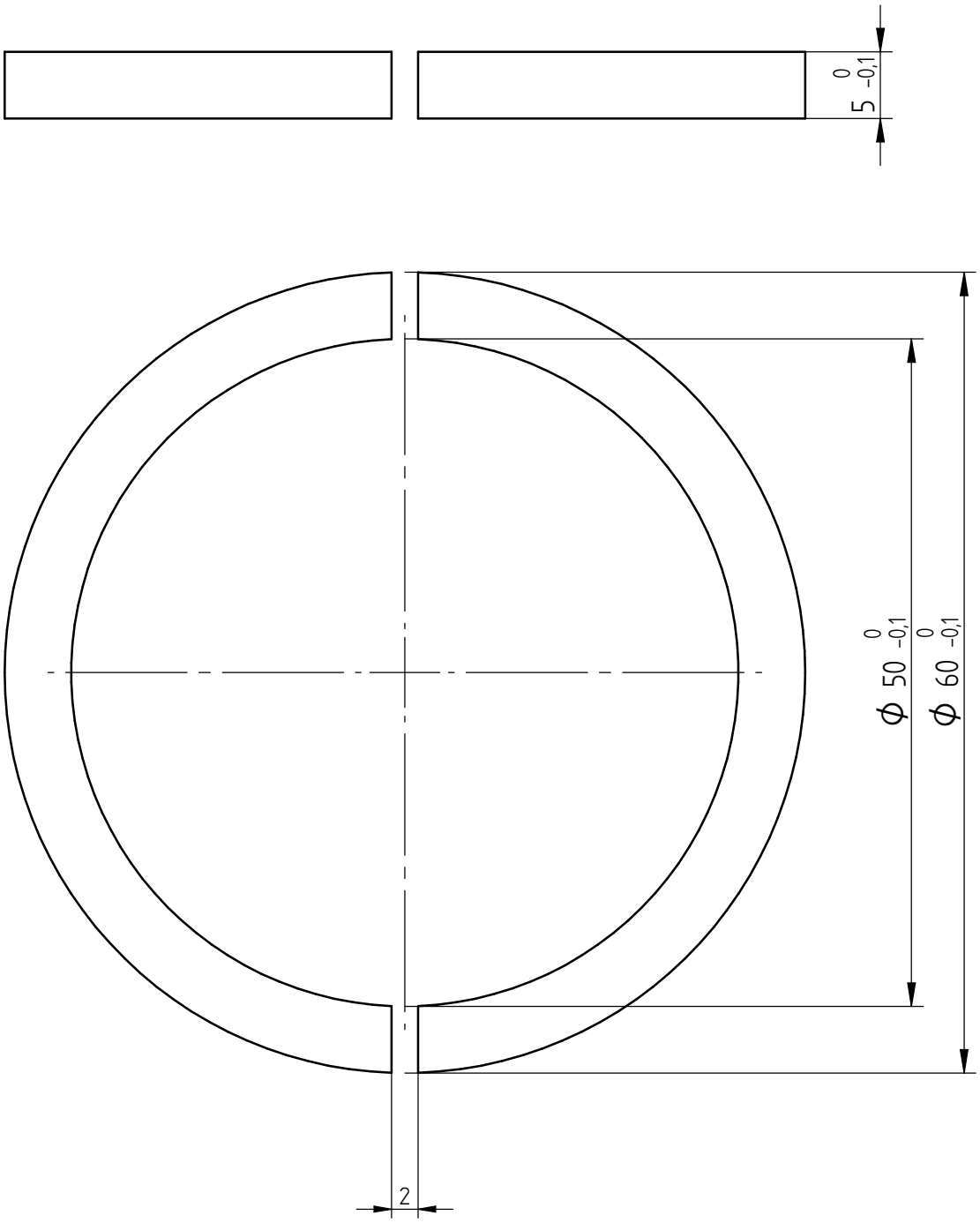

SCALE:	Toleranciamento ISO 8015 Tolerâncias gerais ISO 2768 – mH ISO 13920 Rugosidades Gerais ISO 1302 Cantos e Chanfros ISO 13715		MATERIAL: RK442		
	NAME	DATE	TITLE: Disc Type Key D50		DWG NO LA-013
DRAWN	Luis Pina				
CHECKED	Luis Pina		FEUP	SIZE A4	WEIGHT: / REV
ENG APPR	CM Silva				QUANTITY: 6 / SHEET 1 OF 1
MGR APPR					

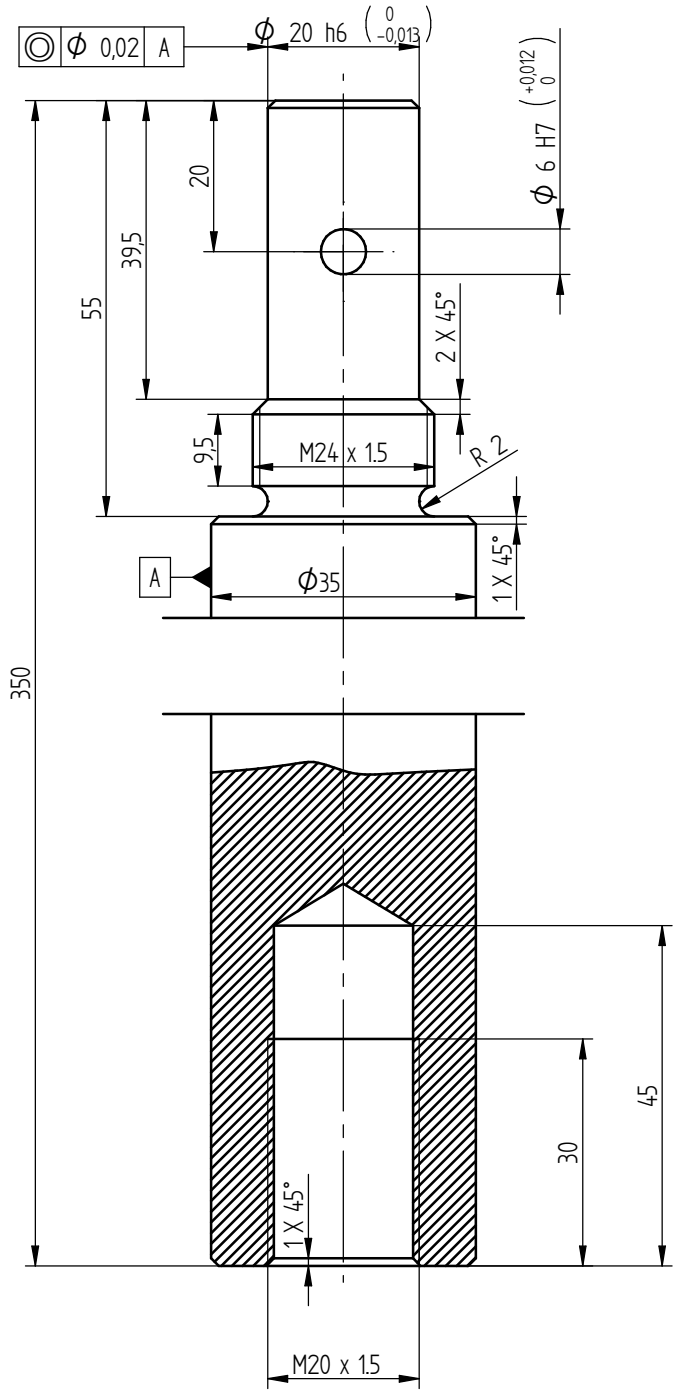

SCALE: 1:1	Tolerancimento ISO 8015 Tolerâncias gerais ISO 2768 – mH ISO 13920 Rugosidades Gerais ISO 1302 Cantos e Chanfros ISO 13715		MATERIAL:		
	NAME	DATE	TITLE: Cylinder Rod Extension		DWG NO LA-02
DRAWN	Luis Pina				
CHECKED	Luis Pina		FEUP	SIZE A4	WEIGHT: / REV
ENG APPR	CM Silva				QUANTITY: / SHEET 1 OF 1
MGR APPR					

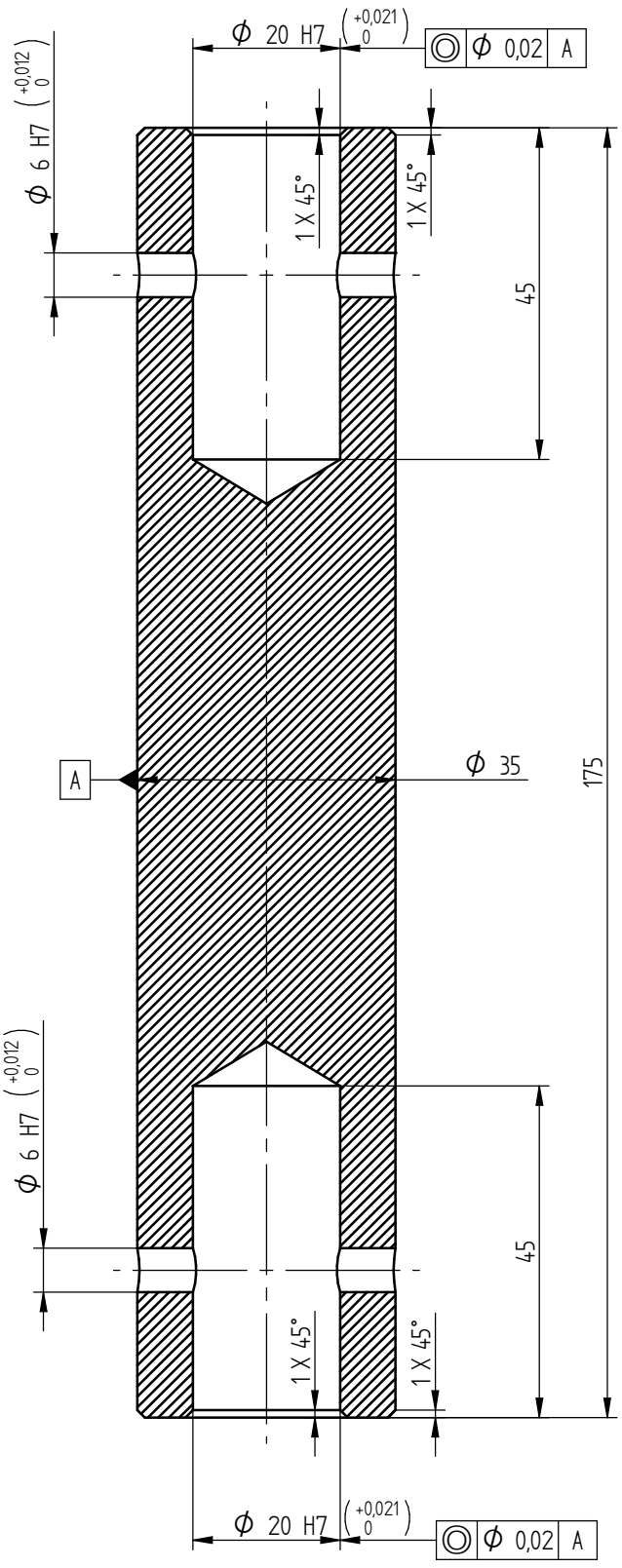

SCALE:	Toleranciamento ISO 8015 Tolerâncias gerais ISO 2768 – mH ISO 13920 Rugosidades Gerais ISO 1302 Cantos e Chanfros ISO 13715		MATERIAL: AISI 304		PERFIL RED35
			MATERIAL: quebrar arestas		
	NAME	DATE	TITLE: Lower Coupling		DWG NO LA-03
DRAWN	Luis Pina				
CHECKED	Luis Pina		FEUP	SIZE A4	WEIGHT: / REV
ENG APPR	CM Silva				QUANTITY: 3 / SHEET 1 OF 1
MGR APPR					

A.3 Upper Assembly

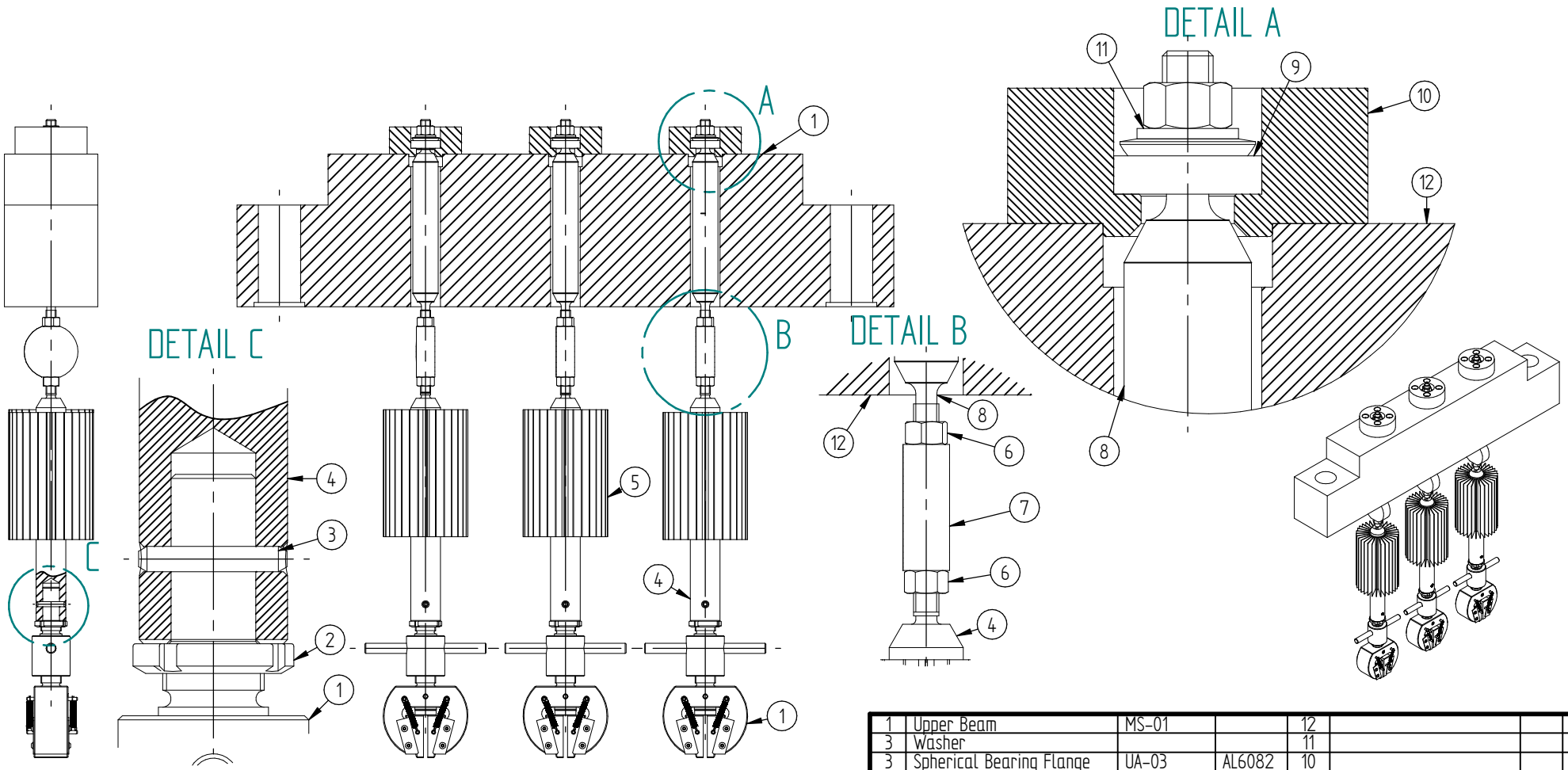

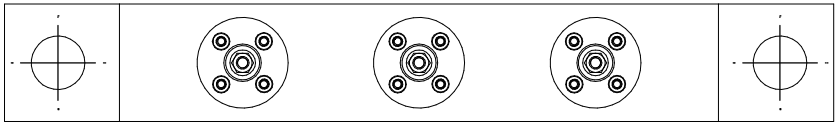

Nº	Designação	Norma ou Desenho Nº	Material	Rf	MOLDE nº-MATRIZ | PROD. SEMI-ACAB	MASSA	OBSERVAÇÕES
1	Upper Beam	MS-01		12			
3	Washer			11			
3	Spherical Bearing Flange	UA-03	AL6082	10			
3	Axial Spherical Bearing			9			
3	Spherical Bearing Extension	UA-02	AISI 304	8			
3	Load Cell			7			
9	M12x1.75 Nut			6			
3	Heat Sink			5			
3	Upper Coupling	UA-01	RK442	4			
3	Pin 6 x 20			3			
6	KM5 locknut		AL 7075	2			
3	Mec. Wedge Action Grip	GP-00	AL 7075	1			

SCALE:	Toleranciamento ISO 8015 Tolerâncias gerais ISO 2768 - mH ISO 13920 Rugosidades Gerais ISO 1302 Cantos e Chanfros ISO 13715	OBSERVAÇÕES:

	NAME	DATE	TITLE: Upper Assembly	DWG NO UA-00
DRAWN	Luis Pina			
CHECKED	Luis Pina		FEUP	REV
ENG APPR	CM Silva		SIZE A4	WEIGHT:
MGR APPR				QUANTITY: SHEET 1 OF 1

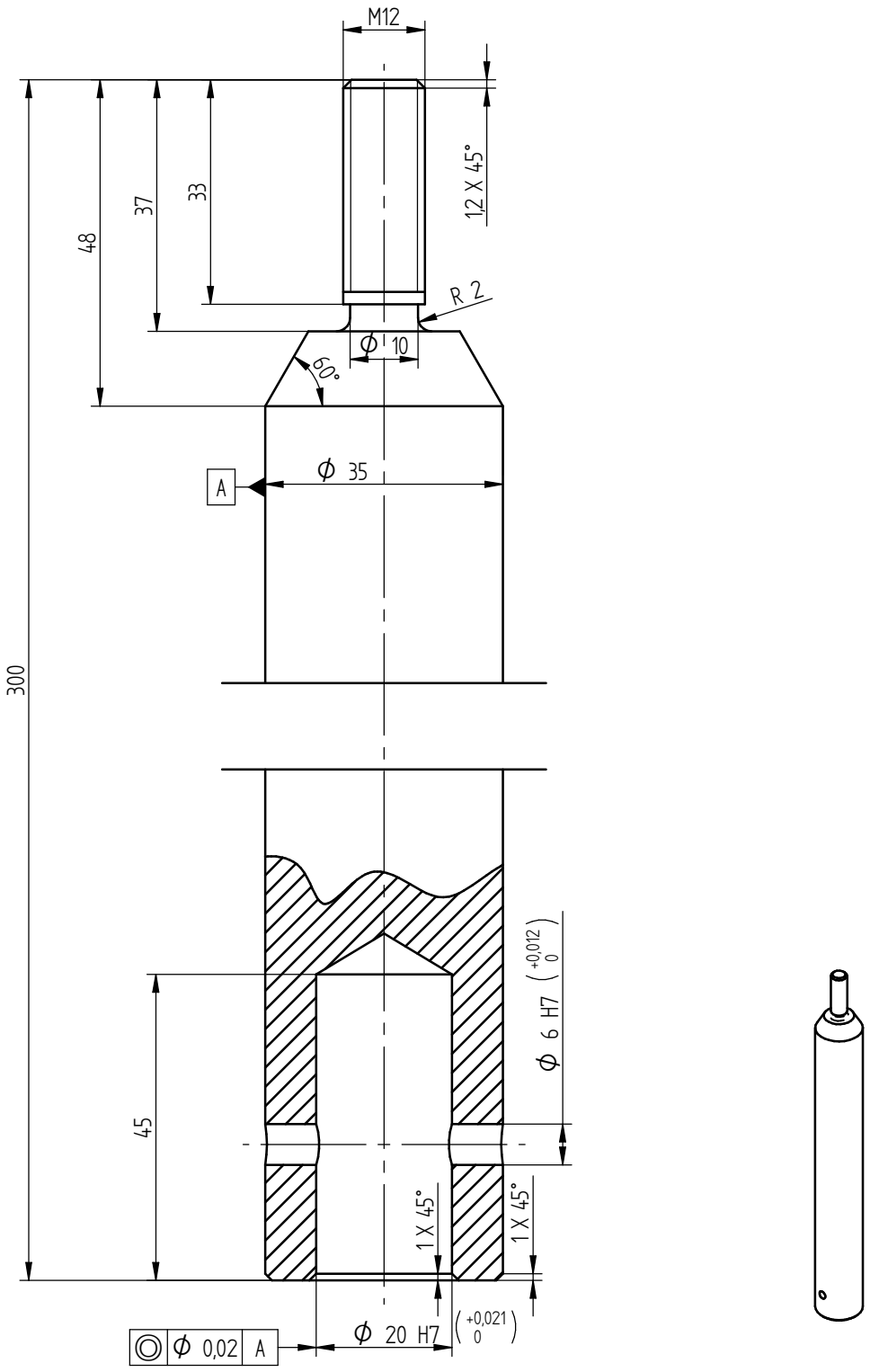

SCALE: 1:5	Toleranciamento ISO 8015 Tolerâncias gerais ISO 2768 – mH ISO 13920 Rugosidades Gerais ISO 1302 Cantos e Chanfros ISO 13715		MATERIAL: AISI 304 PERFIL RED35		
	NAME	DATE	TITLE: Upper Coupling		DWG NO UA-01
DRAWN	Luis Pina				
CHECKED	Luis Pina		FEUP	SIZE A4	WEIGHT: / REV
ENG APPR	CM Silva				
MGR APPR					QUANTITY: 3 / SHEET 1 OF 1

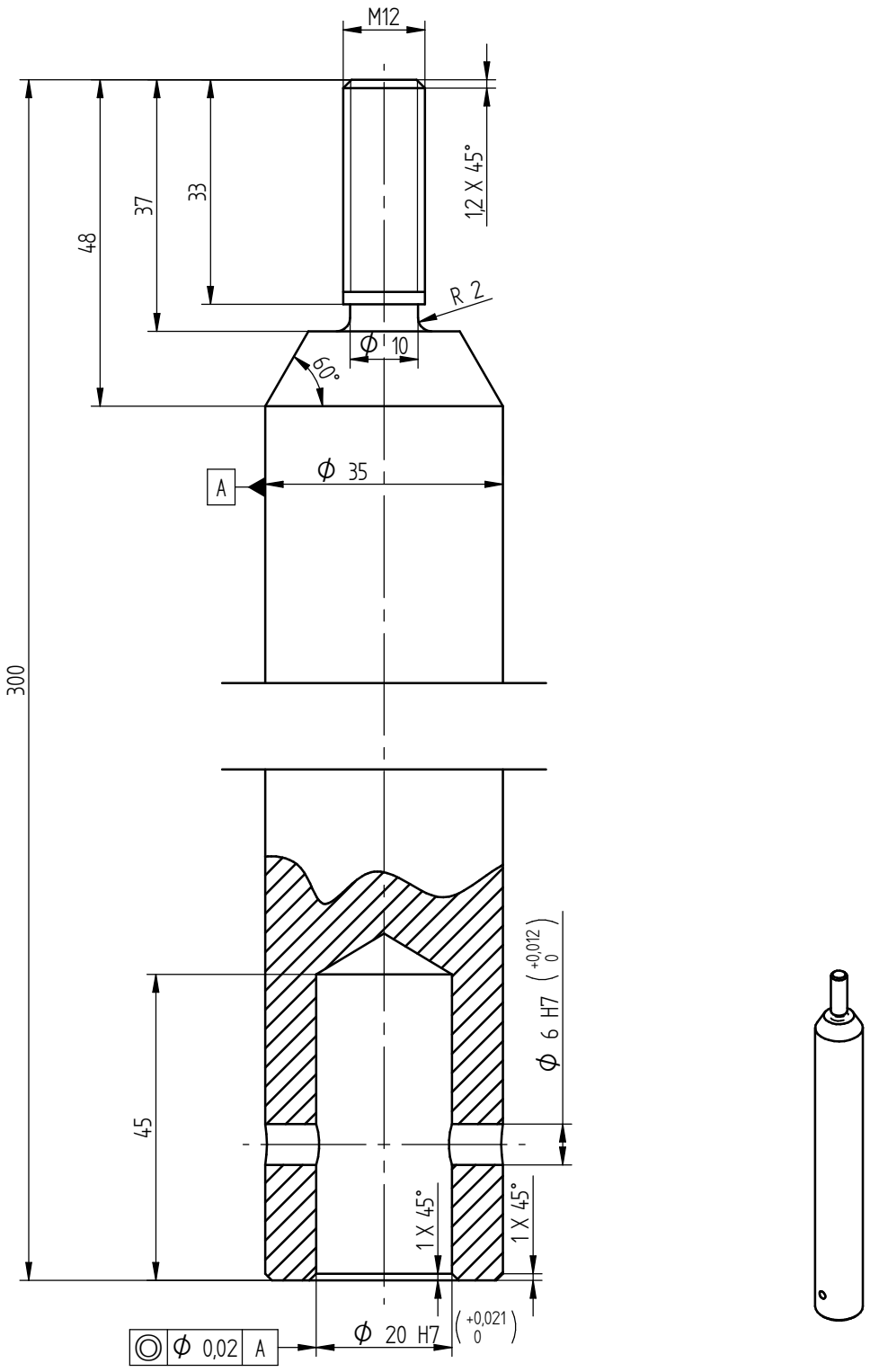

SCALE: 1:5	Toleranciamento ISO 8015 Tolerâncias gerais ISO 2768 – mH ISO 13920 Rugosidades Gerais ISO 1302 Cantos e Chanfros ISO 13715		MATERIAL: AISI 304 PERFIL RED35		
	NAME	DATE	TITLE: Upper Coupling		DWG NO UA-01
DRAWN	Luis Pina				
CHECKED	Luis Pina		FEUP	SIZE A4	WEIGHT: / REV
ENG APPR	CM Silva				
MGR APPR					QUANTITY: 3 / SHEET 1 OF 1

SECTION A-A

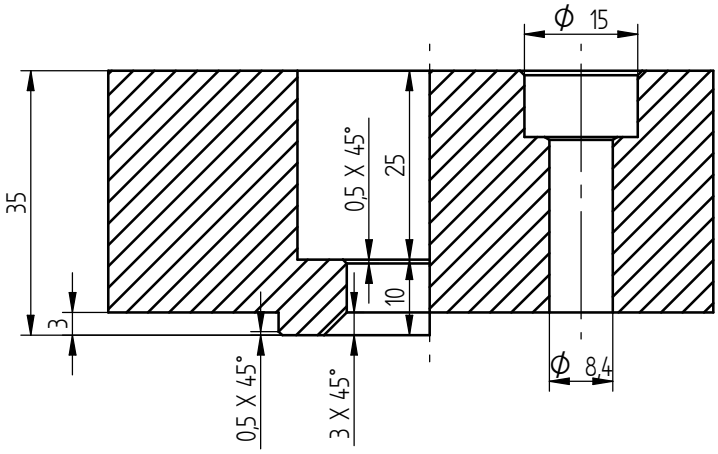

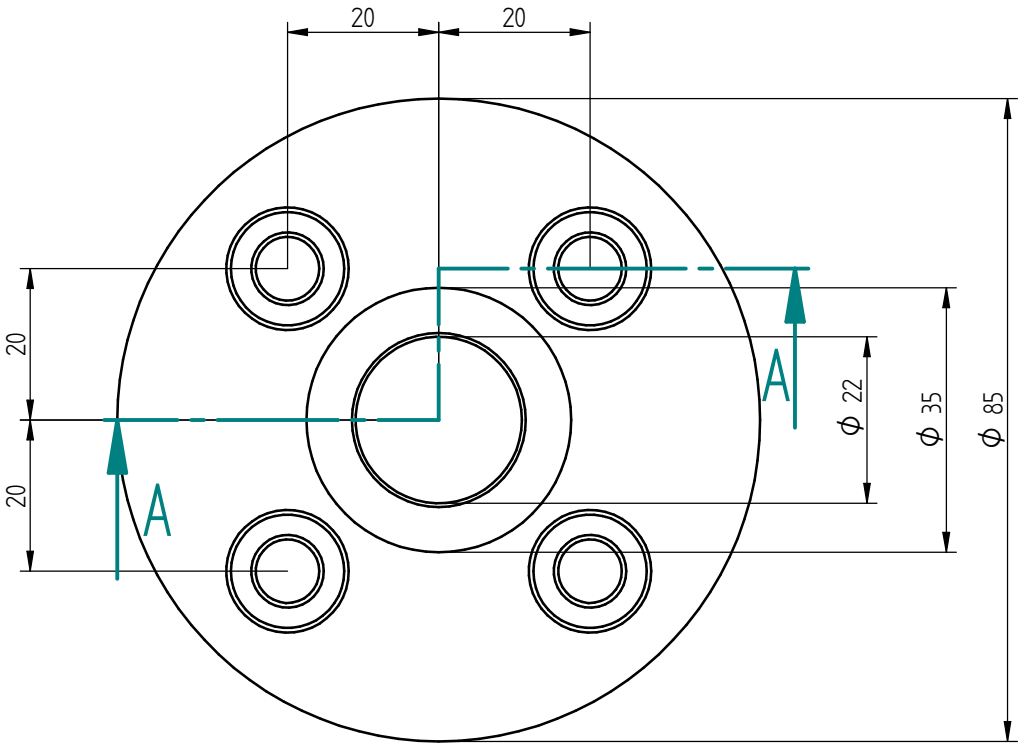

SCALE:	Tolerancimento ISO 8015 Tolerâncias gerais ISO 2768 - mH ISO 13920 Rugosidades Gerais ISO 1302 Cantos e Chanfros ISO 13715		MATERIAL: AL6082		
	NAME	DATE	TITLE: Spherical Bearing Flange		DWG NO UA-03
DRAWN	Luis Pina				
CHECKED	Luis Pina		FEUP	SIZE A4	WEIGHT: / REV
ENG APPR	CM Silva				
MGR APPR					QUANTITY: / SHEET 1 OF 1

A.4 Mechanical Structure

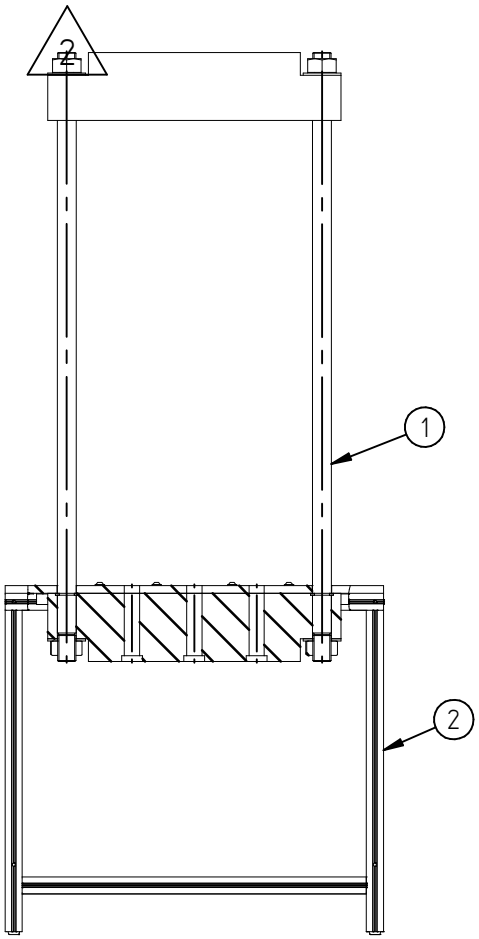

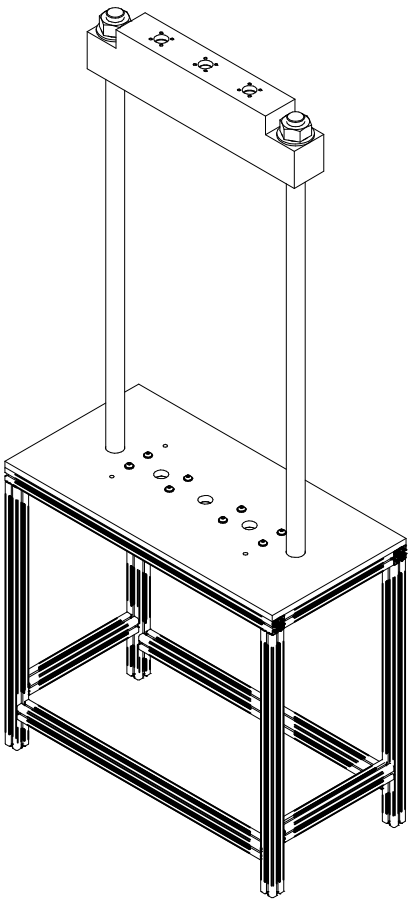

Nº	Designação	Norma ou Desenho Nº	Material	Rf	MOLDE nº-MATRIZ I PROD. SEMI-ACAB	MASSA	OBSERVAÇÕES
8	Washer			4			
8	Screw			3			
1	Support Frame	MS-02		2			
1	Test Frame	MS-01		1			

SCALE:	Toleranciamento ISO 8015 Tolerâncias gerais ISO 2768 - mH ISO 13920 Rugosidades Gerais ISO 1302 Cantos e Chanfros ISO 13715	OBSERVAÇÕES:			
	NAME	DATE	TITLE: Mechanical Structure		DWG NO MS-00
DRAWN	Luis Pina				
CHECKED	Luis Pina		FEUP	SIZE A4	WEIGHT: / REV
ENG APPR	CM Silva				QUANTITY: / SHEET 1 OF 1
MGR APPR					

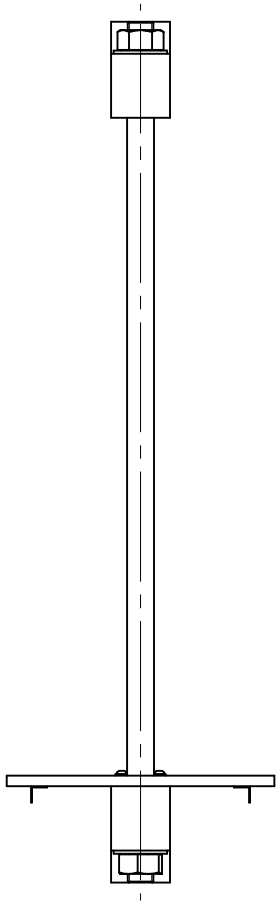

SECTION A-A

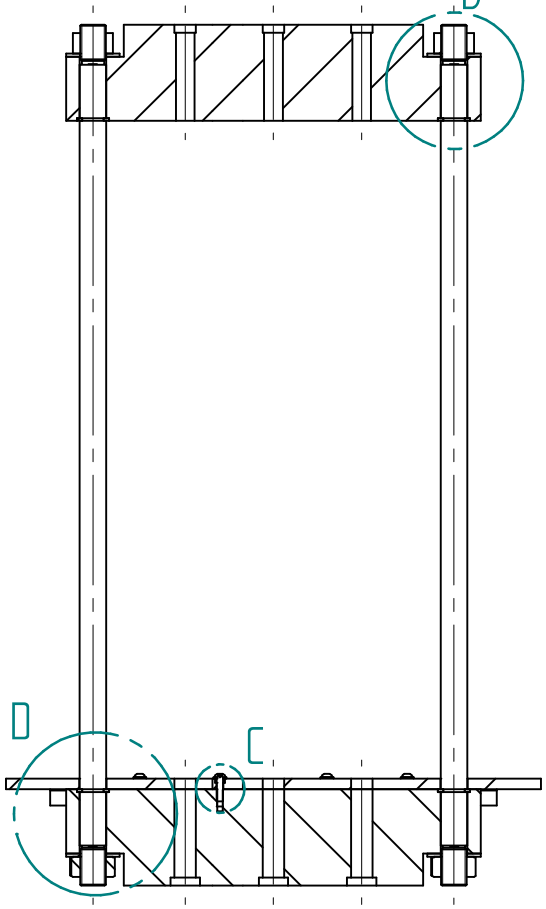

DETAIL B

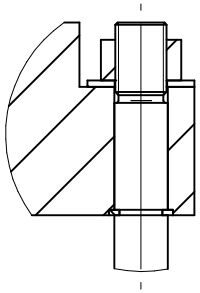

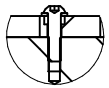

DETAIL C

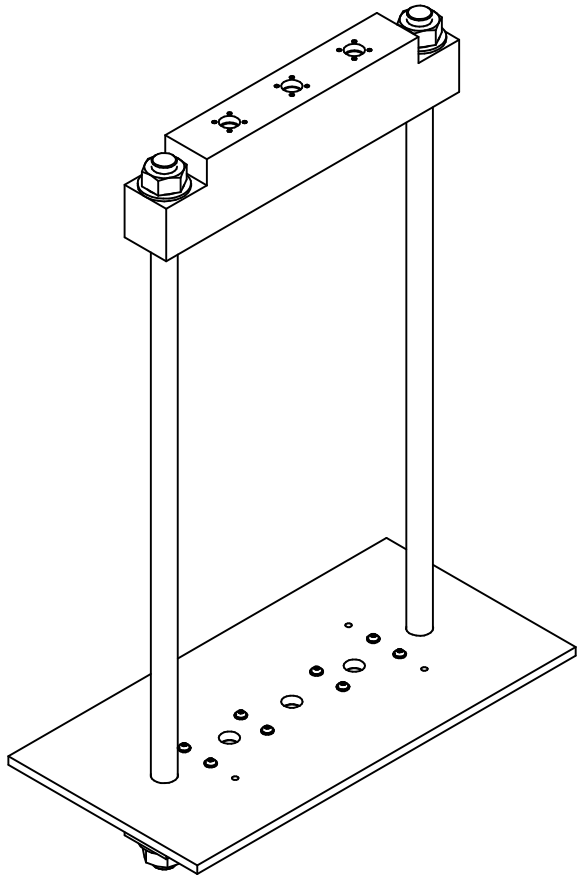

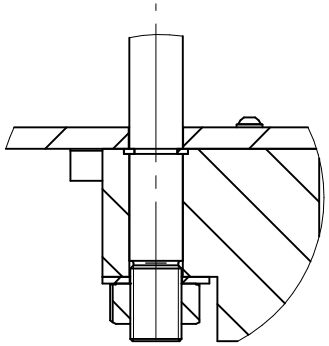

DETAIL D

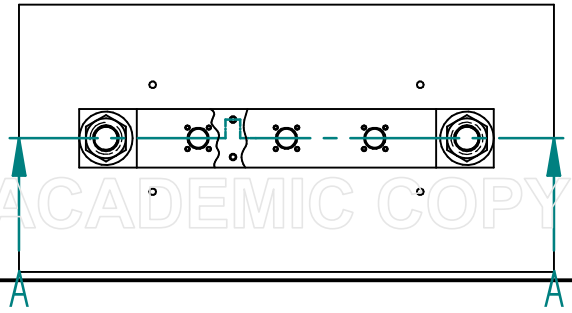

Nº	Designação	Norma ou Desenho Nº	Material	Rf	MOLDE nº-MATRIZ | PROD. SEMI-ACAB	MASSA	OBSERVAÇÕES
8	Washer			10			
8	Screw M12 x 45	ISO 7849		9			
2	L - profile			8			
1	Aluminium Plate	MS-015		7			KMS
4	Nut M48			6			
4	Washer M48			5			
4	Chaveta Meio Disco	MS-014	RK442	4			
2	Coluna	MS-013	CK45	3			Cuddel
1	Trave Superior	MS-012	AL 7075	2			KMS
1	Trave Inferior	MS-011	AL 7075	1			KMS

SCALE:

Toleranciamento ISO 8015
Tolerâncias gerais ISO 2768 - mH ISO 13920
Rugosidades Gerais ISO 1302
Cantos e Chanfros ISO 13715

OBSERVAÇÕES:

	NAME	DATE
DRAWN	Luis Pina	
CHECKED	Luis Pina	
ENG APPR	CM Silva	
MGR APPR		

TITLE: ESTRUTURA

DWG NO MS-01

FEUP

SIZE A4

WEIGHT:

REV

QUANTITY:

SHEET 1 OF 1

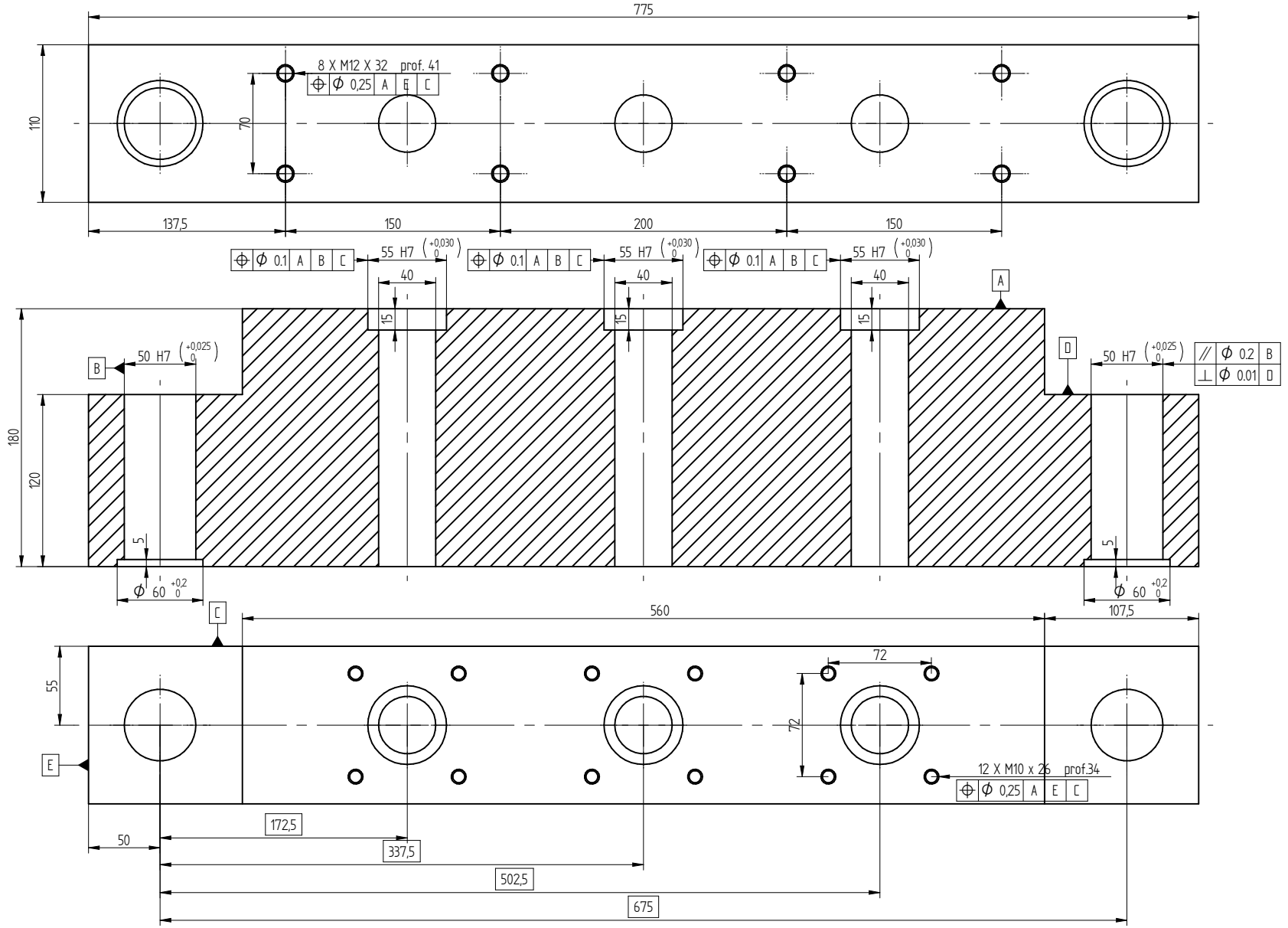

SCALE:	Toleranciamento ISO 8015 Tolerâncias gerais ISO 2768 – mH ISO 13920 Rugosidades Gerais ISO 1302 Cantos e Chanfros ISO 13715		MATERIAL: ALUMINIO 7075 T651	
			NOTAS:	
	NAME	DATE	TITLE: TRAVE INFERIOR	DWG NO 201
DRAWN	Luis Pina	21/02/2016		
CHECKED	Luis Pina	07/06/2016	FEUP	REV
ENG APPR	CM Silva		SIZE A4 / WEIGHT:	
MGR APPR			QUANTITY:	SHEET 1 OF 1

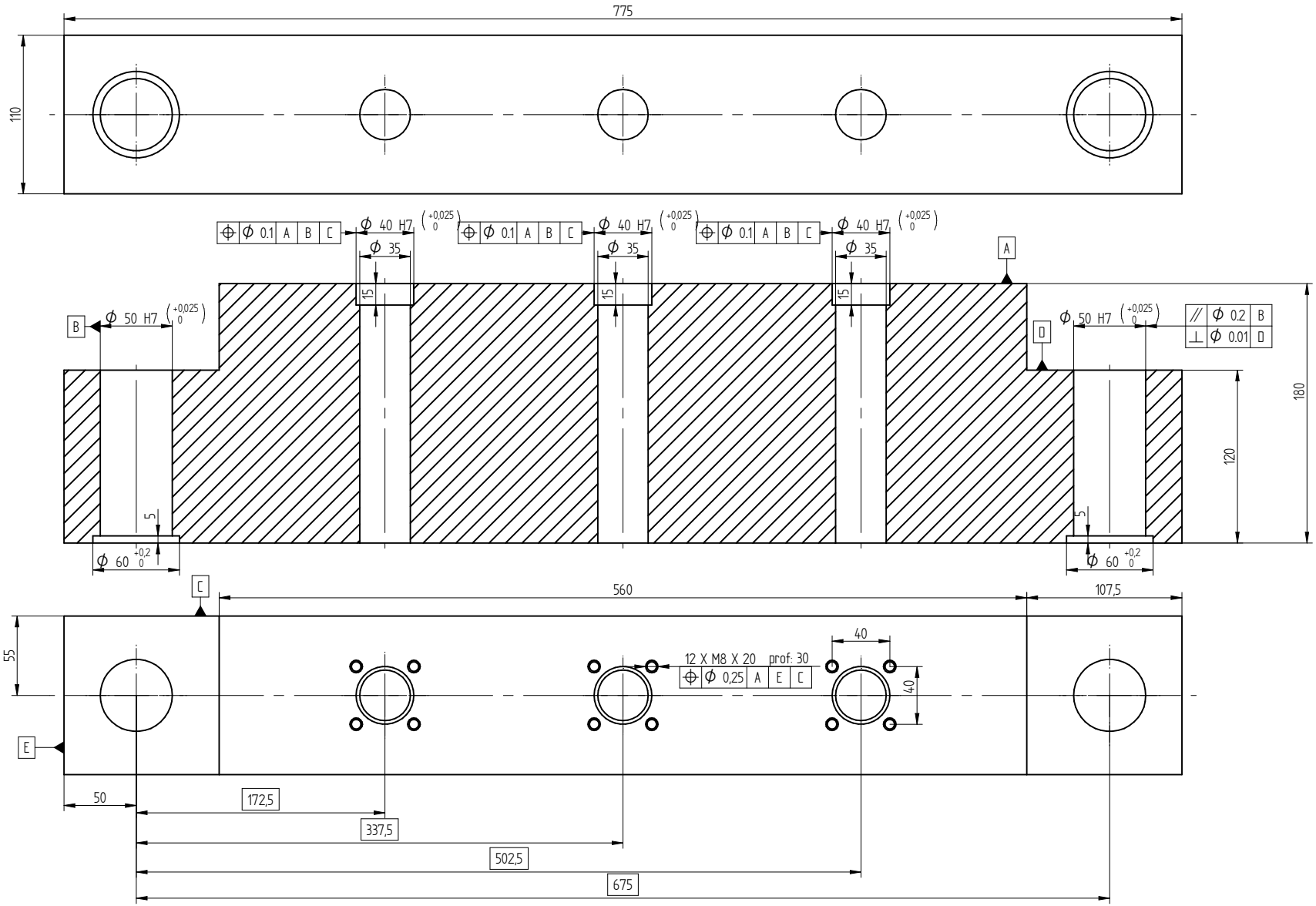

SCALE:	Toleranciamento ISO 8015 Tolerâncias gerais ISO 2768 – mH ISO 13920 Rugosidades Gerais ISO 1302 Cantos e Chanfros ISO 13715		MATERIAL: ALUMINIO 7075 T651		
	NAME	DATE	TITLE: TRAVE SUPERIOR		DWG NO 202
DRAWN	Luis Pina	21/02/2016			
CHECKED	Luis Pina	21/02/2016	FEUP	SIZE A4	WEIGHT: / REV
ENG APPR	CM Silva				QUANTITY: / SHEET 1 OF 1
MGR APPR					

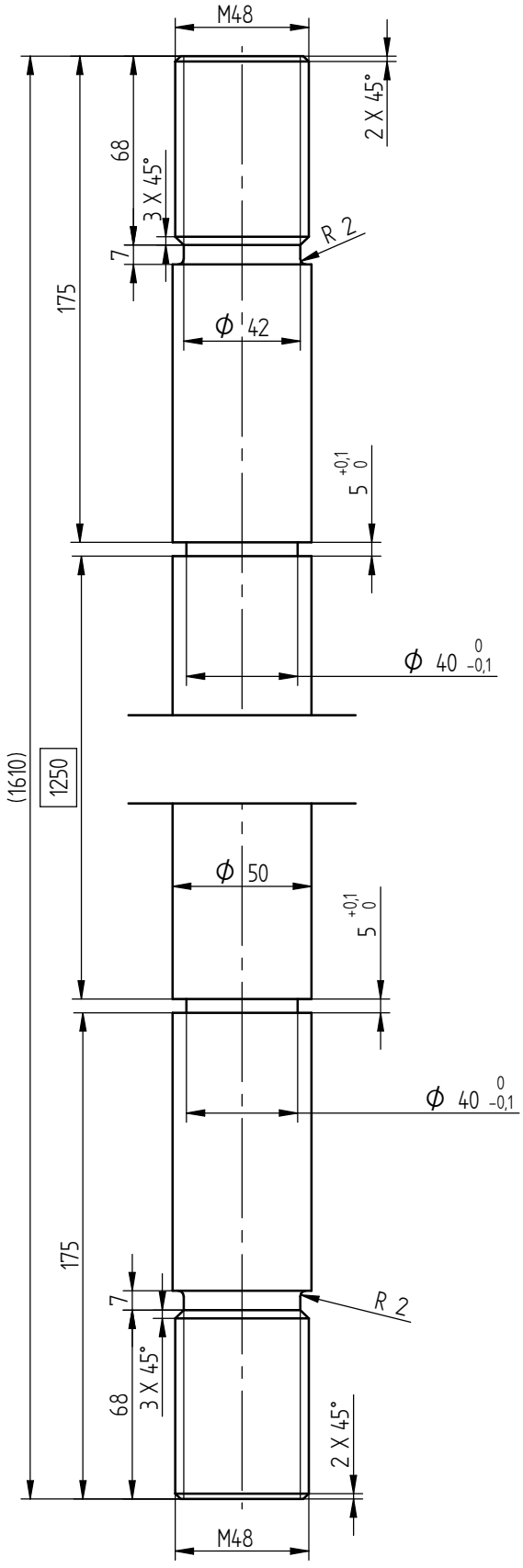

SCALE:	Toleranciamento ISO 8015 Tolerâncias gerais ISO 2768 – mH ISO 13920 Rugosidades Gerais ISO 1302 Cantos e Chanfros ISO 13715		MATERIAL: HASTE CROMADA			
	NAME	DATE	TITLE: COLUNA			DWG NO 203
DRAWN	Luis Pina	21/02/2016				
CHECKED	Luis Pina	21/02/2016	FEUP	SIZE A4	WEIGHT:	REV
ENG APPR	CM Silva				QUANTITY: 2	SHEET 1 OF 1
MGR APPR						

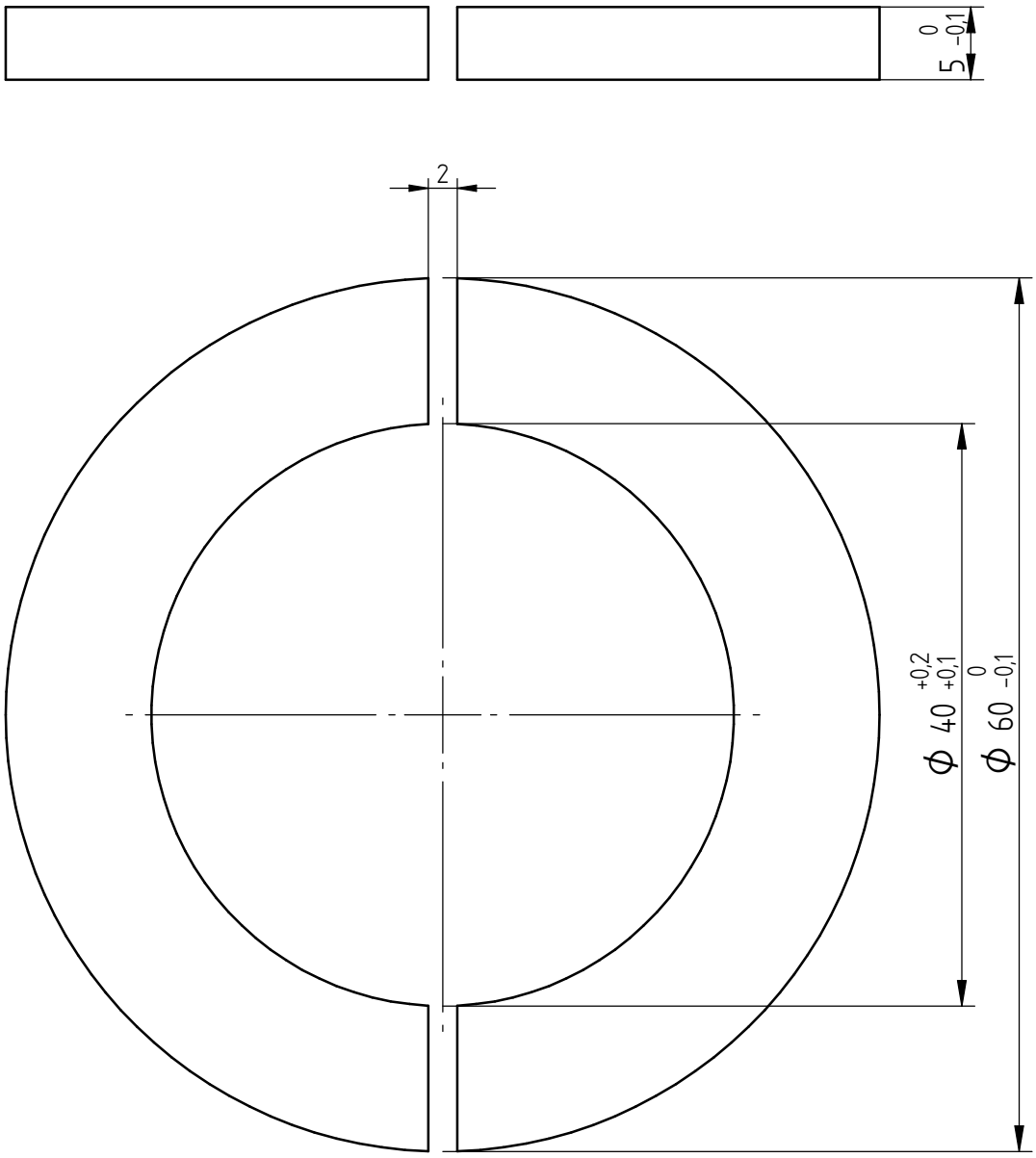

SCALE:	Tolerancimento ISO 8015 Tolerâncias gerais ISO 2768 – mH ISO 13920 Rugosidades Gerais ISO 1302 Cantos e Chanfros ISO 13715		MATERIAL: RK442		
	NAME	DATE	TITLE: DISCO CHAVETA		DWG NO 204
DRAWN	Luis Pina	21/02/2016			
CHECKED	Luis Pina	21/02/2016	FEUP	SIZE A4	WEIGHT: / REV
ENG APPR	CM Silva				
MGR APPR					QUANTITY: / SHEET 1 OF 1

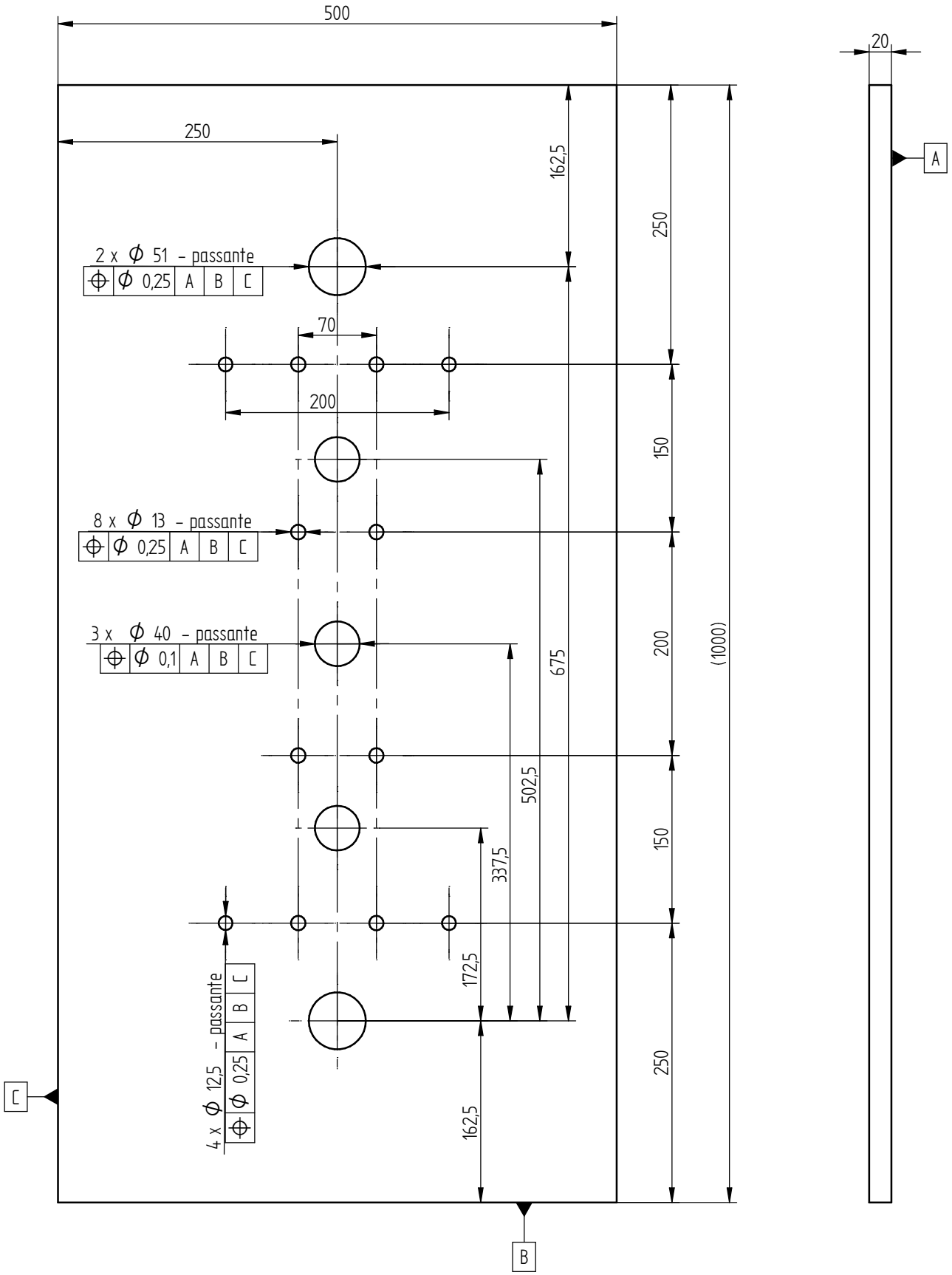

SCALE: 1:5	Toleranciamento ISO 8015 Tolerâncias gerais ISO 2768 – mH ISO 13920 Rugosidades Gerais ISO 1302 Cantos e Chanfros ISO 13715		MATERIAL: AL7000		
	NAME	DATE	TITLE: Aluminium Plate		DWG NO MS-015
DRAWN	Luis Pina				
CHECKED	Luis Pina		FEUP	SIZE A4	WEIGHT: / REV
ENG APPR	CM Silva				
MGR APPR					QUANTITY: / SHEET 1 OF 1

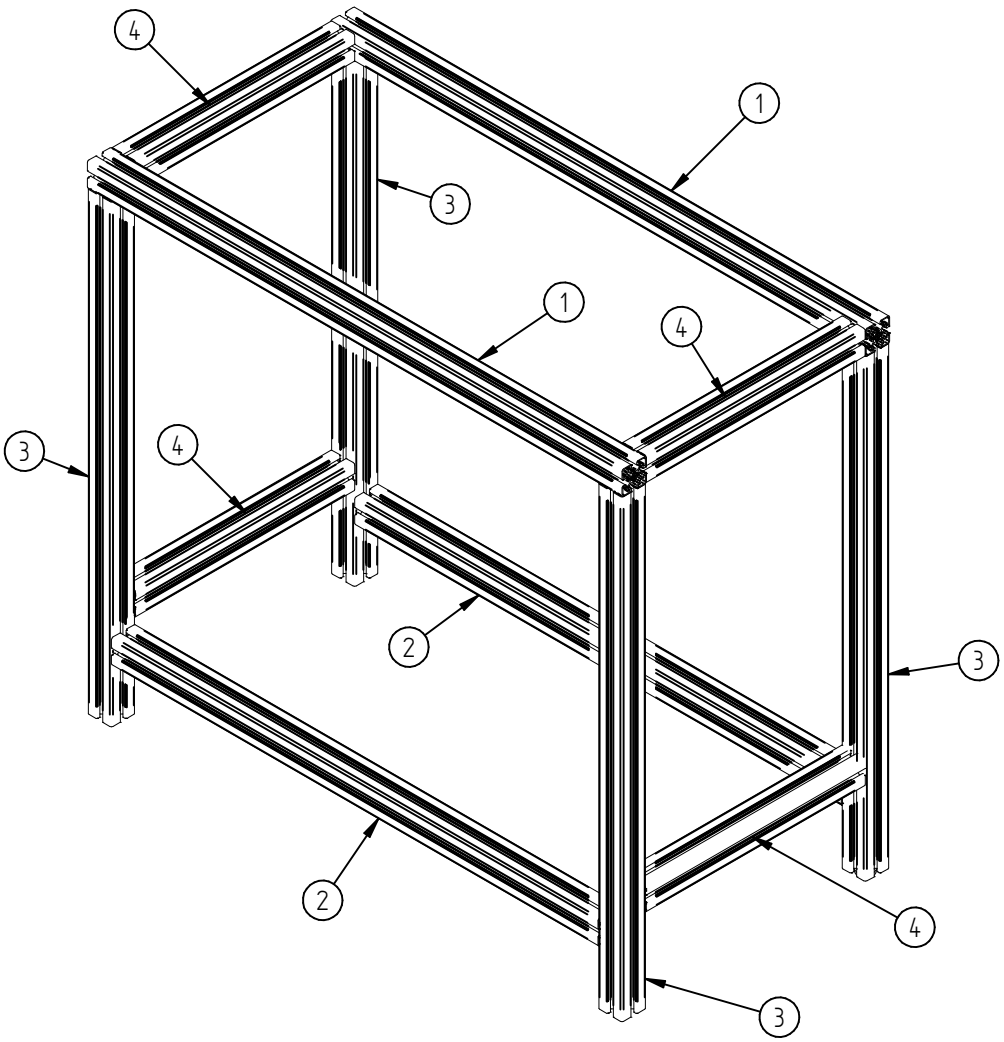

Nº	Designação	Norma ou Desenho Nº	Material	Rf	MOLDE nº-MATRIZ | PROD. SEMI-ACAB	MASSA	OBSERVAÇÕES
4	Screw S12x30-T50 LE100			5			
4	Bosch 45x45L 410			4			
4	Bosch 45x45L 850	MS-022		3			
2	Bosch 45x45L 910			2			
2	Bosch 45x45L 1000	MS-021		1			

SCALE: 1:10	Toleranciamento ISO 8015 Tolerâncias gerais ISO 2768 - mH ISO 13920 Rugosidades Gerais ISO 1302 Cantos e Chanfros ISO 13715	OBSERVAÇÕES:

	NAME	DATE				
DRAWN	Luis Pina		TITLE: Support Frame			DWG NO MS-02
CHECKED	Luis Pina		FEUP	SIZE A4	WEIGHT:	REV
ENG APPR	CM Silva				QUANTITY:	SHEET 1 OF 1
MGR APPR						

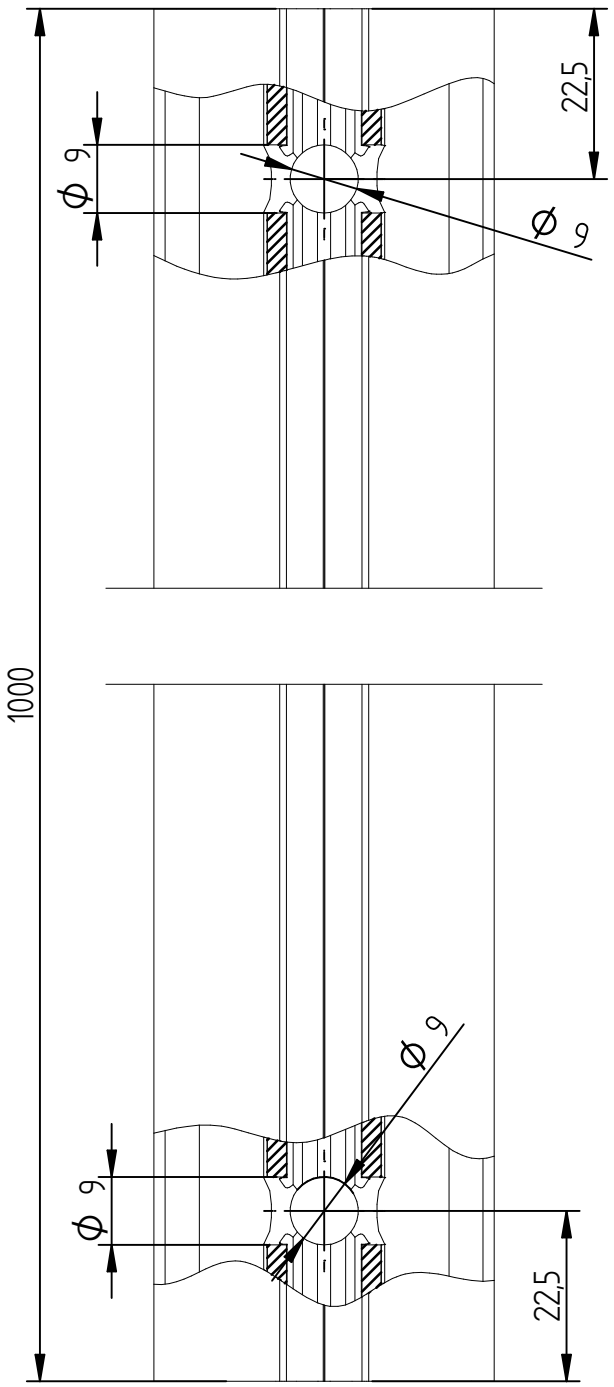

SCALE:	Tolerancimento ISO 8015 Tolerâncias gerais ISO 2768 – mH ISO 13920 Rugosidades Gerais ISO 1302 Cantos e Chanfros ISO 13715		MATERIAL:		
	NAME	DATE	TITLE: Bosch Profile 45x45L 1000		DWG NO MS-021
DRAWN	Luis Pina				
CHECKED	Luis Pina		FEUP	SIZE A4	WEIGHT: / REV
ENG APPR	CM Silva				
MGR APPR					QUANTITY: 4 / SHEET 1 OF 1

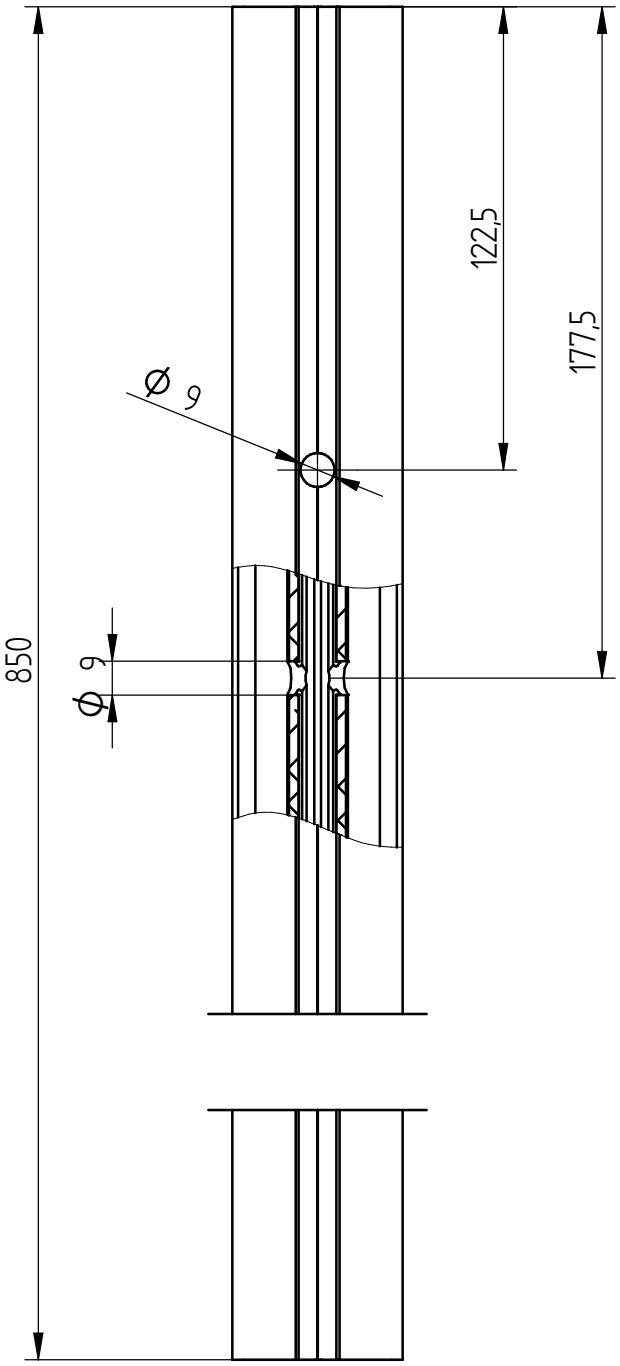

SCALE: 1:2	Tolerancimento ISO 8015 Tolerâncias gerais ISO 2768 – mH ISO 13920 Rugosidades Gerais ISO 1302 Cantos e Chanfros ISO 13715		MATERIAL:		
	NAME	DATE	TITLE: Bosch Profile 45x45L 850		DWG NO MS-022
DRAWN	Luis Pina				
CHECKED	Luis Pina		FEUP	SIZE A4	WEIGHT: / REV
ENG APPR	CM Silva				QUANTITY: 4 / SHEET 1 OF 1
MGR APPR					

Appendix B

Electric Circuit

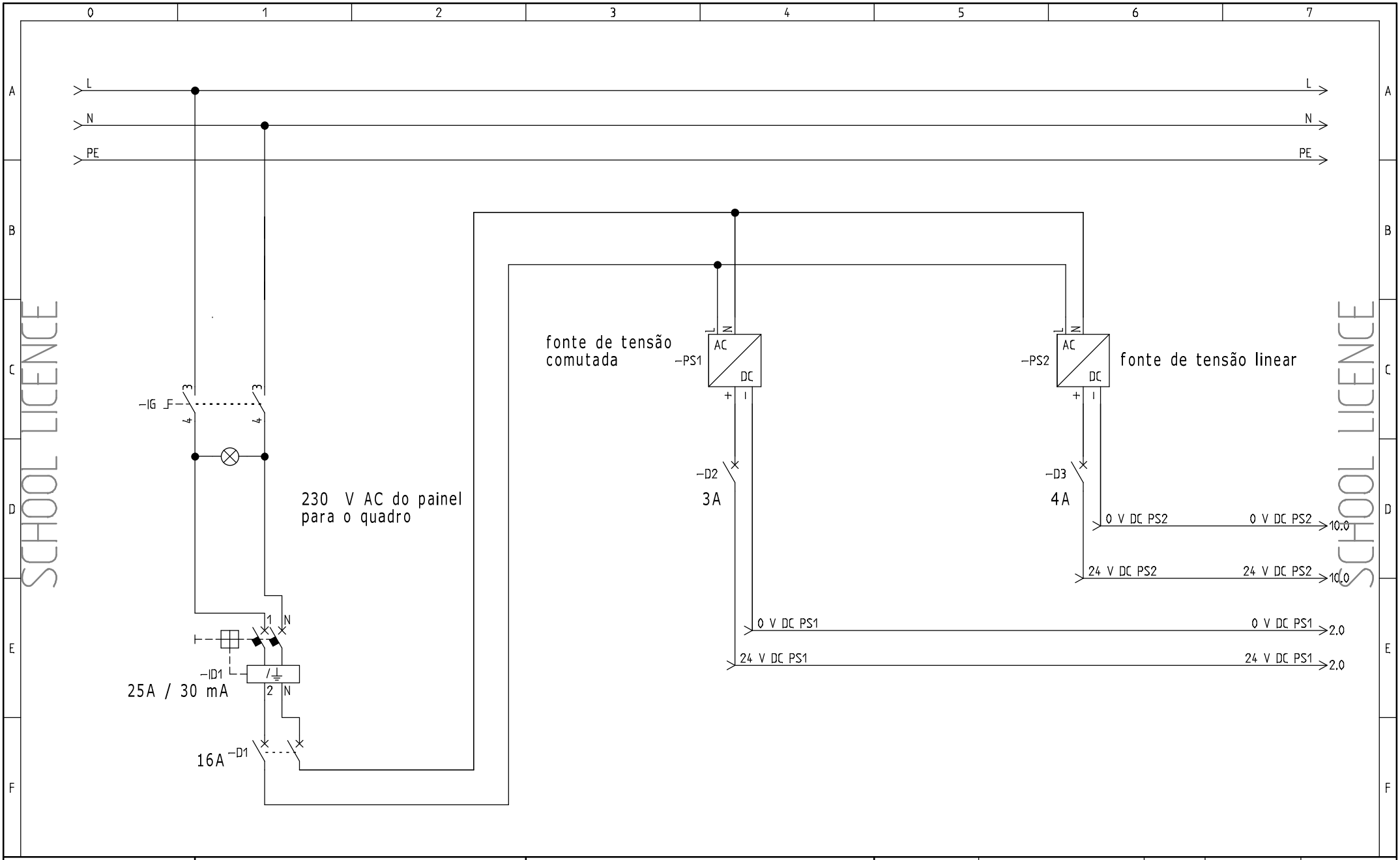

- Logo -	POTÊNCIA	esquema geral_V4 funcional	Project:	Drawing no.:	Init.:	Rev.:	Sheet: 1
			Date: 03-06-2016	Function:	Location:	Total sheets: 20	Next sheet: 2

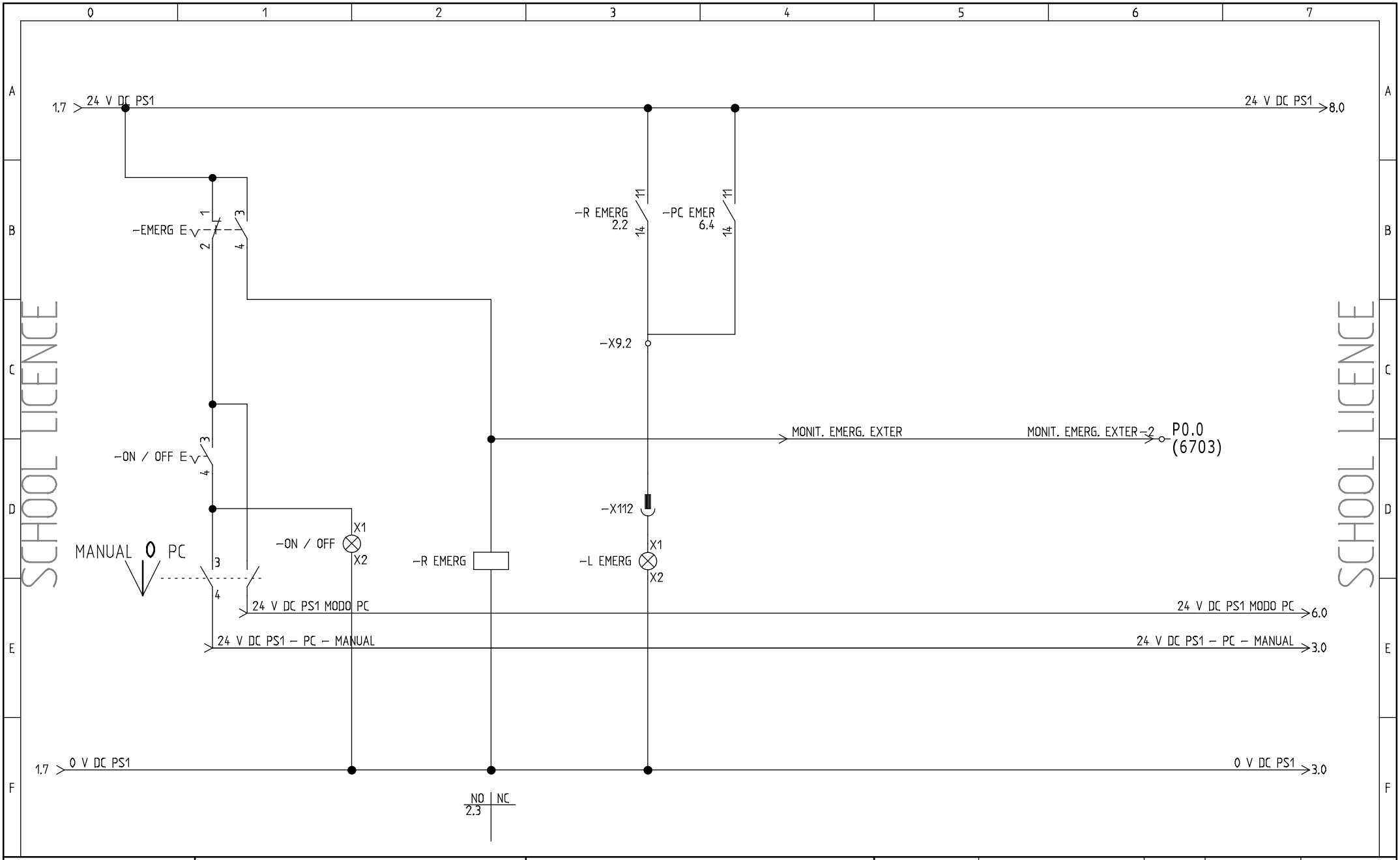

– Logo –	COMANDO MANUAL/PC /EMERGÊNCIA	esquema geral_V4 funcional	Project:	Drawing no.:	Init.:	Rev.:	Sheet: 2
			Date: 03-06-2016	Function:	Location:	Total sheets: 20	Next sheet: 3

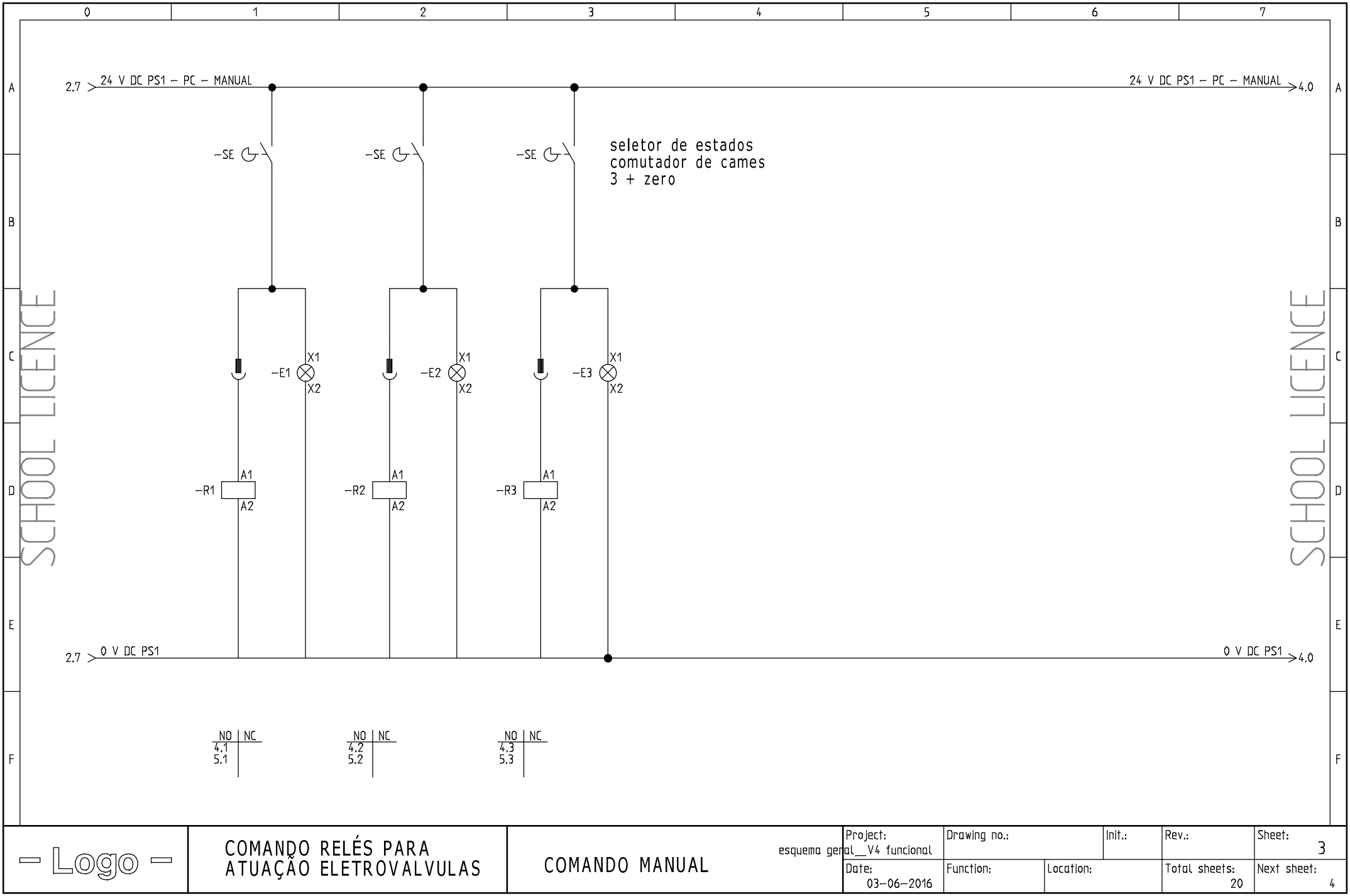

– Logo –	COMANDO RELÉS PARA ATUAÇÃO ELETROVALVULAS	COMANDO MANUAL	esquema geral__V4 funcional	Project:	Drawing no.:	Init.:	Rev.:	Sheet: 3
				Date: 03-06-2016	Function:	Location:	Total sheets: 20	Next sheet: 4

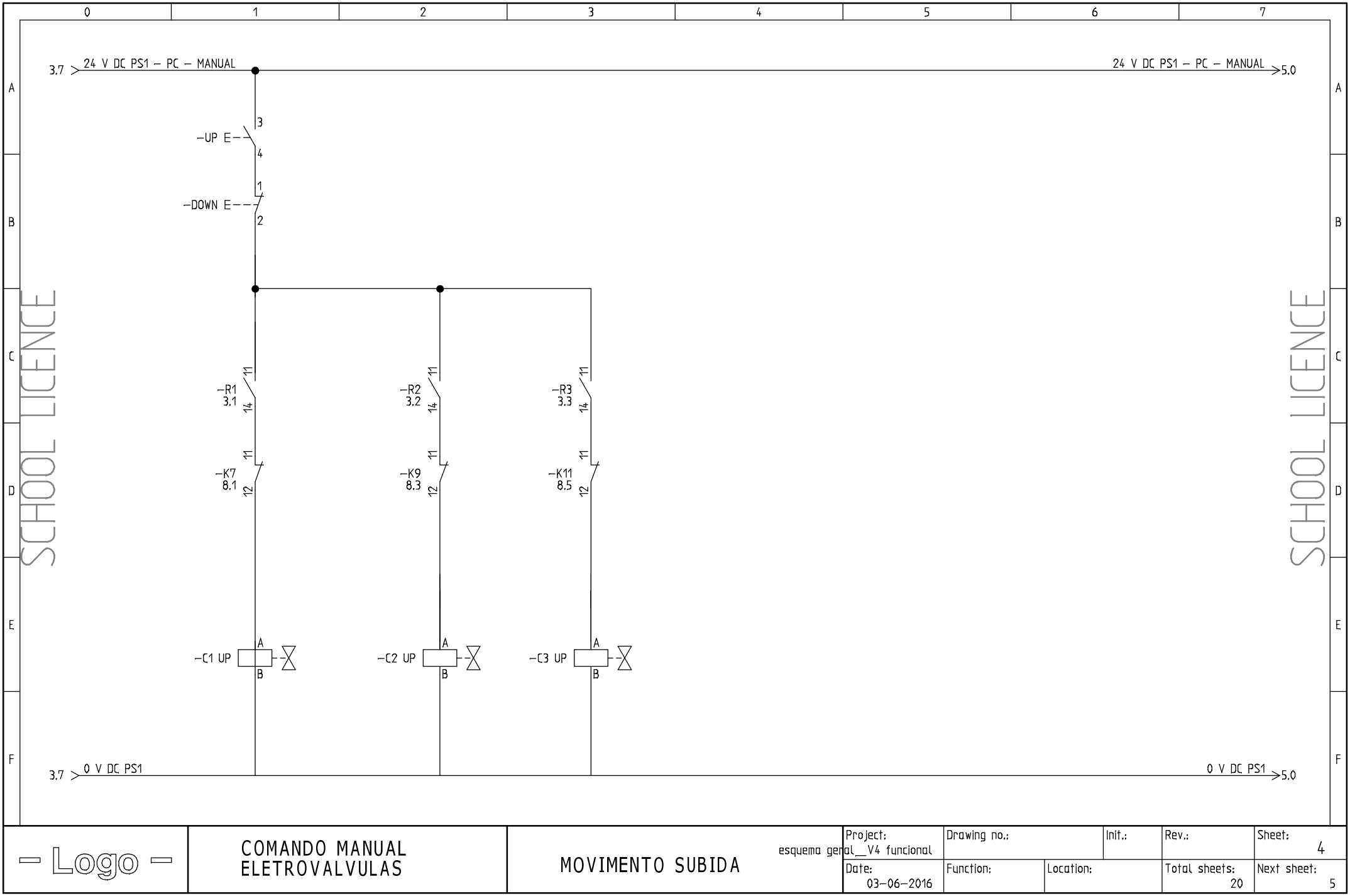

– Logo –	COMANDO MANUAL ELETROVALVULAS	MOVIMENTO SUBIDA	esquema geral_V4 funcional	Project:	Drawing no.:	Init.:	Rev.:	Sheet: 4
				Date: 03–06–2016	Function:	Location:	Total sheets: 20	Next sheet: 5

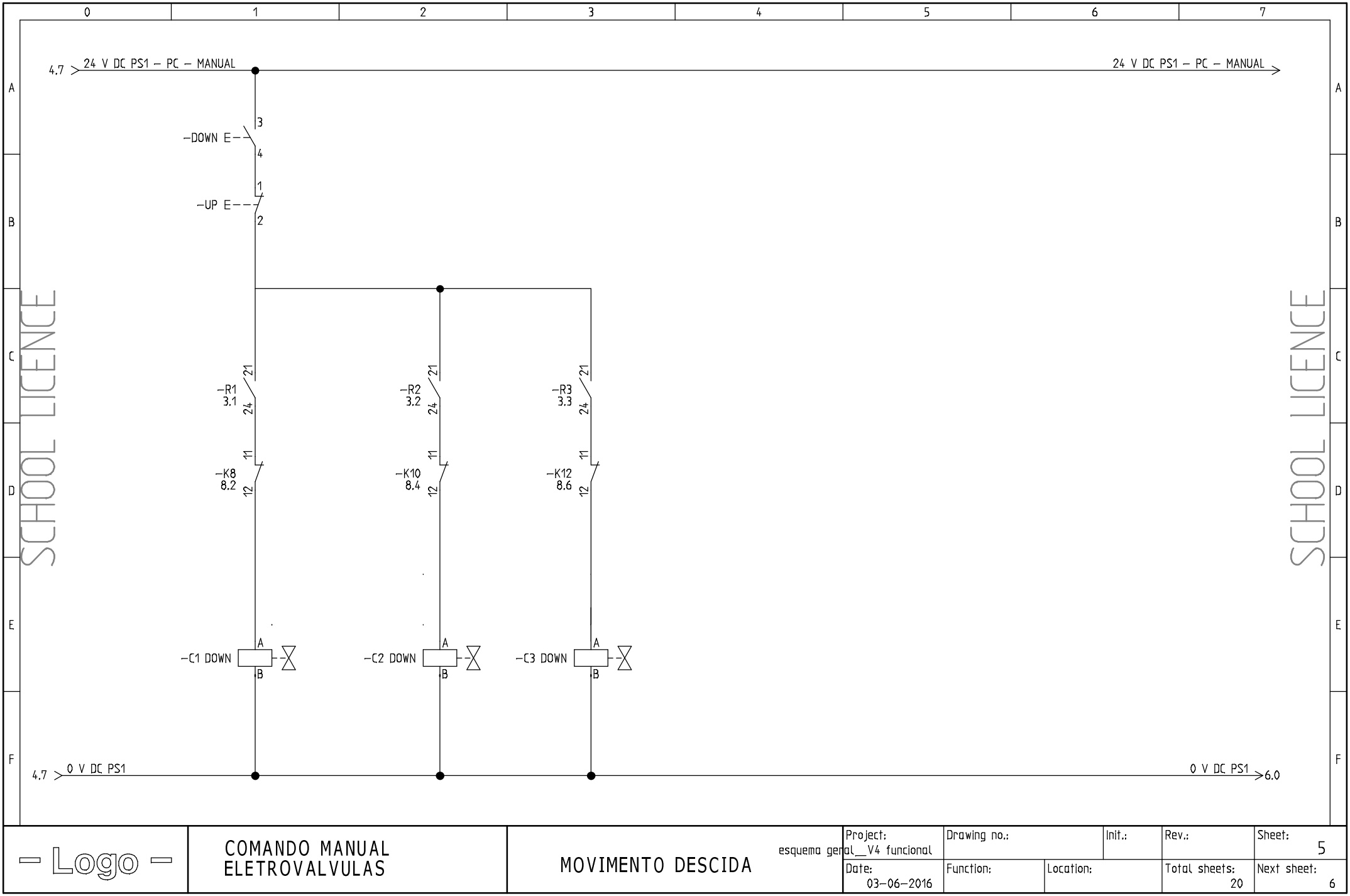

– Logo –	COMANDO MANUAL ELETROVALVULAS	MOVIMENTO DESCIDA	esquema geral_V4 funcional	Project:	Drawing no.:	Init.:	Rev.:	Sheet: 5
				Date: 03–06–2016	Function:	Location:	Total sheets: 20	Next sheet: 6

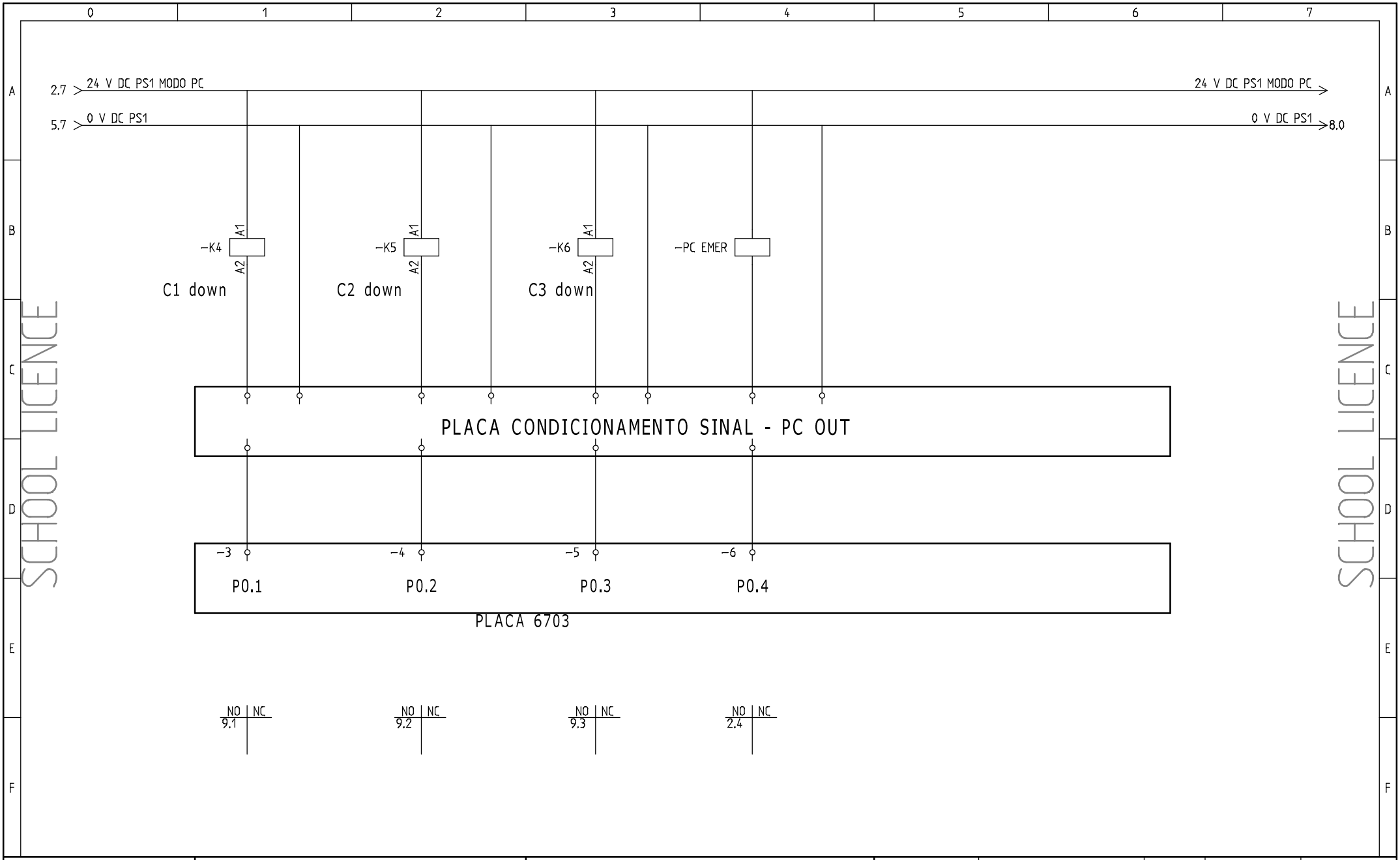

- Logo -	COMANDO DAS ELECTROVÁLVULAS VIA PC	PC OUT	esquema geral_V4 funcional	Project:	Drawing no.:	Init.:	Rev.:	Sheet: 6
				Date: 03-06-2016	Function:	Location:	Total sheets: 20	Next sheet: 7

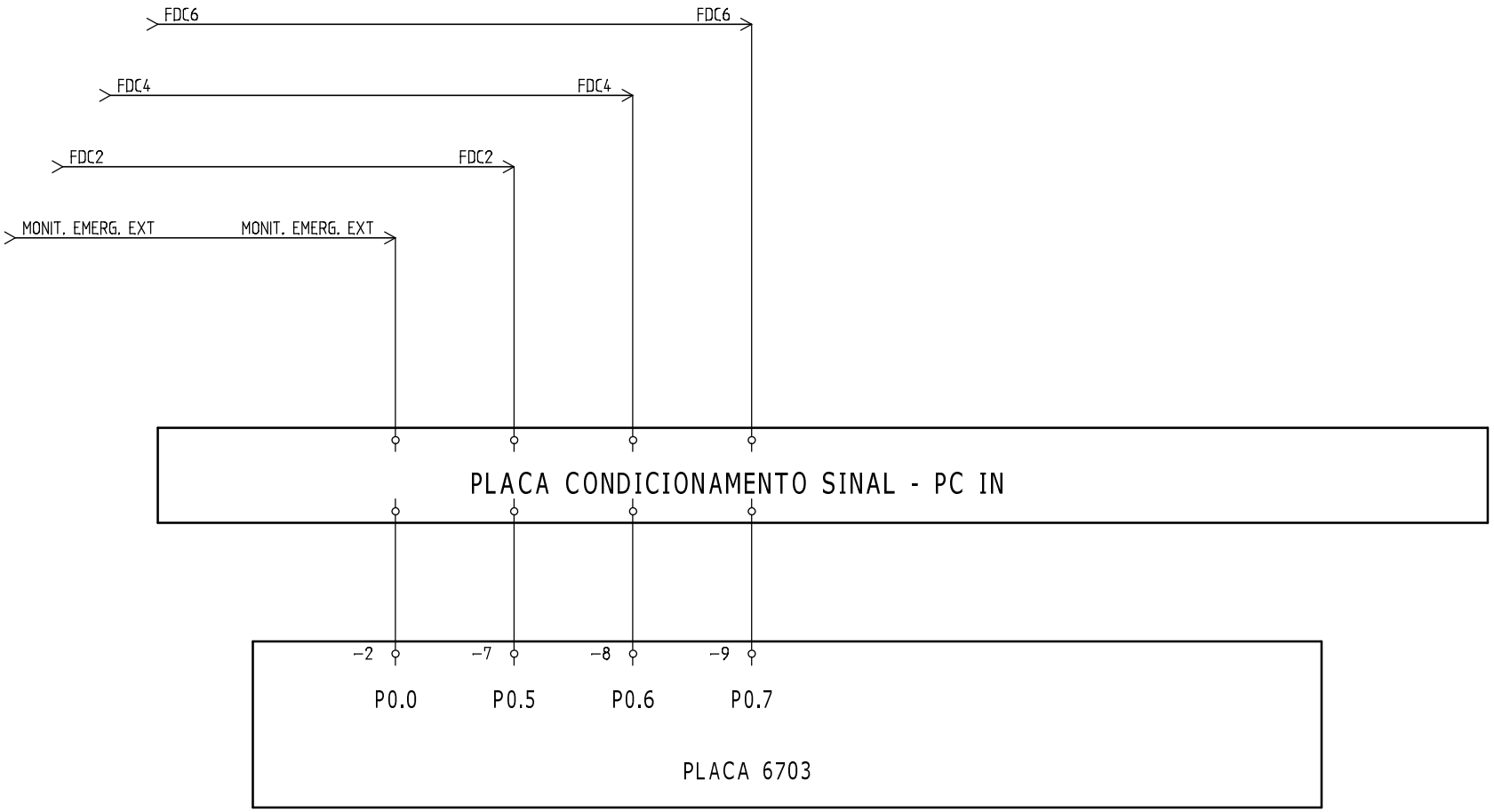

- Logo -		PC IN	Project: esquema geral__V4 funcional	Drawing no.:	Init.:	Rev.:	Sheet: 7
			Date: 03-06-2016	Function:	Location:	Total sheets: 20	Next sheet: 8

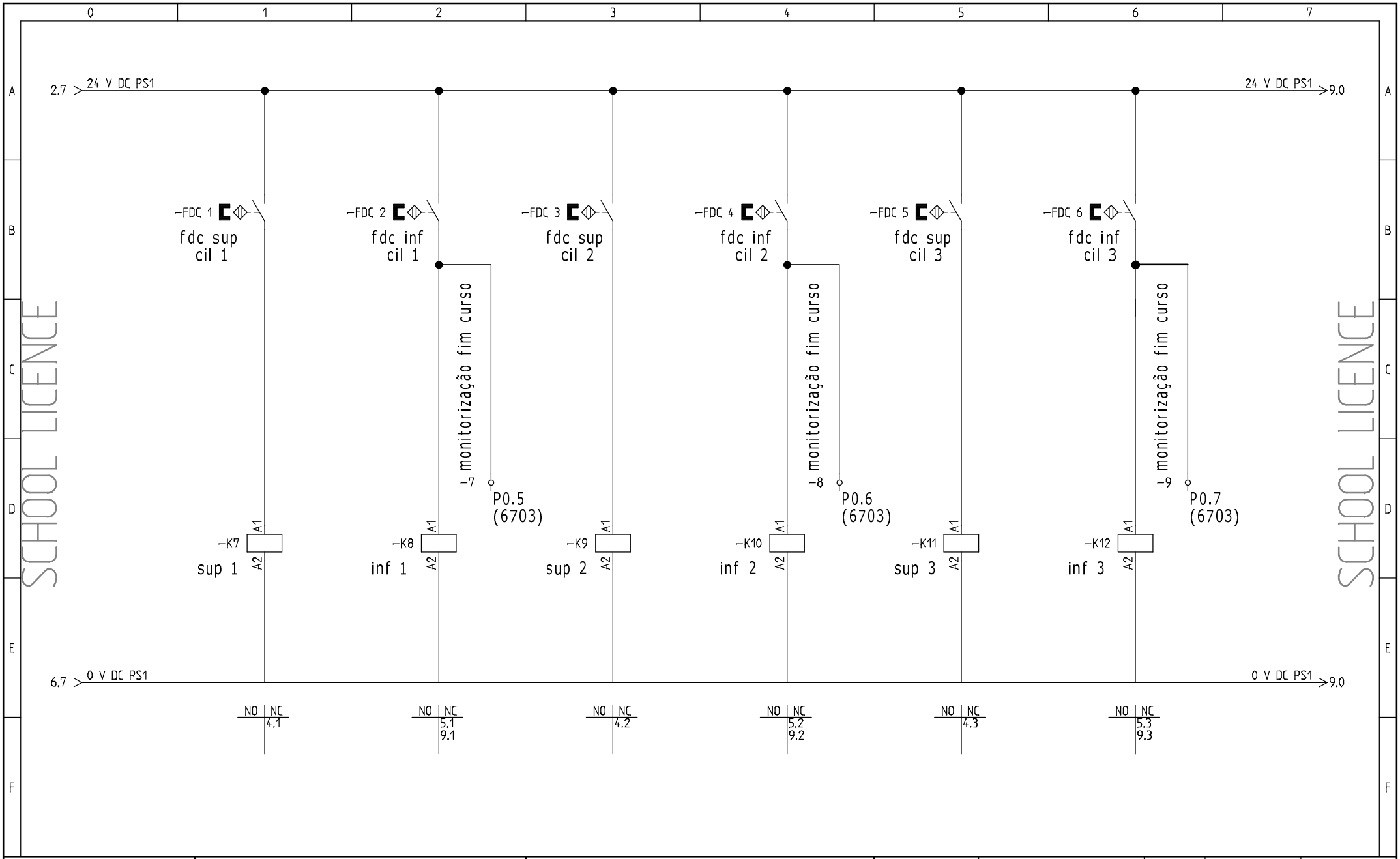

— Logo —	FIM CURSO DOS CILINDROS	esquema geral_V4 funcional	Project:	Drawing no.:	Init.:	Rev.:	Sheet: 8
			Date: 03-06-2016	Function:	Location:	Total sheets: 20	Next sheet: 9

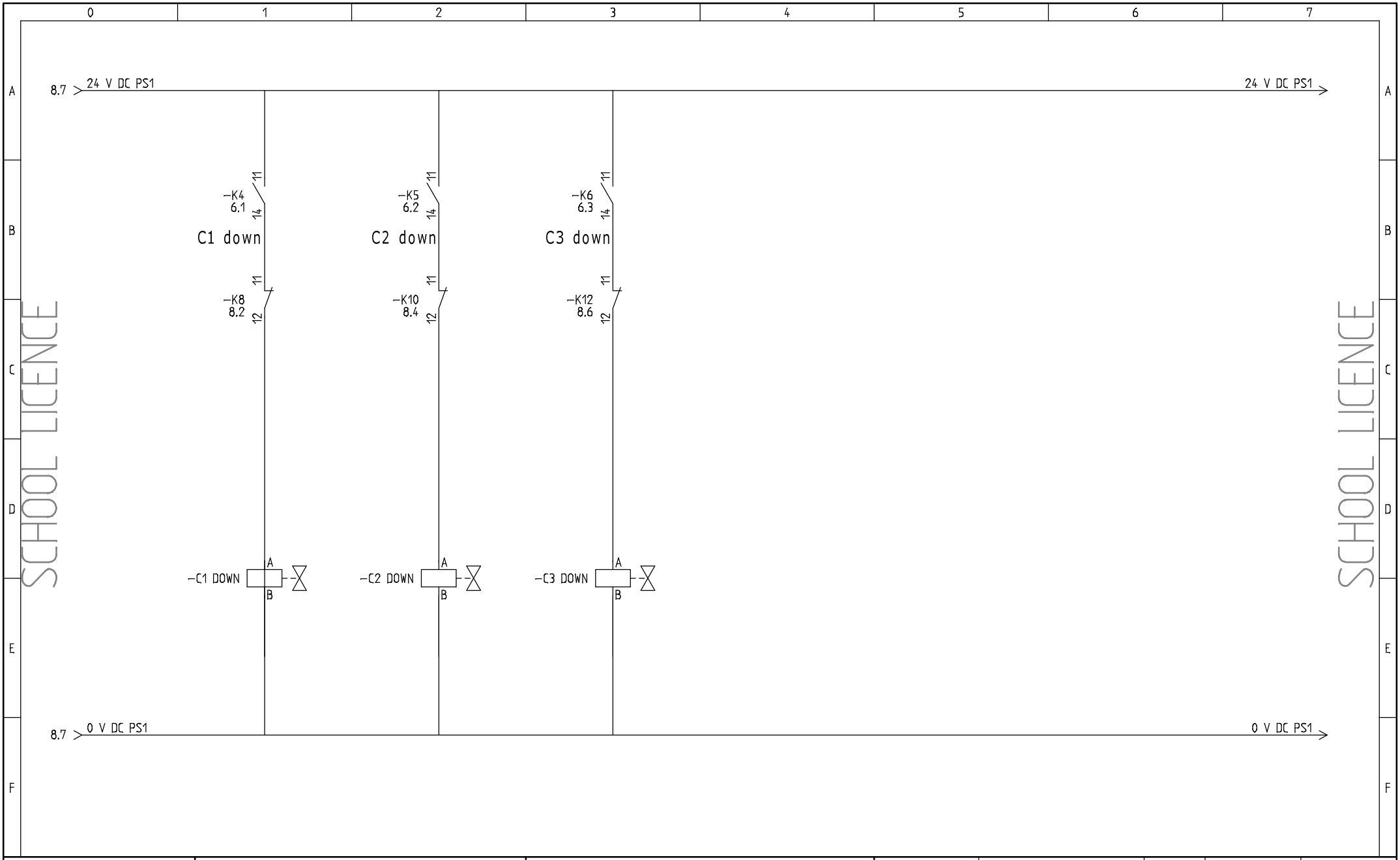

- Logo -	COMANDO DAS ELECTROVÁLVULAS VIA PC	esquema geral_V4 funcional	Project:	Drawing no.:		Init.:	Rev.:	Sheet: 9
			Date: 03-06-2016	Function:	Location:		Total sheets: 20	Next sheet: 10

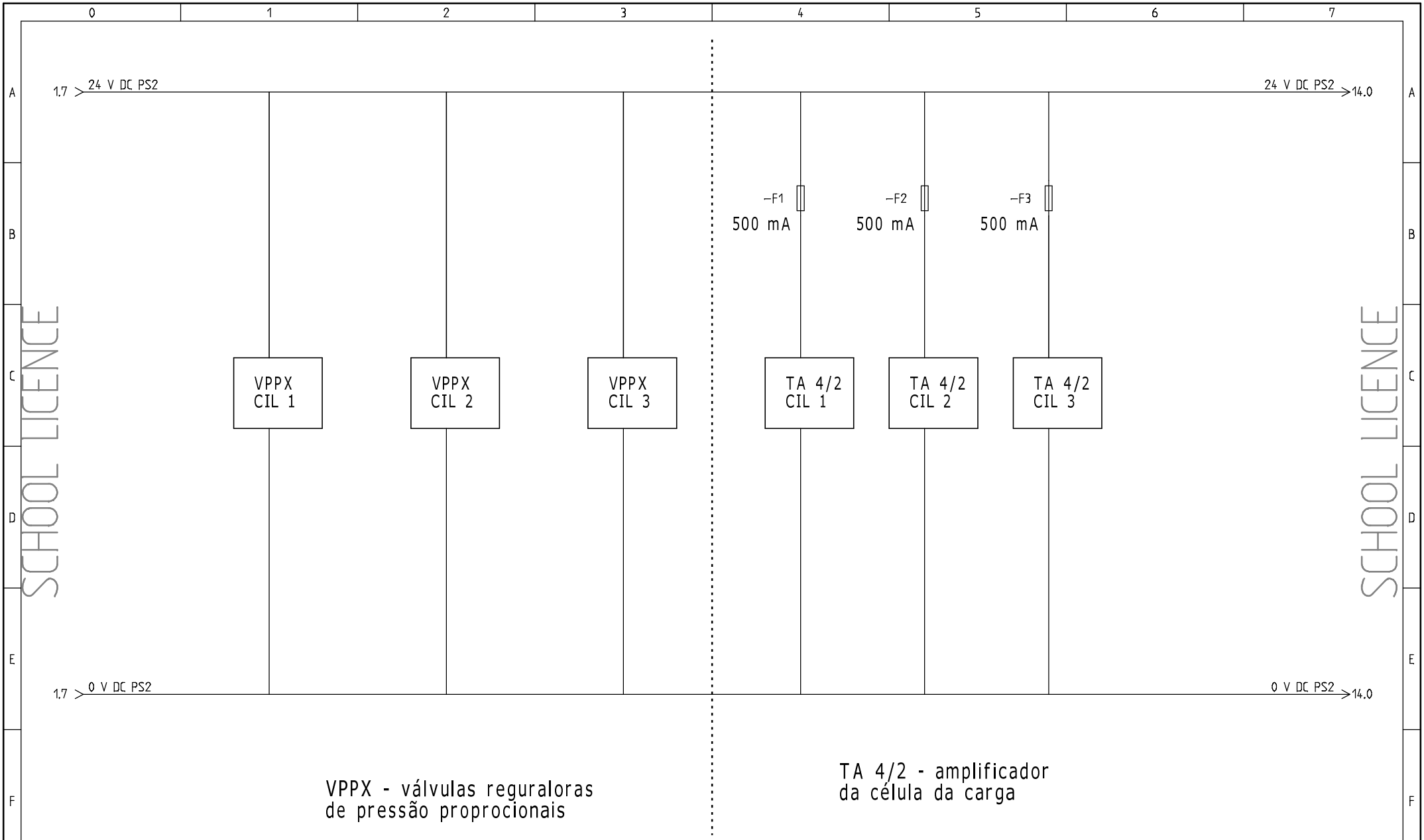

— Logo —		esquema geral_V4 funcional	Project:	Drawing no.:	Init.:	Rev.:	Sheet: 10
			Date: 03-06-2016	Function:	Location:	Total sheets: 20	Next sheet: 11

1 - do not connect TxPc

2 - 24 v dc supply voltage — + 24 V DC PS2

3 - analog input W- — AO GND 1 placa 6703

4 - analog input W+ — AO 1 (V) placa 6703

5 - do not connect Rx Pc

6 - analog output X — AI 6 placa 6010

7 - gnd or 0 v dc — 0 V DC PS2

8 - input for ext sensor signal + — AO 4(V) placa 6703

SCHOOL LICENCE

– Logo –	VPPX - CIL 1	VALVULA REGULADORA DE PRESSÃO PROPORCIONAL	Project: Esquema geral_V4 funcional	Drawing no.:		Init.:	Rev.:	Sheet: 11
			Date: 03-06-2016	Function:	Location:		Total sheets: 20	Next sheet: 12

SCHOOL LICENCE

M12 8 PINOS

1 - do not connect TxPc

2 - 24 v dc supply voltage — + 24 V DC PS2

3 - analog input W- — AO GND 3 placa 6703

4 - analog input W+ — AO 3 (V) placa 6703

5 - do not connect Rx Pc

6 - analog output + — AI 7 placa 6010

7 - gnd or 0 v dc — 0 V DC PS2

8 - input for ext sensor signal + — AO 2 (V) placa 6703

SCHOOL LICENCE

— Logo —	VPPX - CIL 2	VALVULA REGULADORA DE PRESSÃO PROPORCIONAL	Project: Esquema geral_V4 funcional	Drawing no.:	Init.:	Rev.:	Sheet: 12
			Date: 03-06-2016	Function:	Location:	Total sheets: 20	Next sheet: 13

1 - do not connect TxPc

2 - 24 v dc supply voltage — + 24 V DC PS2

−X7.1

3 - analog input W- — AO GND 5 placa 6703

4 - analog input W+ — AO 5 (V) placa 6703

5 - do not connect Rx Pc

6 - analog output + — AI 8 placa 6010

7 - gnd or 0 v dc — 0 V DC PS2

8 - input for ext sensor signal + — AO 0 (V) placa 6703

SCHOOL LICENCE

− Logo −	VPPX - CIL 3	VALVULA REGULADORA DE PRESSÃO PROPORCIONAL	Project: Esquema geral_V4 funcional	Drawing no.:		Init.:	Rev.:	Sheet: 13
			Date: 03−06−2016	Function:	Location:		Total sheets: 20	Next sheet: 14

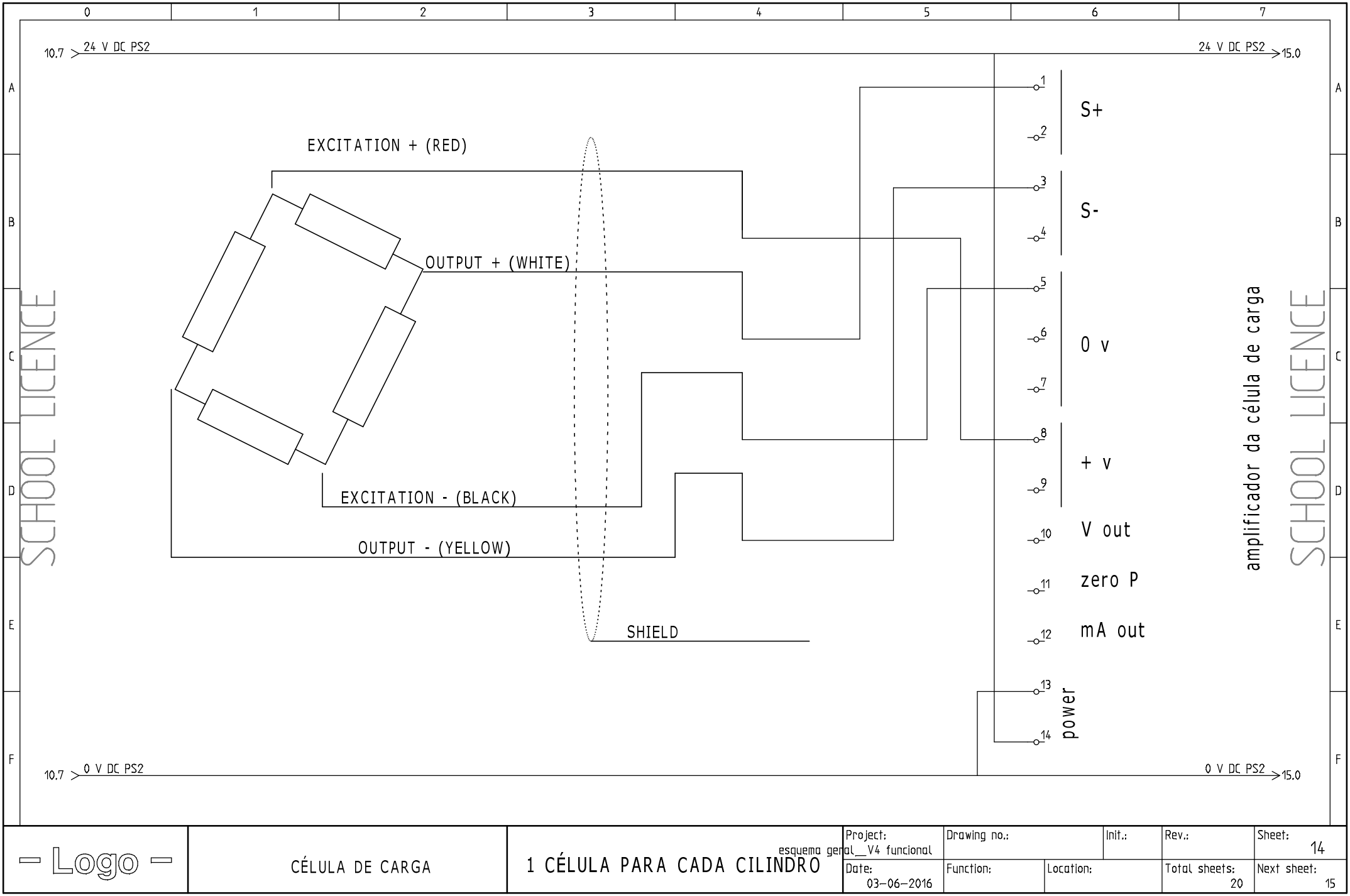

— Logo —	CÉLULA DE CARGA	1 CÉLULA PARA CADA CILINDRO	Project: esquema geral__V4 funcional	Drawing no.:		Init.:	Rev.:	Sheet: 14
			Date: 03-06-2016	Function:	Location:		Total sheets: 20	Next sheet: 15

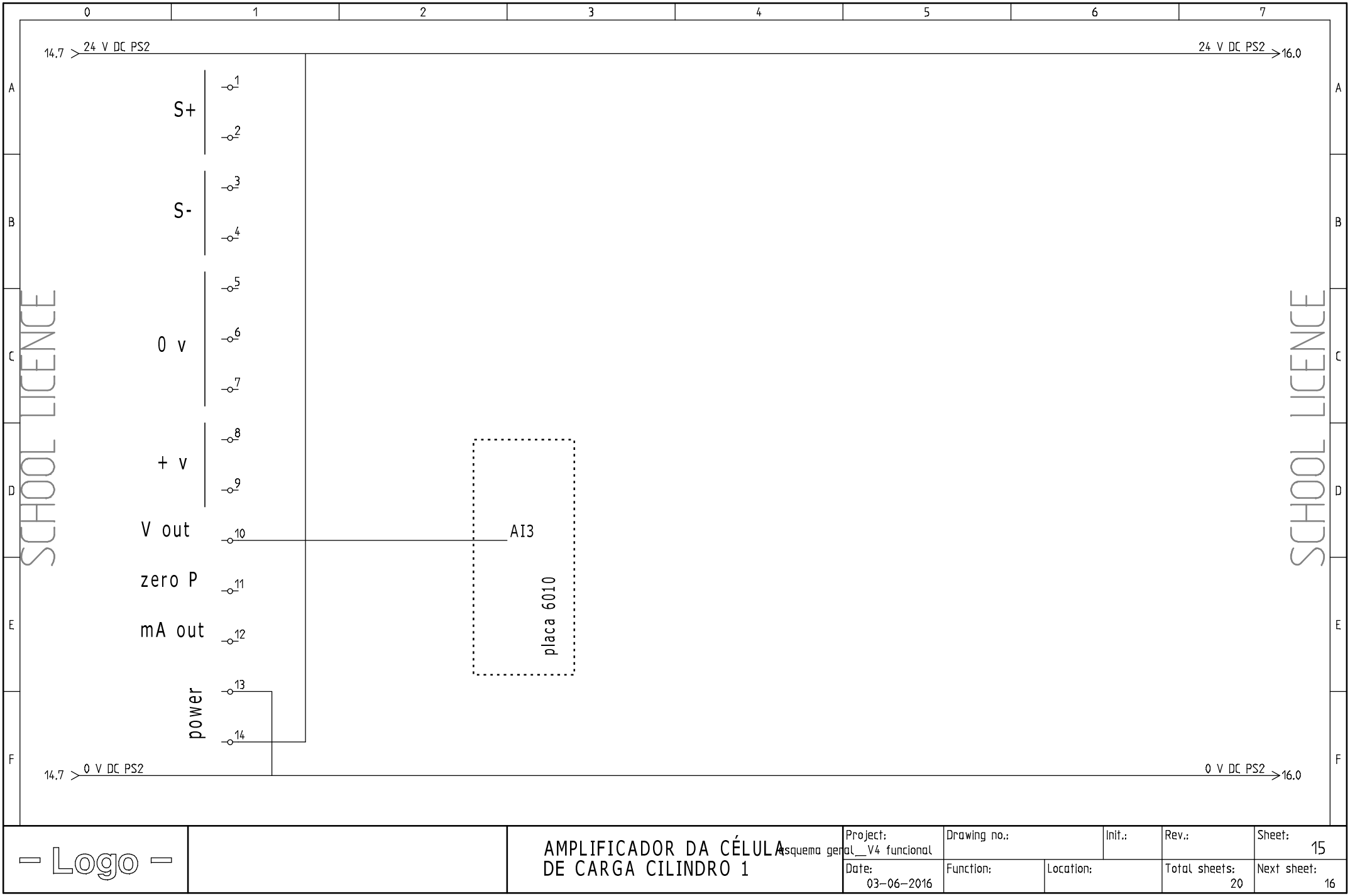

— Logo —

AMPLIFICADOR DA CÉLULA DE CARGA CILINDRO 1

Esquema geral_V4 funcional

Project:	Drawing no.:		Init.:	Rev.:	Sheet: 15
Date: 03-06-2016	Function:	Location:		Total sheets: 20	Next sheet: 16

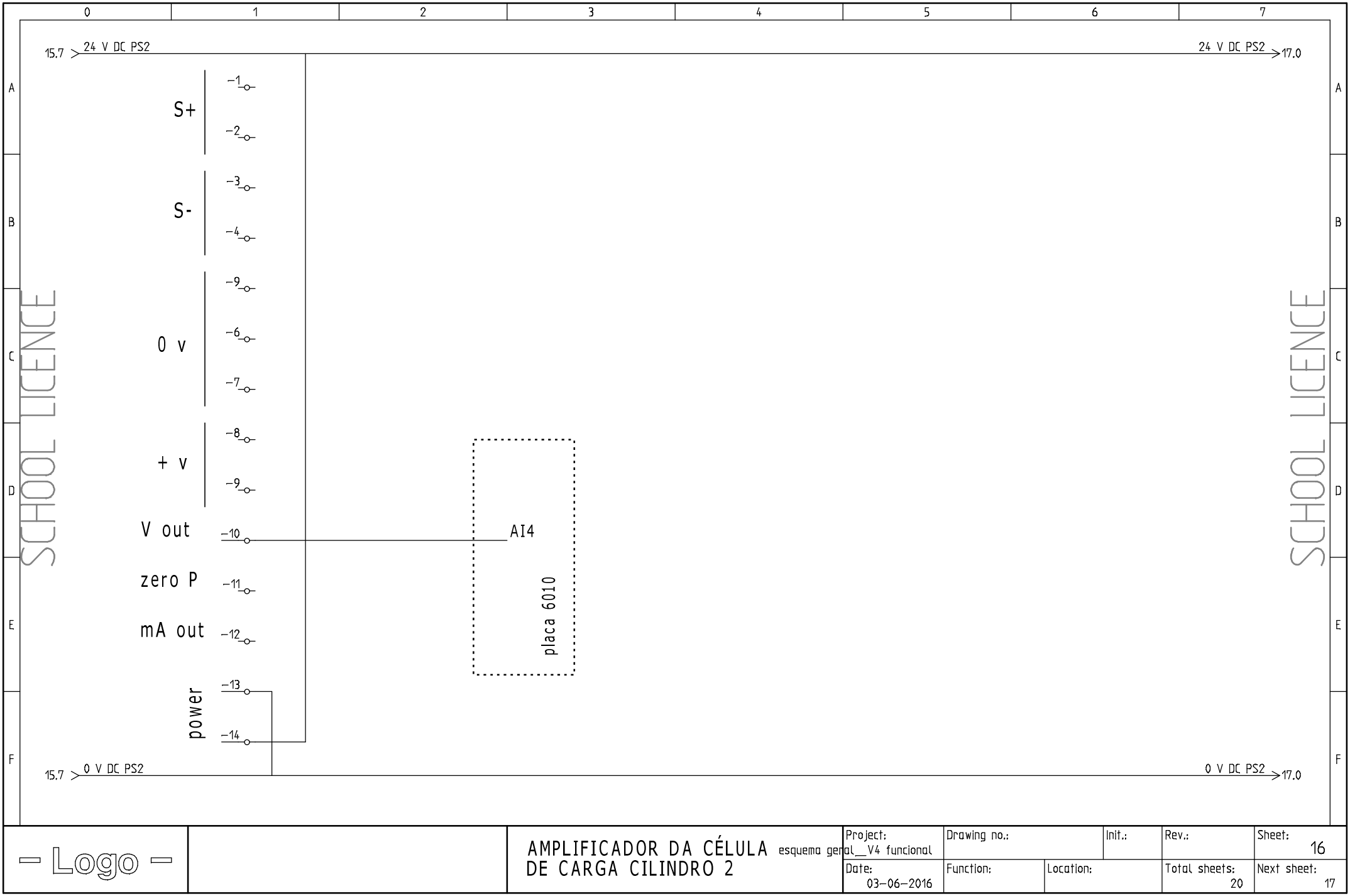
0
1
2
3
4
5
6
7
A
B
C
D
E
F
15.7
24 V DC PS2
24 V DC PS2
17.0
S+
S-
0 v
+ v
V out
zero P
mA out
power
-1
-2
-3
-4
-9
-6
-7
-8
-9
-10
-11
-12
-13
-14
AI4
placa 6010
SCHOOL LICENCE
SCHOOL LICENCE
15.7
0 V DC PS2
0 V DC PS2
17.0
- Logo -
AMPLIFICADOR DA CÉLULA DE CARGA CILINDRO 2
esquema geral_V4 funcional
Project:
Drawing no.:
Init.:
Rev.:
Sheet: 16
Date: 03-06-2016
Function:
Location:
Total sheets: 20
Next sheet: 17

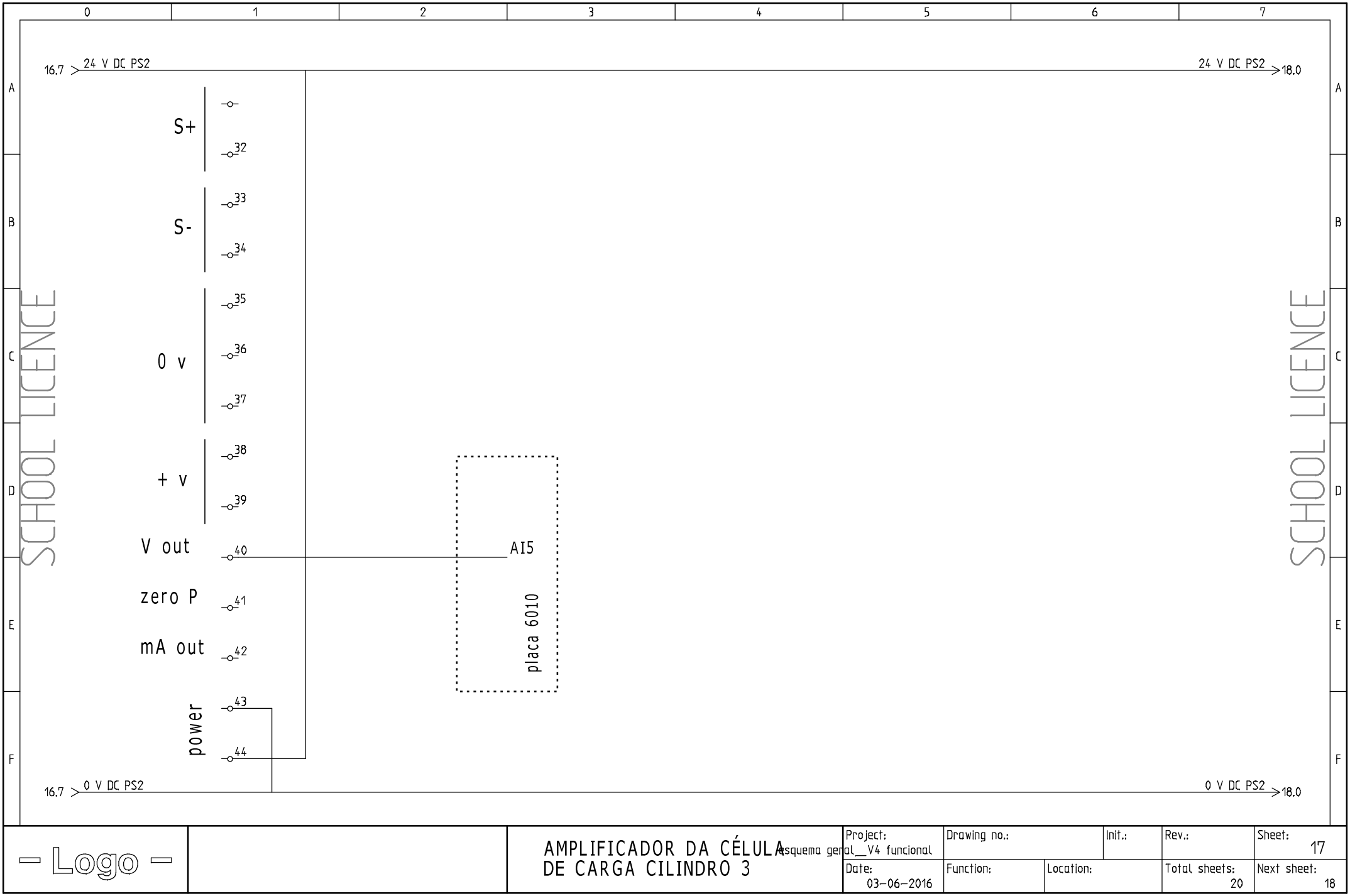
0
1
2
3
4
5
6
7
A
B
C
D
E
F
16.7
24 V DC PS2
24 V DC PS2
18.0
S+
32
S-
33
34
0 v
35
36
37
+ v
38
39
V out
40
zero P
41
mA out
42
power
43
44
AI5
placa 6010
16.7
0 V DC PS2
0 V DC PS2
18.0
SCHOOL LICENCE
SCHOOL LICENCE
— Logo —
AMPLIFICADOR DA CÉLULA DE CARGA CILINDRO 3
Esquema geral_V4 funcional
Project:
Drawing no.:
Init.:
Rev.:
Sheet: 17
Date: 03-06-2016
Function:
Location:
Total sheets: 20
Next sheet: 18

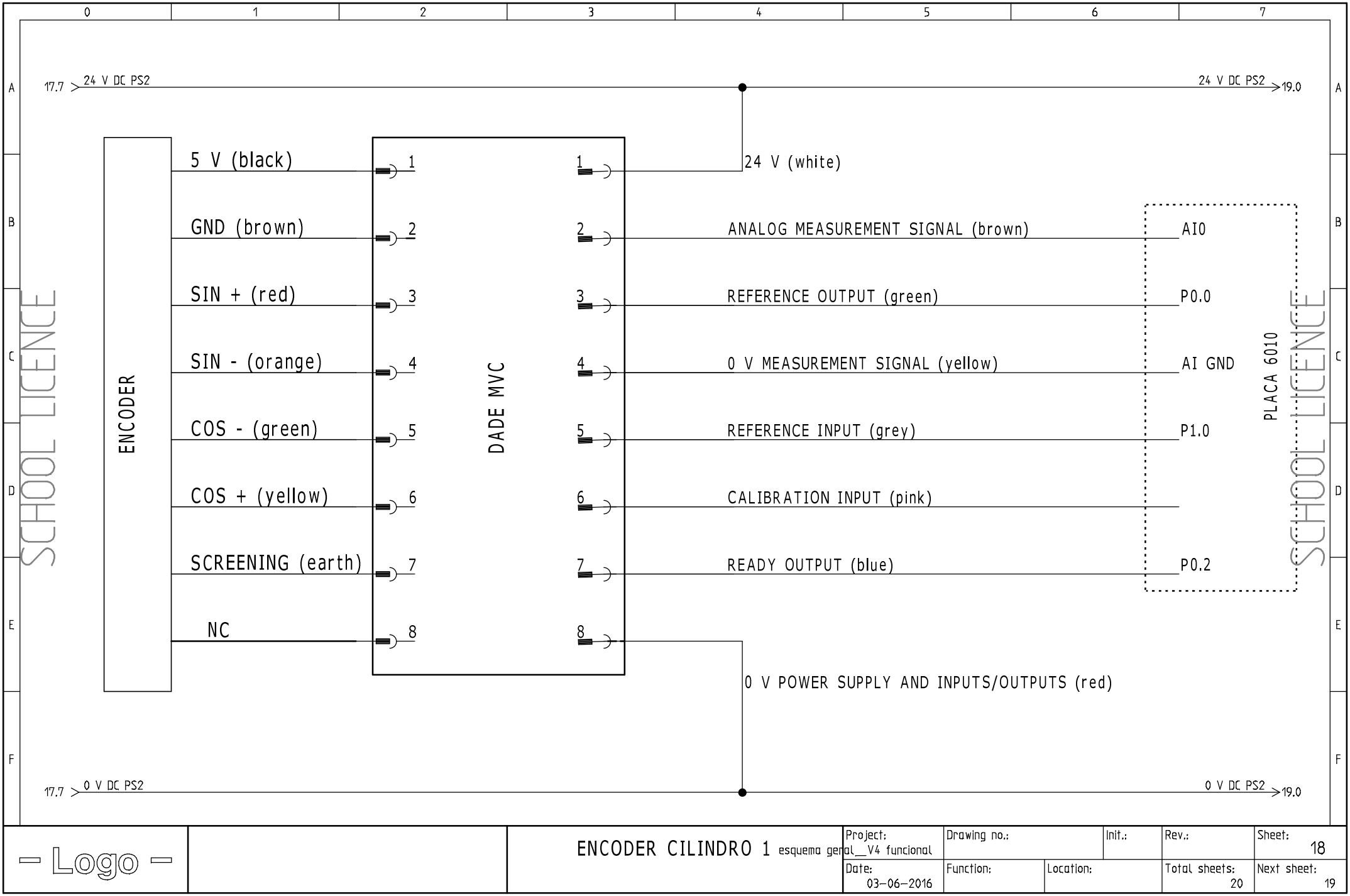

– Logo –		ENCODER CILINDRO 1 esquema geral_V4 funcional	Project:	Drawing no.:	Init.:	Rev.:	Sheet: 18
			Date: 03-06-2016	Function:	Location:	Total sheets: 20	Next sheet: 19

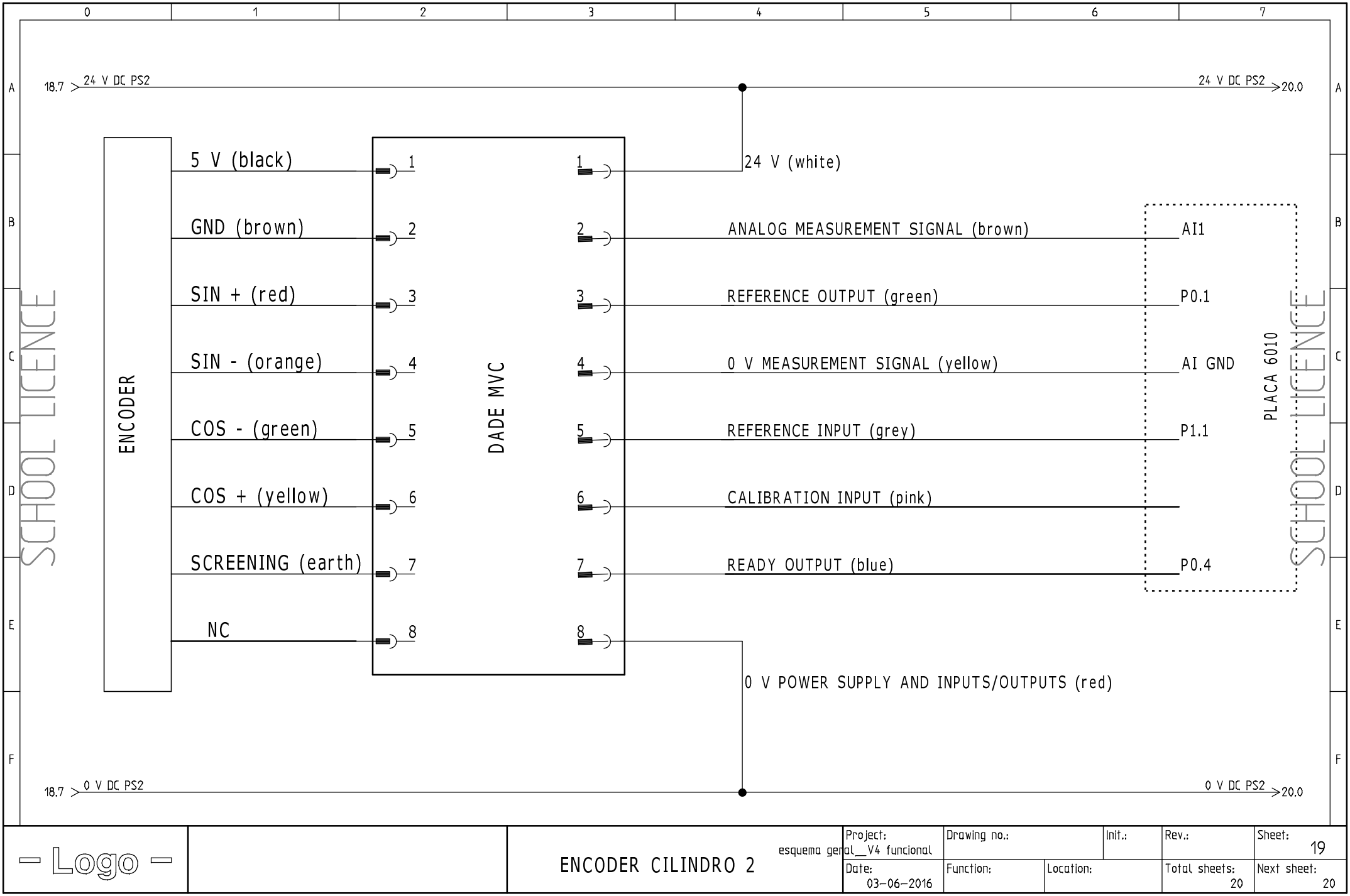

– Logo –		ENCODER CILINDRO 2 esquema geral_V4 funcional	Project:	Drawing no.:	Init.:	Rev.:	Sheet: 19
			Date: 03-06-2016	Function:	Location:	Total sheets: 20	Next sheet: 20

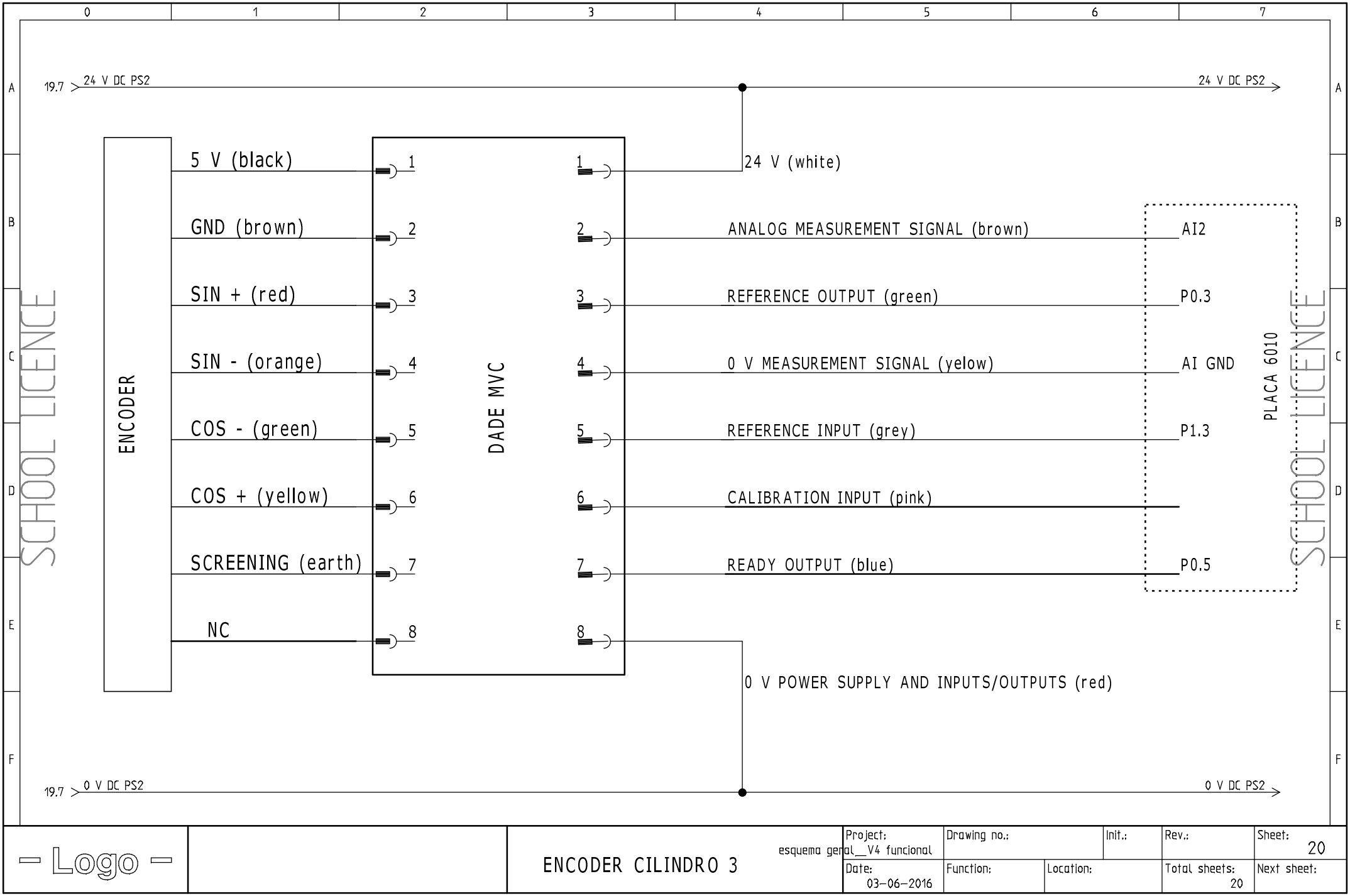

– Logo –		ENCODER CILINDRO 3	Project: esquema geral_V4 funcional	Drawing no.:	Init.:	Rev.:	Sheet: 20
			Date: 03-06-2016	Function:	Location:	Total sheets: 20	Next sheet:

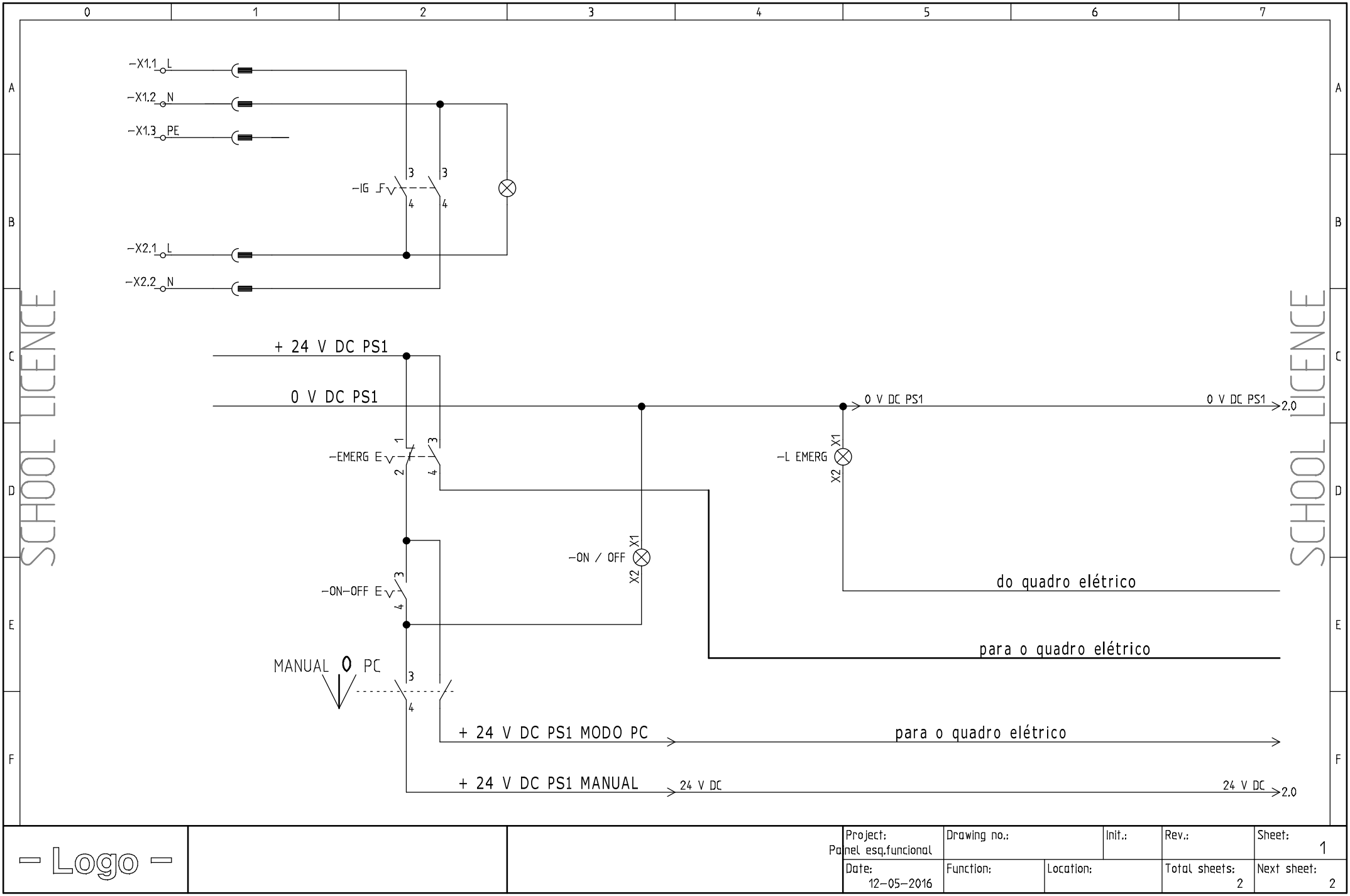

- Logo -			Project: Painel esq.funcional	Drawing no.:	Init.:	Rev.:	Sheet: 1
			Date: 12-05-2016	Function:	Location:	Total sheets: 2	Next sheet: 2

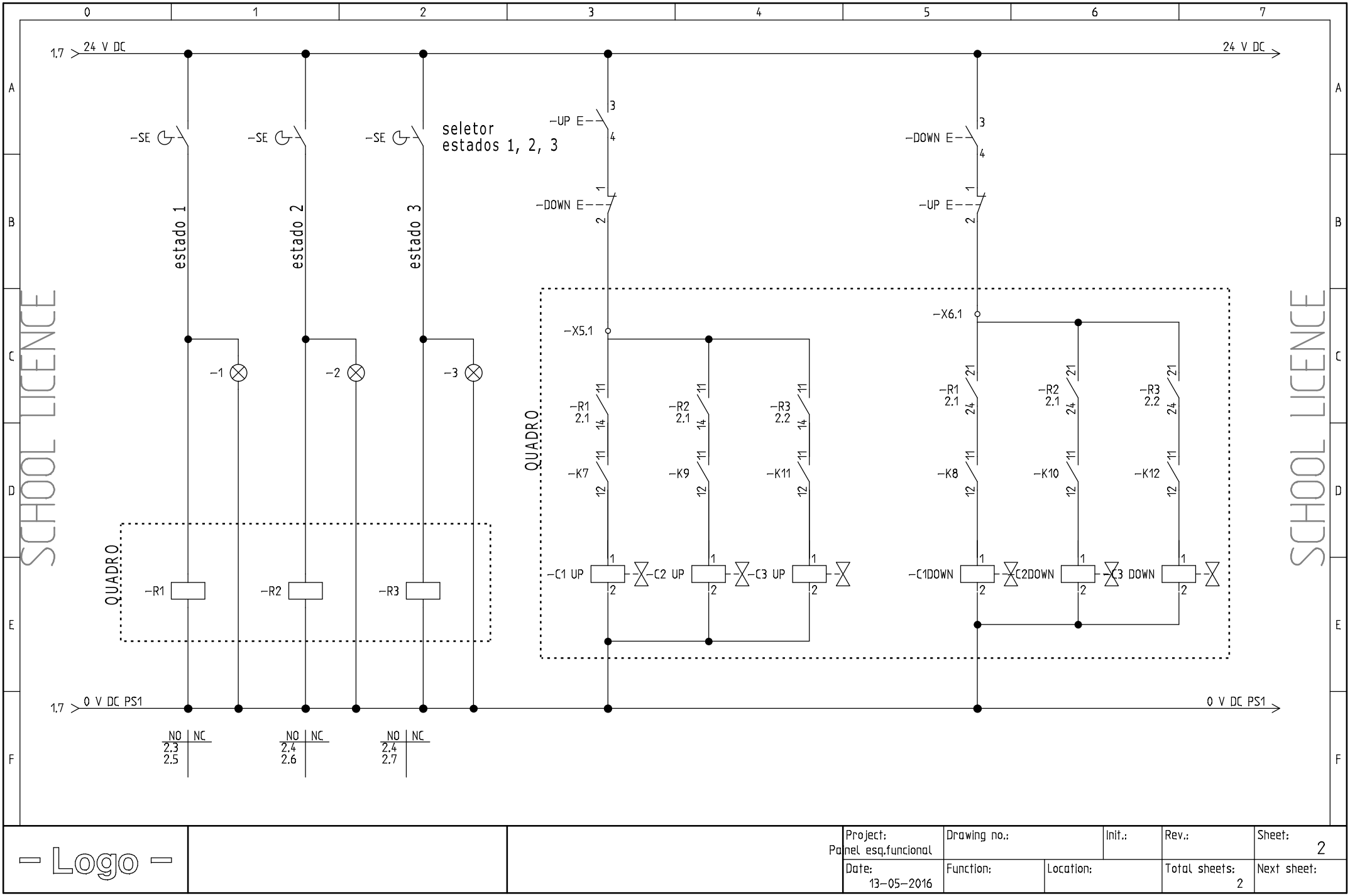

- Logo -			Project: Painel esq.funcional	Drawing no.:	Init.:	Rev.:	Sheet: 2
			Date: 13-05-2016	Function:	Location:	Total sheets: 2	Next sheet:

References

[1] Walter Brockmann, Paul Ludwig Geiß, Jürgen Klingen, Bernhard Schröder, and B Mikhail. *Adhesive bonding*. Wiley-VCH Verlag GmbH & Co. KGaA Weinheim, 2009.

[2] Lucas FM da Silva, Andreas Öchsner, and Robert D Adams. *Handbook of Adhesion Technology*. Springer Science & Business Media, 2011.

[3] Hugo Freire. Desenvolvimento de um dispositivo experimental para medir a resistência à fluência de ligações adesivas. Master's thesis, Faculdade de Engenharia da Universidade do Porto, 2013.

[4] JP Davim, AG Magalhães, and Faria de Oliveira. *Ensaios mecânicos e tecnológicos*. 1992.

[5] INSTRON. 3360 series | dual column tabletop models.

[6] INSTRON. 3119 series | environmental chambers.

[7] INSTRON. Multi station systems | 5900 series.

[8] ZWICK. Creep testing machine kappa multistation for plastics.

[9] MTS. *647 Side-Loading Hydraulic Wedge Grips*.

[10] INSTRON. *2712-04x | Series Pneumatic Side-Action Grips*.

[11] SHIMADZU. *Manual Screw Flat Grips*. C224-E066A.

[12] MTS. *The Advantage Mechanical Wedge Grips*. 300178-01a.

[13] Euro Inox. Stainless steel at high temperatures.

[14] Granta Design. Ces Edupack.

[15] INSTRON. 2716 series | manual wedge action grips.

[16] José Simões Morais. *Desenho Técnico Básico*. Gráficos Reunidos, Lda, 27th edition, 2007.

[17] Gustav Niemann. *Elementos de Máquinas*. 1971.

[18] Theodore L Bergman, Frank P Incropera, David P DeWitt, and Adrienne S Lavine. *Fundamentals of heat and mass transfer*. John Wiley & Sons, 2011.

[19] INA. *Spherical plain bearings, plain bushes, rod ends*. Catalogue 238.

[20] Joseph E Shigley, Charles R Mischke, and Richard G Budynas. *Mechanical engineering design*. McGraw-Hill,, 2004.

[21] Lucas FM da Silva, Andreas Öchsner, and Robert D Adams. *Aços*. Springer Science & Business Media, 2011.

[22] CARBOLITE GERO. *Vertical Split Tube Furnace - VST / TVS*.

[23] FESTO. Standard cylinders ddpc, with measured-value transducer DADE.

[24] AVENTICS. *TA 4/2*. TA4.516.R3.

[25] SMC. *TA 4/2*. TA4.516.R3.

[26] FESTO. Proportional pressure regulators VPPX.

[27] FESTO. Service unit combinations MSB, MS series.

[28] FESTO. One-way flow control valves.

[29] FESTO. Proximity sensors SMT/SME-8, for T-slot.

[30] AEP Transducers. *TS-TSA*.

[31] AEP Transducers. *TA 4/2*. TA4.516.R3.